UNIVERSITY OF
KWAZULU-NATAL

INYUVESI
YAKWAZULU-NATALI

THE EFFECT OF GRAPHENE AS A HYDROPHOBIC ADDITIVE ON THE POLLUTION PERFORMANCE AND ACCELERATED AGEING OF COATINGS WHEN APPLIED TO AC HIGH VOLTAGE CERAMIC INSULATOR MATERIALS

By

Barend, Jacobus, Gert, Wessel du Plessis

220112742

In partial fulfilment of the academic requirements for the degree of

Master of Science in High Voltage Electrical Engineering,

College of Agriculture, Engineering and Science

University of KwaZulu-Natal

July 2023

Supervisors: Prof. L. Jarvis, Dr. R. Stephen, & Mr. J.C. Bekker

Industrial Supervisor: Dr. W.L. Vosloo

COLLEGE OF AGRICULTURE, ENGINEERING AND SCIENCE

DECLARATION 1 - PLAGIARISM

As the candidate's Supervisor, Prof. Leigh Jarvis, I agree to the submission of this dissertation.

Signed: ……..... **Date**: **10/07/2023**

I Barend (J.G.W) du Plessis declare that:

(i) **The research reported in this dissertation, except where otherwise indicated, is my original research.**

(ii) **This dissertation has not been submitted for any degree or examination at any other university.**

(iii) **This dissertation does not contain other persons' data, pictures, graphs, or other information, unless specifically acknowledged as being sourced from other persons.**

(iv) **This dissertation does not contain other persons' writing, unless specifically acknowledged as being sourced from other researchers. Where other written sources have been quoted, then:**

a) their words have been re-written, but the general information attributed to them has been referenced.
b) Where their exact words have been used, their writing has been placed inside quotation marks, and referenced.

(v) **This dissertation does not contain text, graphics or tables copied and pasted from the Internet, unless specifically acknowledged, and the source being detailed in the dissertation and in the References sections.**

Signed: ……..... **Date**: **10/07/2023**

COLLEGE OF AGRICULTURE, ENGINEERING AND SCIENCE

DECLARATION 2 - PUBLICATIONS

DETAILS OF CONTRIBUTION TO PUBLICATIONS that form part and/or include research presented in this dissertation (include publications in preparation, submitted, *in press* and published and give details of the contributions of each author to the experimental work and writing of each publication)

Publication 1: SAUPEC 2024 (24 – 25 January 2024)

Mr. B.J.G.W. du Plessis – Main Author

Prof. L. Jarvis – Main Supervisor

Dr. R. Stephen – Co-Supervisor

Dr. W.L. Vosloo – Industrial Supervisor

Mr. J.C. Bekker – Co-Supervisor

Signed: ……..... **Date**: **10/07/2023**

ACKNOWLEDGEMENTS

I would like to express my sincere gratitude to the following individuals who have played a significant role in the completion of my study:

First and foremost, I would like to extend my deepest appreciation to **Prof. Leigh Jarvis**, my esteemed supervisor. Your unwavering support, insightful guidance, and dedication to my academic growth have been invaluable throughout this research journey. Your expertise and encouragement have consistently pushed me to strive for excellence, and I am truly grateful for the opportunity to work under your mentorship.

I am equally grateful to **Dr. Rob Stephen**, my co-supervisor, for his invaluable contribution to this study. Your constructive feedback, meticulous attention to detail, and expertise in the subject matter have greatly enriched the quality of my research. Your dedication to pushing the boundaries of knowledge and your commitment to my academic development have been instrumental in shaping the final outcome of this study.

I would also like to express my deepest gratitude to **Dr. Wallace Vosloo**, my industrial supervisor. Your guidance, mentorship, and practical insights have been instrumental in bridging the gap between academia and industry. Your extensive experience and deep understanding of the field have provided me with invaluable perspectives that have significantly influenced the direction and applicability of my research. Your support and enthusiasm for my work have been truly inspiring, and I am grateful for the opportunity to have collaborated with you.

Finally, I would like to extend my appreciation to **Mr. Nelius Bekker**, another co-supervisor, for his valuable insights, thoughtful suggestions, and continuous support throughout this research journey. Your mentorship and guidance have been instrumental in navigating the challenges encountered during the course of this study, and I am truly grateful for your unwavering commitment to my academic success.

To all those who have contributed to this study, directly or indirectly, I am indebted to your support and encouragement. Your guidance, expertise, and belief in my abilities have motivated me to strive for excellence and have made this research endeavour a rewarding and enlightening experience.

ABSTRACT

This study focuses on the development and pre-testing of a modified insulator coating. The study aims to investigate and evaluate the performance of Pristine Graphene (PG) and Nanoplatelet Graphene (NPG) doped Room-Temperature Vulcanising Silicone Rubber (RTV SR) coatings at different weight percentages (wt%). Key properties such as surface resistivity, hydrophobicity, hydrophobicity transfer/recovery, tracking resistance, and erosion resistance were analysed to assess the effectiveness of the modified coating.

From an electrical insulation resistance perspective, NPG doped RTV SR coatings with over 3 wt% demonstrated more than twice the reduction in surface resistivity compared to the reference RTV SR coating. Furthermore, the Inclined Plane Tests (IPT) confirmed that the addition of NPG particles to the RTV SR mixture lowers the combustion temperature of the ATH (Aluminium-Trihydrate) filler, resulting in faster ignition during electrical discharging or DBA (Dry Band Arcing) events.

However, the project presented promising performance in terms of hydrophobicity, recovery, and transfer properties. A 10 wt% NPG weight fraction led to an approximate 10% increase in static contact angle measurements compared to the unfilled RTV SR coating. The presence of NPG did not hinder the hydrophobicity recovery and transfer mechanisms within the RTV SR matrix.

After pollution application, similar large static contact angles were measured as those observed on a clean 10 wt% NPG doped RTV SR coating surface. This observation led to a hypothesis that physical entanglement and/or interfacial interaction between Low-Molecular-Weight (LMW) silicones and the free-floating NPG sheets within the bulk layer of the modified coating material could result in the transfer of NPG sheets to the surface during polluted surface conditions. Consequently, this encapsulation of pollution particles would develop a pollution layer with a hydrophobicity level comparable to that of a clean NPG doped RTV SR coating surface over time.

Several recommendations are proposed for future research, including the setup of an inclined plane tester to evaluate hydrophobicity resistance and transfer principles, exploration of alternative fillers which do not decrease combustion temperature when adding to virgin RTV SR material, implementation of thermogravimetric analysis to study the modified coating’s chemical and physical phenomena, and conducting outdoor pollution performance and ageing tests in severe marine environments. Additionally, further investigation of the LMW silicones and NPG hydrophobicity transfer "package" hypothesis, accurate measurement of pollution layer thickness and homogeneity, Scanning Electron Microscopy (SEM) studies to determine morphological characteristics, and improvement of NPG mixing and dispersion quality are recommended. Furthermore, evaluation and comparison of PG doped RTV SR samples as well as corona activity analysis between different PG/NPG doped RTV SR weight percentages is also recommended.

The study concludes by emphasising the need for standardised tests and procedures to evaluate the long-term durability of superhydrophobic coatings and highlights the potential of semiconductive coatings, enhanced by graphene, to prevent flashovers, by governing small leakage currents. The reason for the study is to see if RTV SR coating can be modified to be superhydrophobic.

TABLE OF CONTENTS

LIST OF FIGURES

LIST OF TABLES

LIST OF ABBREVIATIONS

A	Ampere
AC	Alternating Current
ASTM	American Society for Testing and Materials
ATH	Aluminum-Trihydrate
CIGRE	International Council on Large Electrical Systems
CAH	Contact Angle Hysteresis
DBA	Dry Band Arcing
DC	Direct Current
EP	Epoxy
ESDD	Equivalent Salt Deposit Density
HR	Hydrophobicity Recovery
HT	Hydrophobicity Transfer
HTM	Hydrophobicity Transfer Material
HTV SR	High Temperature Vulcanised Silicone Rubber
HV	High Voltage
IEC	International Electrotechnical Commission
IP	Intellectual Property
IPMD	Insulator Pollution Monitoring Device
KIPTS	Koeberg Insulator Pollution Test Station
KNPS	Koeberg Nuclear Power Station
kVA	Kilo Volt Ampere
LMW	Low Molecular Weight
MTR	Mobile Test Rig
NPG	Nanoplatelet Graphene
NSDD	Non-Soluble Deposit Density
PD	Particle Discharge
PDMS	Polydimethylsiloxane
PG	Pristine Graphene
PMMA	Poly Methyl Methacrylate

PS	Polystyrene
PU	Polyurethane
PVA	Poly Vinyl Alcohol
RDWT	Rotating Dipping Wheel Test
RH%	Percent Relative Humidity
RRT	Round Robin Tests
RTV SR	Room Temperature Vulcanised Silicone Rubber
R&D	Research and Development
SAIDI	System Average Interruption Duration Index
SAIFI	System Average Interruption Frequency Index
SCL	Specific Creepage Length
SEM	Scanning Electron Microscopy
SPS	Site Pollution Severity
STRI	Swedish Transmission Research Institute
USCL	Unified Specific Creepage Length
V	Volt
W	Watt
WC	Wettability Class

1. INTRODUCTION

1.1 Background

Superhydrophobic Room Temperature Vulcanised Silicone Rubber (RTV SR) coatings are under development, especially for use on ceramic insulators, to improve performance under severe environmental pollution conditions. Eskom (Energy Utility in South Africa) requires independence of supplier's research into the pollution performance of these coatings (ex. Graphene doped RTV SR) when tested with accelerated ageing methods which are broadly accepted, provided there is good correlation between the field and laboratory results [6].

For many years Eskom has followed international guidelines in selecting transmission and distribution insulator products for use in polluted environments. The first Koeberg Insulator Pollution Test Site (KIPTS) test site has been in operation for years, receiving extensive funding from Eskom Research and Development (R&D) [8]. It has become one of the best ranked test facilities in the world in terms of high voltage insulator research [9]. The research done at KIPTS had a profound impact on the insulator product market, as manufacturers altered their designs based on their findings at KIPTS. Due to severe sand dune movement, Eskom decommissioned old KIPTS and is now building a new outdoor insulator pollution test facility 2 km North of KNPS catering for distribution and transmission voltage levels (11, 22, 33, 66, 132 and 400 kV).

The previous test equipment (2x 22 kV 50 kVA transformers and 22 kV rectifiers used to generate positive and negative DC) at the old KIPTS site were extracted and refurbished at appropriate workshops. This equipment was then used to finalise the design of the Mobile Test Rig (MTR) and internal power source also presented in this project.

1.2 Importance of The Research and Motivation

The expected life of an insulator is a key consideration during insulation selection and design. While ceramic insulators made of inorganic materials are not prone to appreciable degradation with age, insulators with Hydrophobicity Transfer Material (HTM) characteristics made, fully or partially, of organic materials are relatively more prone to degradation while ageing, especially under extreme severe environments. This degradation may manifest as a loss of hydrophobicity, surface tracking and erosion that impact electrical performance [10].

Superhydrophobic RTV SR coatings are now under development and have been reviewed by Arshad et al [11]. The superhydrophobic coatings' pollution performance seems promising in reducing the risk of pollution build up on insulators, especially for use on glass cap-and-pin disc insulators. Recent innovative work for enhancing hydrophobic properties of silicone coating is currently concentrating on using fillers to achieve superhydrophobic properties [12 - 27]. When the static contact angle is greater than 150° the surface is described to be superhydrophobic. A sliding angle typically less than 10°, will present self-cleaning ability, giving rise to the behaviour known as "Lotus effect" [12 - 13]. In order to obtain a superhydrophobic surface showing the "Lotus effect" it is necessary to combine two approaches: a low surface energy material and a suitable surface topography with micro and/or nanostructures [14]. Advanced chemical materials and nanotechnology are often important to achieve a "responsive" superhydrophobic surface.

A silicone coating was enhanced with a filler in a previous study which provided initial contact angles above 150° [10]. An insulator was coated with this enhanced silicone material and has been installed for long term evaluation at different test stations. The tested solution under consideration had no apparent benefit and no performance of the superhydrophobic coating was found. Measured leakage currents did not show any major difference, when compared to conventional silicone coatings. The superhydrophobic characteristics tended to disappear as confirmed by the contact angle observed before installation and after three years at the test stations (Martigues, France, coastal and industrial) [10].

Now with the development of wide-scale applicability including facile synthesis and high yield, graphene is ready to be used for practical application in the preparation of polymer nanocomposites [28]. Thus far little research has been done to explore the coating based on graphene nanosheets and silicone rubber.

Research is ongoing to explore solutions able to maintain advantages of superhydrophobicity in long term. Therefore, will the partial hydrophobicity transfer characteristics of the RTV SR coated insulator will be compared with the full hydrophobicity transfer characteristics enhancement when adding graphene into the silicone rubber host for this project. If superhydrophobic coatings when applied to ceramic insulators are proven to be successful, the impact of its use within Eskom and the Southern African power industry will significantly improve the insulation performance and reliability of the power network.

The work that is performed with the MTR can place Eskom in the forefront of research in high voltage insulators. More insight will be achieved in the testing of high voltage insulators and could lead to improved design and selection of insulators for the distribution and transmission networks. Lastly, the reliability and performance of the Eskom network can be improved by reducing the figures of the System Average Interruption Duration Index (SAIDI), System Average Interruption Frequency Index (SAIFI) and transmission system minutes.

1.3 Research Aims and Objectives

- Conduct a comprehensive literature review on insulator RTV SR coatings. Answer questions for e.g., what is the state of current insulator technology; what are the main causes for insulator pollution flashover?

- Conduct a literature review on existing ceramic and polymeric insulator indoor and outdoor pollution test theories. Answer questions for e.g., how are HTM insulators pollution performance obtained and which test methods are commonly utilized?

- Conduct a literature review on existing silicone hydrophobic and superhydrophobic coatings' preparation, application and characterization. Answer questions for e.g., how is the hydrophobicity level measured; what are superhydrophobic coatings?

- Conduct a literature review on existing graphene doped polymer matrixes. Understand preparation, application and characterization. Answer questions for e.g., what is graphene and the polymer matrix.

- Conduct actual erosion and tracking tests using the IPT for different coated porcelain tiles with fixed Specific Creepage Lengths (SCLs) under HVAC and HVDC excitation.

- Complete the final MTR and power source design for manufacturing where 30 insulators' outdoor pollution performance is compared by means of leakage current and environmental data as well as visual observations.

- Understanding, quantifying and proposing recommendations for the pollution performance, erosion and tracking of the graphene doped RTV SR coatings when applied to ceramic insulator materials.

1.4 Hypothesis

Graphene, with its exceptional electrical and mechanical properties, has the potential to enhance the performance of RTV SR coatings. By doping graphene into the coating material, it is expected to improve the pollution performance properties when compared to traditional RTV SR coatings used on ceramic insulators.

The pollution flashover voltage is a critical parameter that determines the insulation performance of ceramic insulators in polluted environments. The hypothesis suggests that the incorporation of graphene can enhance the pollution flashover voltage, making the coated insulators more resistant to flashovers caused by pollution deposits.

Comparing the graphene-doped RTV SR coatings to standard or conventional RTV SR-coated ceramic insulators will provide a benchmark for evaluating the enhancements achieved through graphene doping. It is expected that the graphene-doped coatings will demonstrate good pollution performance properties, highlighting the potential benefits of this innovative approach in insulator design.

1.5 Research Question

What is the optimal dispersion concentration of PG and NPG filler in a RTV SR host to achieve significant improvements in pollution performance and electrical properties comparable to those of superhydrophobic coatings on AC high-voltage ceramic insulator materials?

1.6 Research Scope and Limitations of the Investigation

Due to budget constraints for a 100 kV container test supply circuit and a salt and clean fog chamber, it was decided that the old KIPTS insulator test facility's equipment, must be used in this project to finalise the outdoor insulation pollution MTR design to be used for calibration of the New KIPTS site.

While the MTR is being designed, non-expensive and existing equipment is needed to conduct pre-practical screening tests which can gather valuable data for graphene doped SR RTV coatings before being implemented on the MTR. Finally, it was decided that surface resistivity,

hydrophobicity, hydrophobicity transfer tests and IPT tests will be used to produce the first round of pollution performance and electrical test results of the PG/NPG doped RTV SR material.

1.7 Report Outline

Chapter 1: Introduction

In this chapter, the background of the research is discussed, highlighting the importance of the study and the motivation behind it. The research aims and objectives are stated, along with the hypothesis and research questions. The scope of the investigation and its limitations are outlined, providing an overview of what will be covered in the study.

Chapter 2: Literature Review

This chapter begins with an introduction to the topic and then delves into the evolution of insulating materials. The natural/outdoor pollution theory is explored, including pollution sources, deposits, classification, critical wetting, and environmental considerations. The pollution flashover process and the operational performance of insulators are discussed, focusing on flashover modes and common electrical factors affecting insulators. Hydrophobic coatings are examined, including the basic chemical structure, components, thickness, and application methods of RTV SR coatings. The definition and preparation of superhydrophobic coatings are presented, along with a review of existing studies on graphene doped RTV SR and epoxy resin.

Chapter 3: Research Methodology

This chapter introduces the research methodology. The baseline data of the experimental test samples is given. Five methods are presented for conducting various tests: surface resistivity tests, insulator surface wettability/hydrophobicity tests, hydrophobicity transfer tests, tracking and erosion resistance tests, and outdoor/mobile test rig tests. Each method is described in detail, including overviews, specific procedures, and evaluation criteria.

Chapter 4: Coating Batch 1: Experimental Test Results for PG and NPG Doped RTV SR

This chapter focuses on the experimental test results for the first coating Batch. The background of the study is provided, followed by insulation resistance tests and hydrophobicity tests. Static contact angle measurements and wettability class measurements are discussed as part of the hydrophobicity tests. Hydrophobicity transfer tests and tracking and erosion resistance tests are also conducted and their results are presented. Finally, the chapter concludes with a summary and conclusion based on the findings.

Chapter 5: Coating Batch 2: Experimental Test Results for NPG Doped RTV SR

In this chapter, the experimental test results for the second coating Batch are presented. The background of the study is provided, followed by surface resistivity tests and hydrophobicity tests. Static contact angle measurements and wettability class measurements are discussed as part of the hydrophobicity tests. Hydrophobicity recovery and transfer tests are conducted, and their results are analyzed and discussed. Tracking and erosion resistance tests are performed, with visual

observations and measurements, and the results are discussed. The chapter concludes with a discussion of the results and their implications.

Chapter 6: Conclusion and Recommendations

The final chapter provides a conclusion based on the overall findings of the study. The main conclusions drawn from the research are summarised. Recommendations are provided based on the results and limitations of the study. Future work suggestions are also presented, highlighting areas for further research and exploration.

---

2. LITERATURE REVIEW

2.1 Introduction

As society ever increasingly becomes more dependent on a continuous supply of electrical energy, the cost and reliability of each component in the electricity supply system must be taken into consideration [29]. Power line/substation insulation integrity plays an important role during the transmission of reliable and safe electrical energy.

During service conditions, outdoor high voltage insulators must not only be capable of accommodating high electrical stresses, but also withstand, often severe, environmental effects and therefore it is important to understand the durability performance of a hydrophobic coating against these stresses [30]. A three-tier approach is proposed in [11] for evaluating the performance of advanced/modified coatings, as shown in Figure 1.

- **Tier 1:** Small scale testing of coated samples by applying a single stress.
- **Tier 2:** Laboratory testing of realistic samples of conductors or insulators by applying a specific number of stresses.
- **Tier 3:** Involves a field demonstration at utility stages. In this case real samples are exposed to field conditions for extended period.

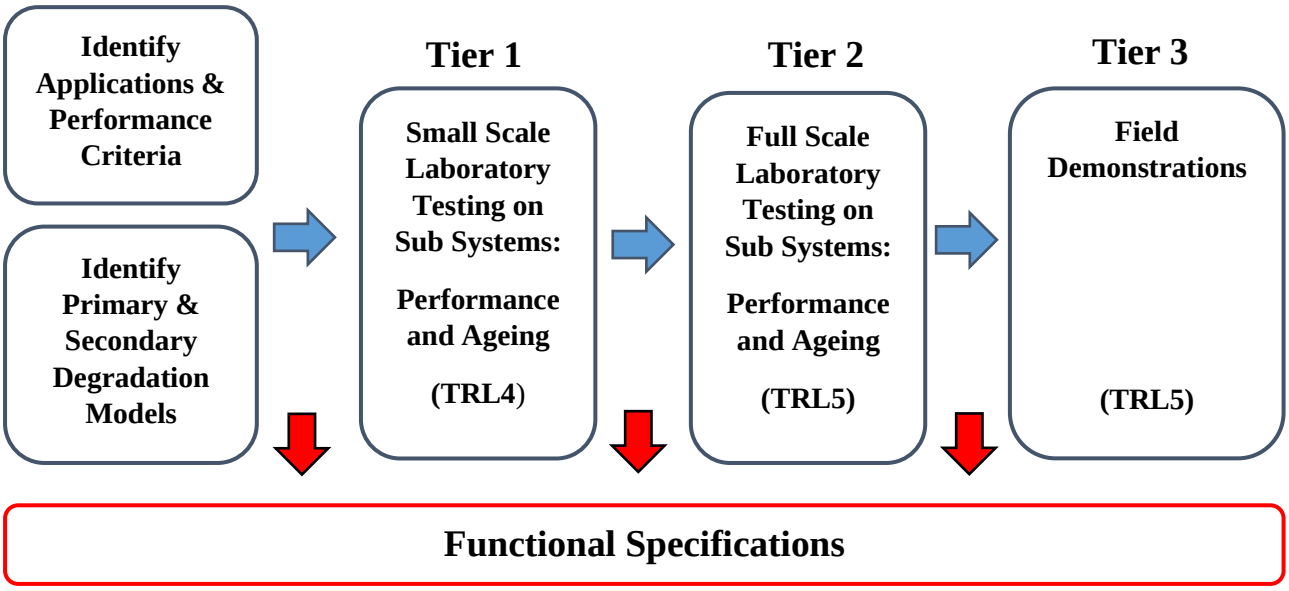

Figure 1: Three-tier approach for testing of functional specifications.

Tier 1 to 3 forms the basis of the research methodology experimental test methods used in Chapter 3. Consideration of the type and characteristics properties of insulators to maintain electrical performance in harsh environments is challenging [11]. However, the International Electrotechnical Commission (IEC) and International Council on Large Electrical Systems (CIGRE) developed an extensive series of test techniques and standards to ensure the compliance

of modern insulators with the recent requirements of electrical networks. These requirements and standards are written by technical experts both from manufacturers and users [31].

2.2 Evolution of Insulating Materials

Since 1880 the power line insulator had many different designs with various concepts and a few fundamental properties which are still valid today. Refinement and development of the modern insulator mainly orbited around its mechanical strength- and electrical performance properties [30].

The first-generation ceramics (glass and porcelain) dominated the insulator market for decades as the preferred outdoor insulation material [30]. These low-cost ceramic materials provided insulators with years of service experience and intensive research led to good understanding of the failure mechanisms involved. However, the reliability of insulation remained unacceptably low in severe polluted areas and where long-term pollution build-up is present over a period of years, e.g., industrial and marine environments [29].

The level of demand for electric power continued to grow and led to the development of a second-generation insulation material manufactured from synthetic polymers. Polymeric materials demonstrated improved flashover performances in highly polluted areas compared to ceramic materials and were easy to produce [32]. Figure 2 below shows the basic evolution of characteristic properties for ceramic- and polymeric insulation materials.

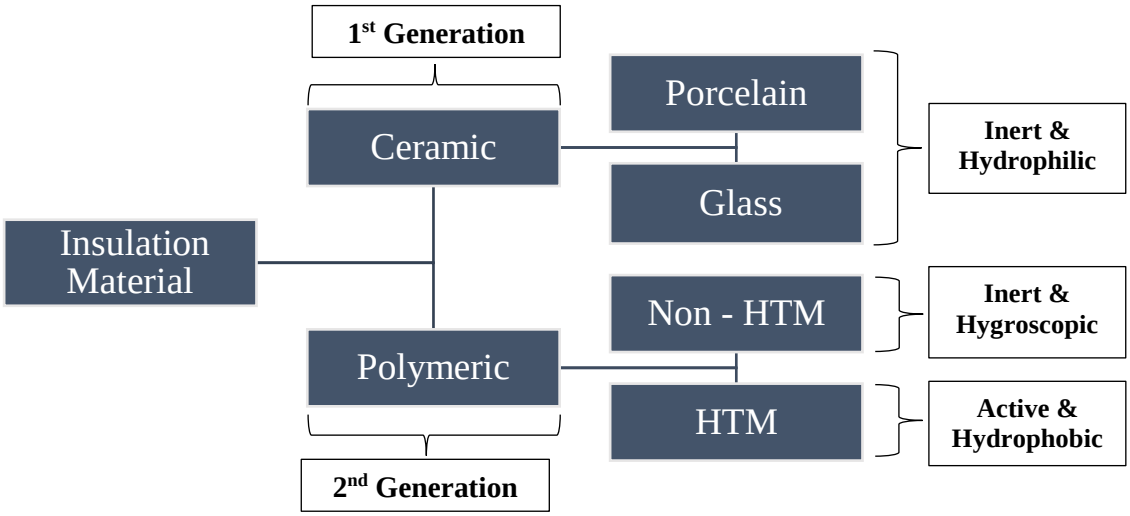

Figure 2: The basic evolution of characteristic properties for insulation materials.

In Dr. W.L. Vosloo's PhD thesis on high-voltage insulator materials, it was found that silicone polymeric material's hydrophobic behaviour differs from that of hydrophilic porcelain material [8]. The stable surface of porcelain does not react with electrolytic pollution layers, maintaining a consistent surface area (A_{pol}) for current flow, as shown in Figure 3 (a). Ceramic insulation materials are described as inert, lacking hydrophobicity diffusion or mechanism. Furthermore, the author explains that the difference in the pollution layer resistivity (ρ) of a hydrophobic silicone polymeric insulation material surface is changed by the LMW silicone partially migrating into the pollution

layer. Therefore, surface area available for current to flow reduces due to an increase in surface resistivity as illustrated in Figure 3 (b) below. Hydrophobic silicone polymeric materials are thus described as active HTM materials which interact with the electrolytic pollution layer. This phenomenon promotes sustained hydrophobicity, even in the presence of pollution and is called pollution encapsulation [8].

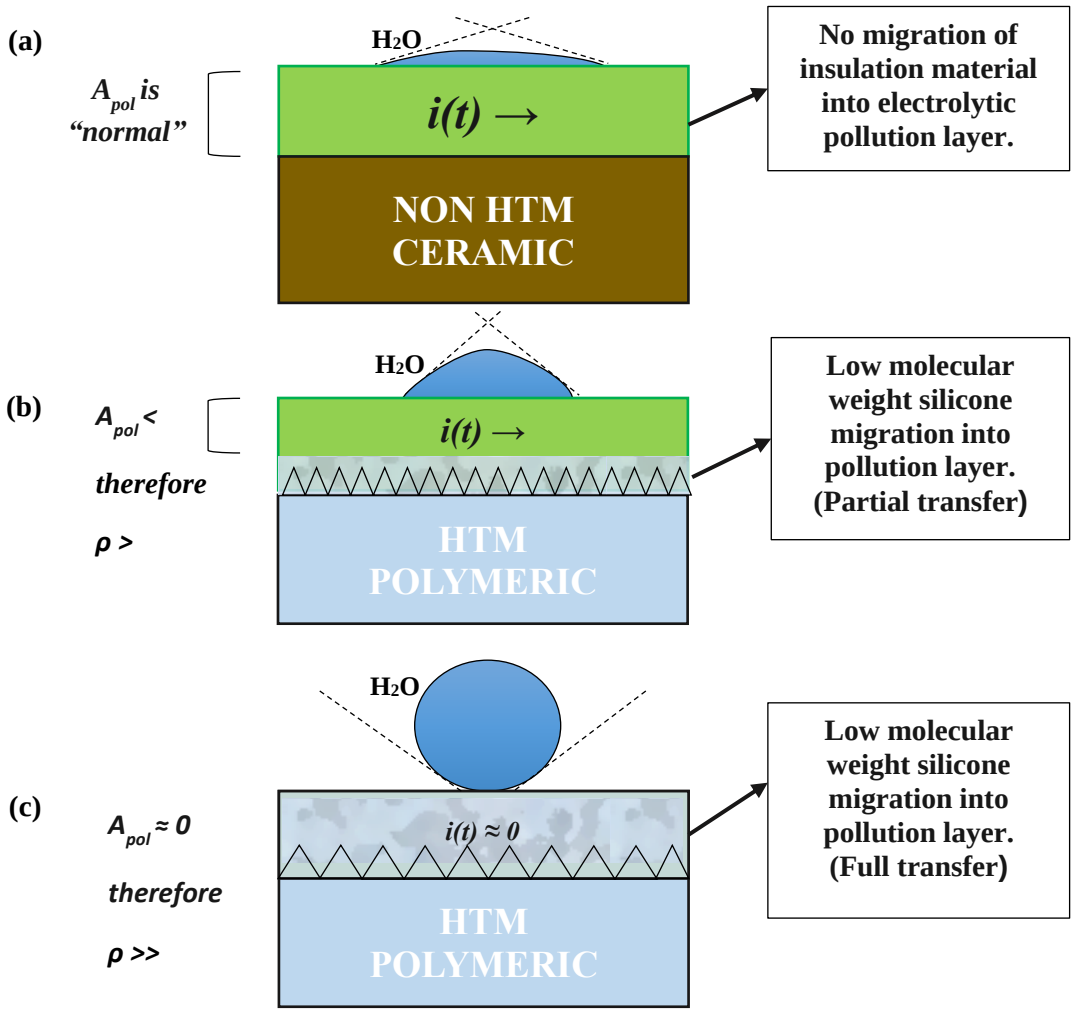

Figure 3: Schematic diagram representing an electrolytic pollution layer with leakage current *i(t)* on a (a) hydrophilic- (e.g., ceramics), (b) hydrophobic silicone polymer- (e.g., RTV SR coating) (partially recovered) and (c) hydrophobic silicone polymer (fully recovered)

Hydrophobic polymer rubbers' unique property of recovering to a hydrophobic surface after pollution deposition presents a clear advantage to the ceramic insulators. However, the hydrophobicity of polymer-based insulators may be lost under repeated environment stresses and their behaviour develops to the same as that for hydrophilic materials [29].

2.3 Natural/Outdoor Pollution Theory

This section briefly covers the widely adopted theory applicable to quantify natural/outdoor pollution on insulators. The section starts by looking at pollution sources and deposits, it continues by discussing the classification of pollution, critical wetting's role in pollution flashover and ends off with environmental considerations for outdoor tests.

2.3.1 Pollution sources and deposits

A pollution source is defined as a source that emits a substance into the atmosphere. The pollution experienced in an insulator's surrounding area is obtained from the effect that the emissions have on that specific area [33].

Two main types of pollution processes, namely pre-deposited (Type-A)- and instantaneous pollution (Type-B) are quantified. Described briefly: Time passes and pre-deposited pollution forms on the insulator. The sources of this pollution pre-deposit are sea salt, industrial products (soluble salts), road salts, bird excrement or desert sands etc. Electrostatic attraction of charged particles along with gravity and the aerodynamic catch of the insulator causes the solution to evidently deposit onto the insulator's surfaces. After a while the insulator is wetted by a natural cause (rain, fog etc.) and forms an instantaneous conducting electrolyte (Type-A), where instantaneous pollution (Type-B) is already a conducting electrolyte (coastal salt fog, crop spraying etc.).

Figure 4 illustrates the principal process by which insulator surfaces are contaminated, also known as Aerodynamic catch [29]. Particles with different densities will flow around the insulator and separate from each other. The heavier particles, such as sand, will be deposited on the leading side, while the lighter particles, such as air, will follow the air current more closely. In other words, the lighter particles will be deposited on the side of the insulator where the air flow's direction is steep.

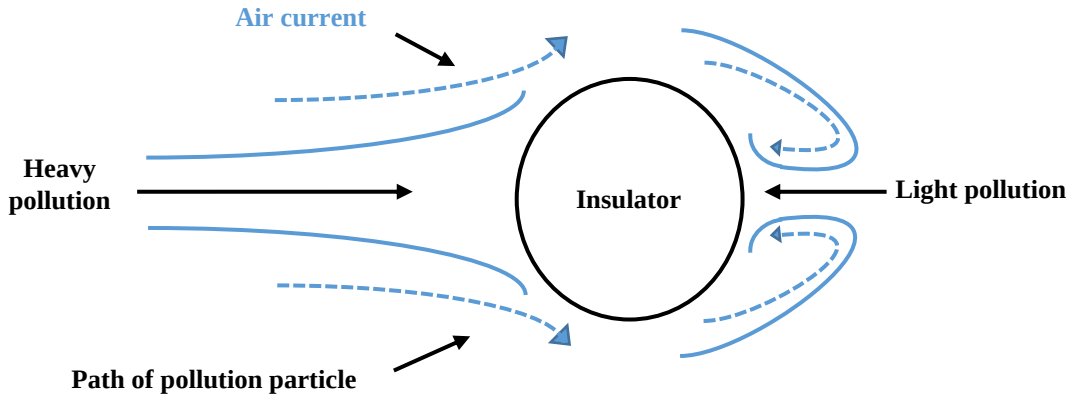

Figure 4: Pollution deposit illustration by aerodynamic action.

2.3.2 Classification of pollution

Two main types of insulator pollution can lead to an insulator flashover as explained earlier. Both Type-A and B pollution types are described further below.

2.3.2.1 Type-A pollution

Type-A pollution is most often associated with inland, desert or industrially polluted areas. A dry salt layer builds up and then eventually becomes wetted by dew, mist, fog or drizzle. Two main components exist; soluble (active) pollution which forms a conductive layer while non-soluble (inert) pollution forms a binding layer for the soluble pollution layer. Non-soluble pollution therefore contributes to the area available for leakage current [6]. Pre-deposited soluble pollution is measured in terms of conductivity (mg/cm^2), while non-soluble pollution is measured in terms of mass (mg) [30].

- *Soluble Pollution (Active)*

Soluble pollution is subdivided into categories of salts which dissolves quickly and hardly in water. Soluble pollution is measured in terms of an equivalent salt deposit density (ESDD) in mg/cm^{2,} and the following examples are given in Table ***1***.

Table 1: Soluble pollution categories and examples [34].

Soluble Pollution Category	Example
Conductive pollution	Metallic dust
High solubility salts	Sodium Chloride (NaCl), Magnesium Dichloride ($MgCl_2$), Sodium Sulphate ($NaSO_4$)
Low solubility salts	Gypsum, fly ash and cement

$$ESDD = \frac{S_a \cdot V_d}{A_{ins}} \quad (1)$$

S_a: Salinity of the water and salt solution at 20°C [kg/m^3]

V_d: Volume of distilled water used [cm^3]

A_{ins}: Area of washed/sampled insulator [cm^3]

- *Non-soluble Pollution (Inert)*

Non-soluble pollution consists of dust, and, clay, oils etc. Non-soluble pollution is measured in terms of non-soluble deposit density (NSDD) in mg/cm^2. Note that this pollution type may also include metallic conductive particles. Non-soluble pollution has the following examples given in Table 2.

Table 2: Non-soluble pollution categories and examples [34].

Non-Soluble Pollution Category	Example
Hydrophilic pollution	Kaolin, cement, clay, SiO_2 , etc.
Hydrophobic pollution	Silicone grease, oil, etc.

The water and salt solution from the ESDD measurements is used to perform the NSDD measurement afterwards. The liquid is filtered through a pre-dried, clean and weighed filter paper of grade GF/A 1,6 µm or similar, then the contaminated filter paper is dried and weighed [6]. The NSDD value is calculated using:

$$NSDD = \frac{M_2 - M_1}{A_{ins}} \quad (2)$$

M_1: Weight of dry clean filter paper [mg]

M_2: Weight of dry contaminated filter paper [mg]

2.3.2.2 Type-B pollution

Type-B pollution is when an insulator changes from an acceptably clean, low conductive state to flashover in a short time (< 1 hour) and then returns to a low conductive state when the event has passed [30]. The instantaneous events can be detected by surface conductance or leakage current measurements. Coastal areas are most often associated with Type-B pollution environments and a salty fog is usually deposited onto the insulator surface. Crop spraying, chemical mists and acid rain from agricultural and industrial emissions respectively are also examples of pollution which contain quick dissolving salts.

2.3.2.3 Site severity classes vs ESDD

Five classes of Site Pollution Severity (SPS) classes are qualitatively defined, from very light pollution to very heavy pollution. For Type-A pollution, the ESDD/NSDD values corresponding to each SPS class is shown in Figure 5 below for the reference cap-and-pin insulator [34].

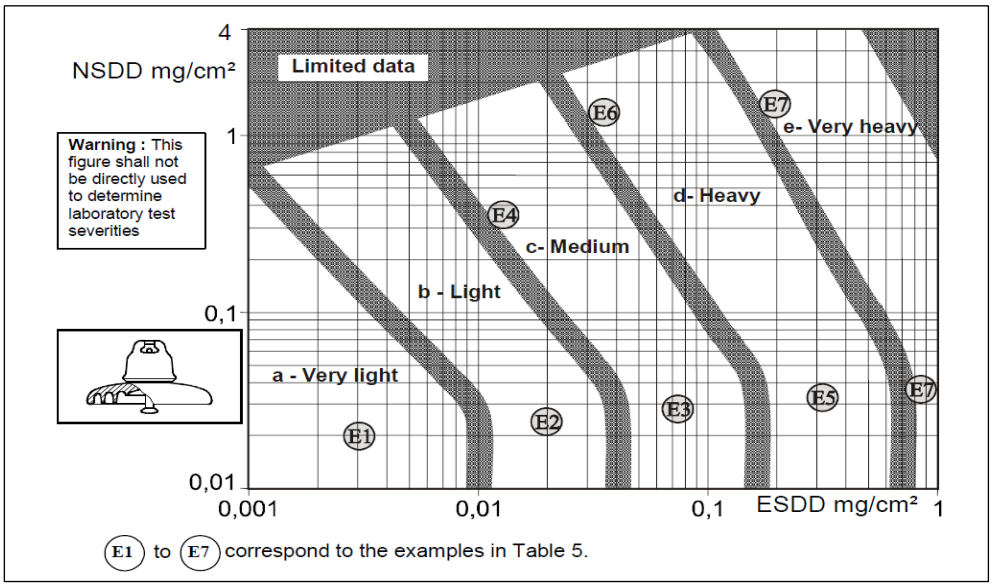

Figure 5: Type A pollution severity - Relation between ESDD/NSDD and SPS for the reference cap and pin insulator [34].

A measured NSDD value of above 2 mg/cm^2 requires an increase by one level for the site severity class [34]. The site severity class should be increased by one level if a high NSDD is expected, e.g., if the insulator is in the vicinity of a cement factory [34]. The relationship between the respective pollution severity classes and the ESDD value over a period of a year is given by

Table ***3*** and contain maximum values from regular field measurements were taken for the reference cap-and-pin insulator.

Table 3*:* ESDD in relation to site severity class [34].

Surface Deposit Index, ESDD [mg/cm^2 monthly maximum]	**Pollution Severity Class**	
V < 0.06	I	Light
0.06 – 0.12	II	Medium
> 0.12 – 0.24	III	Heavy
> 0.24	IV	Very Heavy

2.3.3 Critical wetting

Pollution flashover most likely occurs due to conductivity of the pollution surface under critical wetting. When the highest surface conductivity is reached, critical wetting occurs. A wetting rate is considered critical whenever the pollution layer is wetted completely such that a pollution flashover is likely to occur. Furthermore, the wetting rate is also considered critical when the pollution layer is not completely wiped away from the insulator surface. Critical wetting rates for the various pollution types can be described as shown in Table 4 [34].

Table 4: Soluble and non-soluble pollution's critical wetting rates [34].

Pollution Category	**Critical Wetting Rates**
Conductive pollution	Wetting is always critical.
High solubility salts	Wetting is critical for a low wetting rate, e.g., mist, dew or light rain.
Low solubility salts	The wetting is critical under high wetting rate such as heavy rain.
Hydrophilic solution	Enhances pollution wetting.
Hydrophobic pollution	Inhibits pollution wetting.

2.3.4 Environmental considerations

The typical pollution environments are greatly influenced by weather conditions such as temperature, humidity, rain, fog, wind, solar radiation, snow and ice, lightning and air density. Therefore, weather conditions have a significant impact on the electrical and/or mechanical performance of HV insulators [30]. There are a number of environment factors that affect the performance of HV insulators and are summarized as follows [34]:

- The speed and direction of the wind, precipitation (rain), relative humidity and the position of the pollution sources all determine the final pollution deposits on an insulator surface. Therefore, the environment type and location plays a major role in insulator pollution flashover.

- Ultraviolet solar radiation can cause chalking, crazing, and cracking on the ageing of non-ceramic materials.

- The direction and speed of the wind temperature, ice and snow can influence the mechanical forces on an insulator.

- Lightning activity, soil resistivity and mining activity can affect the insulator flashover performance.

2.4 The Pollution Flashover Process

The pollution flashover process for insulators with a hydrophilic surface is described in CIGRE Electra publication No.64 [35] and is summarised as follows:

i. Insulator becomes coated with a layer of pollution with soluble salts/dilute acids/ alkalis. Wetting process is necessary if pollution is non-conducting and dry in order for flashover to occur.
ii. The surface is either wetted completely or partially by fog, mist, light rain, sleet, melting snow or ice and causes the pollution layer to become conductive.
iii. A leakage current starts to flow and generates heat effects which starts to dry out parts of the insulator.
iv. Non-uniform drying causes the conducting pollution layer to form broken bands and interrupts flow of leakage current.
v. The line-to-earth voltage applied across these small dry bands, causes air breakdowns to occur and DBA starts to bridge each other in the form of leakage current surges/arcs.
vi. If the resistance of the undried part is low enough, the arc can burn continuously and span the insulator entire surface.

The pollution flashover process is a combination of interactions between the insulator, pollutants, wetting conditions, and applied voltage [31]. An example of this is presented in Figure 6.

Figure 6: High voltage pollution flashover on glass cap-and-pin insulator [36].

From the pollution flashover process it has been explained, in the previous section, that the flashover probability becomes very high if the insulator leakage current approaches a certain threshold value. The value can be defined as the highest peak (I_{max}) of leakage current that is recorded during a given time period on an insulator continuously energised at its service voltage. It has been considered as a suitable parameter to indicate how close a glass or porcelain insulator is to flashover [30]:

$$I_{max} = \left(\frac{SCL}{15.32}\right)^2 \ [mA] \ (3)$$

with Specific Creepage Length (SCL) given. Small currents in the order of several mA can cause severe damage to non–ceramic insulating materials [30]. This leads to electrical and/or mechanical breakdown of the insulator.

The main factor which influences insulator leakage current magnitude is the surface layer resistance (R_{pol}) for the idealised case of a uniform electrolytic pollution layer. Dividing the surface electrolytic pollution layer into small sections dl along the insulator creepage distance as shown in Figure 7.

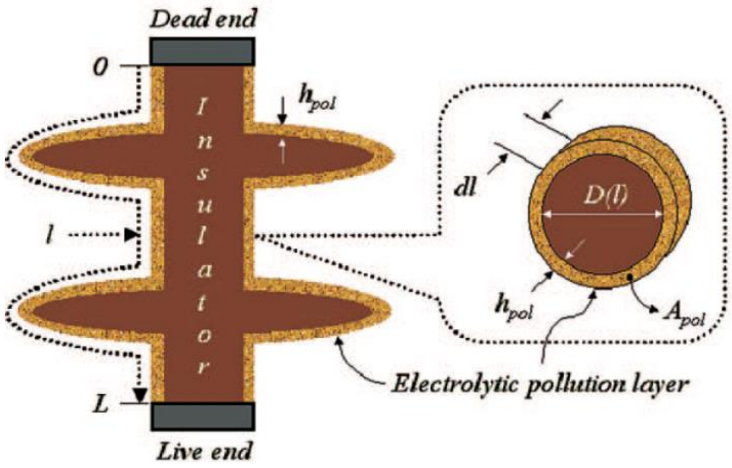

Figure 7: Visual representation of the electrolytic pollution layer leakage current parameters [30].

Below, the following basic surface resistance formula of a uniform electrolytic pollution layer on the insulator surface is obtained [30]:

$$R_{pol} = \left(\frac{\rho_{pol} \cdot l}{A_{pol}}\right)^2 \approx R_{c\,[at\,V_c]}\,[M\Omega]\ (4)$$

dl [mm] denotes the diameter at position (*l*) along the insulator creepage length and h_{pol} [mm] denotes the thickness of the uniform electrolytic pollution layer (see Figure 7).

When the insulator surface resistance reaches a critical low value, the critical flashover voltage [kV] proposed by Rizk and modified by Holtzhausen is given by the following formula [30]:

$$V_c = k_1 \times 10^{-3} \times \left(\frac{R_c \times 10^6}{l}\right)^{k_2} \times l\ [kV_{peak}],\ (5)$$

where R_c denotes the critical insulator resistance. The critical insulator flashover voltage V_c is directly proportional to the critical resistance of the insulator (R_c), which is the same as the value of the surface resistance of the pollution layer (R_{pol} at V_c). Constants k_1 and k_2 are given by [30]:

- $k_1 = 7.6$
- $k_2 = 0.35$

Finally, the equation of R_{pol} shows that the surface layer resistance of an insulator is directly proportional to the total creepage distance. Therefore, the power frequency pollution flashover performance of an insulator can be improved by increasing the total SCL [30]. Note that dry band arc resistances are ignored for these equations.

2.5 Operational Performance of Insulators

2.5.1 Flashover modes

Whenever a conducting electrolyte pollution layer is present on an insulator surface, the applied voltage can significantly reduce by order of magnitude. A hydrophilic surface (ceramic insulators) will wet out completely and be covered with an electrolytic film. In contrast, hydrophobic materials, such as RTV SR, the water droplets beads into separate small droplets preventing the formation of a continuous conductive layer [31]. Different flashover modes are described below.

2.5.1.1 Power frequency flashover

The insulator, under both dry and wet conditions, must withstand a (1) power frequency operating voltage (U_n) and an (2) overvoltage (U_m). The arcing distance has a significant effect on the dry and wet power frequency flashover voltage test [30]. When a conducting electrolytic pollution layer is present on the insulator surfaces, the power frequency flashover voltage is reduced.

Each sample insulator is subjected to a voltage equal to 80% of the average flashover value of the reference insulator after a Rotating Dipping Wheel Test (RDWT). The voltage will be maintained for 30 minutes. The temperature rise of the shank of each insulator (measured immediately after the test) shall not exceed 20 °C [37]. The insulator must also withstand the pollution condition to which it is subjected.

2.5.1.2 Lightning and switching impulse flashover

The insulator must withstand dry lightning and the wet switching impulse overvoltage flashovers. Switching impulses typically do not cause flashover for ≤300 kV system voltages and therefore only (1) lightning impulse flashover tests are the main consideration for lower system voltages, i.e., ≤ 300 kV.

While (2) switching impulse flashover is the main consideration for system voltages of ≥ 300 kV. For large air gaps, the streamer or leader breakdown mechanisms operate such that the switching impulse has more time to bridge the gap [30]. The magnitude of the switching impulse is related to the system voltage and the magnitude of lightning impulses depends on the severity of the lightning, as well as the quality of the grounding of the towers.

2.5.2 Common electrical factors affecting insulators

2.5.2.1 Corona discharges

A potential gradient is formed between conductor surfaces when voltage is applied between two different poles. Under the influence of the potential gradient, the free electrons in the air acquire greater velocities sufficient to strike a neutral molecule with

enough force to dislodge one or more electrons from it. The collision produces another ion and one or more free electrons cumulatively ionizes the air outside and finally conducts due to the flow of these ions. Therefore, electric discharges, corona, start to occur around the conductors giving rise to a faint luminescent glow, along with the hissing sound accompanied by the liberation of ozone, which is readily identified due to its characteristic odour [38]. An example of corona activity is given in Figure 8.

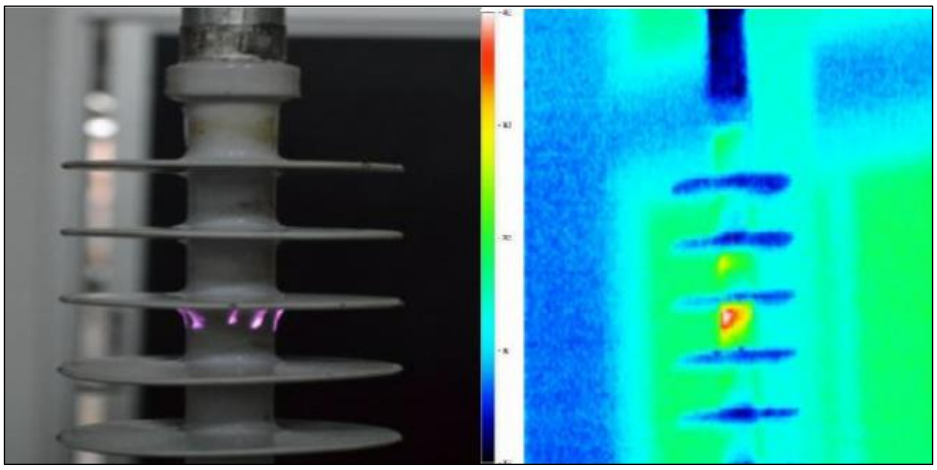

Figure 8: Partial corona discharge and dry band arcing during tracking and erosion test. Thermal image on the right-hand side [39].

Corona also generates ultraviolet radiation, ozone, and acids (in the presence of moisture). These are environmentally unacceptable and have a negative effect on polymeric insulating materials. In order to prevent corona discharges, live-end corona rings are applied for system voltages greater than 200 kV [30].

2.5.2.2 Resistance to power arc damage

The insulator, including other HV equipment, cables, terminations, must be able to withstand the current associated with the system under flashover conditions [30]. In order to compensate for thermal shock that could lead to mechanical failure, it is recommended to use arcing horns or rings on long rod insulators to divert the arc away from the insulating material.

2.5.2.3 Instantaneous- or rapid conductive fog flashover

When flashover occurs within a short period of time (<1 hour), then the flashover mode is described as an instantaneous/rapid pollution event. The clean insulator went from a low conductive state to a high conductive state after being contaminated with conductive fog, and then returned to a low conductive state after the event. Liquid electrolytes such as salt spray, salt fog or industrial acid fog forms the conductive fog layer. Coastal and chemical plant areas mostly experience this type of rapid conductive fog flashover events. Hydrophobic insulator surfaces are therefore recommended for HV electrical insulation in coastal areas [34]. A bird streamer flashover is also classified as an instantaneous pollution flashover event as described above. Bird excrement over an insulator string forms a

continuous conductive stream, which causes the length of the air gap to be reduced, and therefore leading to flashover [30]. Bird guards are used to deter birds from transmission tower to prevent bird stream flashover.

2.5.2.4 Voltage transfer

The highest electrical stress is located on the live end of the insulator under clean and dry conditions as shown in Figure 9 (a) below. When the insulator becomes polluted and wetted, the voltage is distributed over the surface of the insulator in areas where the smallest radius of curvature exists e.g., the shed tips, Figure 9 (b). Over time a dry band forms and most of the stress in transferred to the dry region as shown in Figure 9 (c) [31].

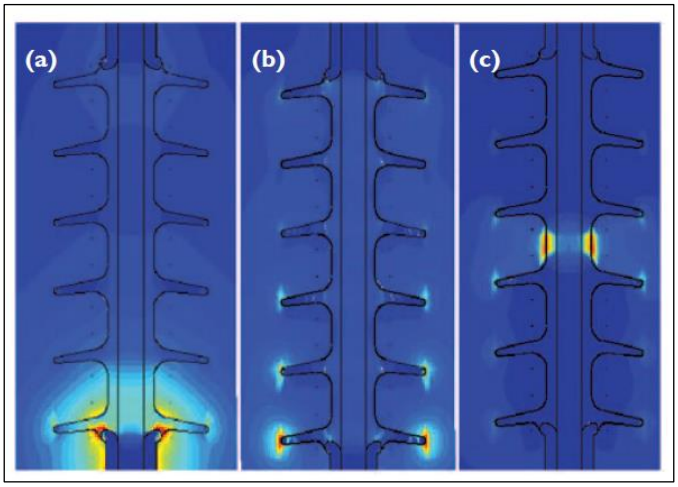

Figure 9: Electric field simulations of insulators: (a) clean and dry; (b) evenly polluted and wet; and (c) evenly polluted and wet with dry band. (Red = Highest Electrical Stress) [31].

2.5.2.5 Tracking and erosion activity

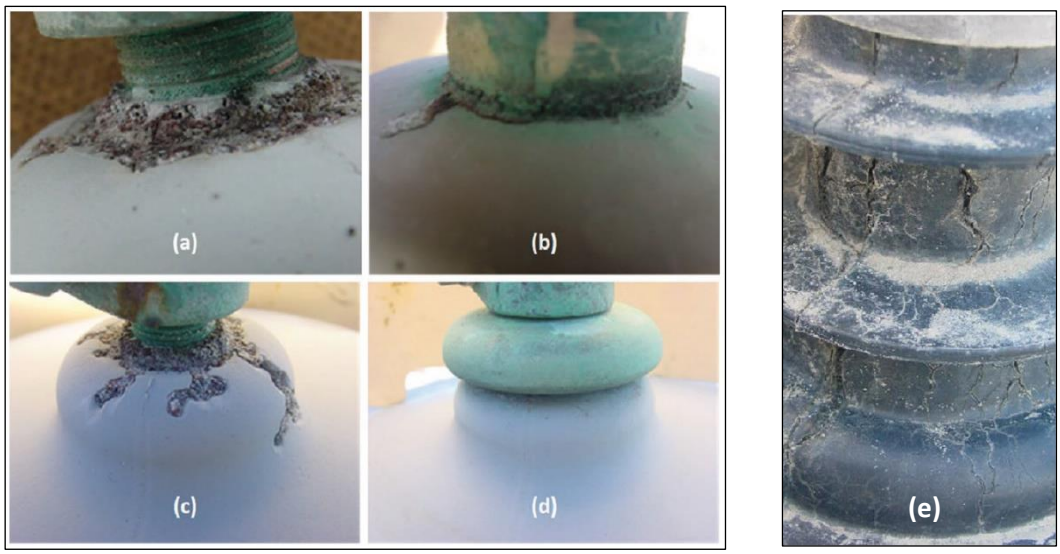

Figure 10: Insulator failures: Severe localized material erosion at the metal to insulating material interfaces (a), (b) and (c). A stress release designed solution was applied by the manufacturer to a previously non-energised pole of the same unit shown in (d) - the result showing that the solution was working well after being energised and exposed to natural ageing as can be seen in (d), (e) Severe erosion and tracking observed on insulator product [9].

Environmental stress as well as electrical discharges causes tracking and erosion during wetting events. A tracking path/erosion of material reduces the SCL of the insulator and may cause the insulator to flashover in the conditions described earlier. Insulator materials' properties determine the outcome of the tracking and erosion activity that occurred on the insulator's surface. Examples of tracking and erosion activity near the metal interface on in-service insulators is shown in Figure 10.

2.6 Hydrophobic Coatings

This section focusses on Silicone Rubber (SR) which is the prevalent product of choice to lend a ceramic insulator surface the requisite HTM properties. Other materials with enhanced performance displaying superhydrophobic characteristics are still under investigation and are not yet ready for wider field adoption [10]. The preparation and characterization of graphene doped RTV SR and epoxy resin are elaborated in Sections 2.6 and 2.7. First, the basic chemical structure existing service experience, alternatives are investigated for a RTV SR coating in the sections below.

2.6.1 RTV SR coating's basic chemical structure

Today, RTV SR coatings are applied in a liquid form to ceramic insulators using various techniques to improve the inert material's pollution performance in severe polluted areas [10]. A RTV SR coating is formed by a chemical process called vulcanisation which involves different components dispersed into a solvent that evaporates moisture, thereafter, triggered by air forming a solid rubber layer. Crosslinks are formed between the individual polymer chains and results in a polymeric material which is more elastic or rigid depending on the crosslink density created [10].

Silicone is the base filler material for RTV SR coatings and consists of repeating silicon-oxygen (siloxane) groups with two substituted groups each bonded to the silicone atoms [10]. Typically, substituted groups may be methyl types such as for Polydimethylsiloxane (PDMS) – a type of silicone used in RTV SR coatings, as shown in Figure 11. Silicone polymer formulations exhibit low surface energy that does not allow water to spread out over the surface (hydrophobic) and contains a small but not negligible amount of short-chain, LMW siloxane chains (blue and green circles in Figure 11) which migrates to the materials' surface in the presence of a electrolytic pollution layer as explained earlier (pollution encapsulation).

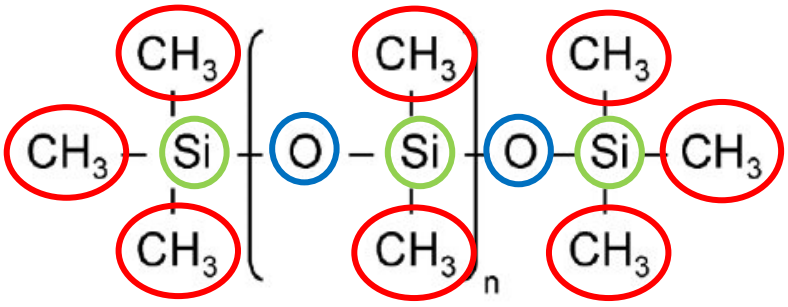

Figure 11: Molecular chemical structure of PDMS, with n = the molecular size. Green: silicon atoms; Blue: oxygen atoms; Red: methyl groups.

Due to the unique chemical structure, silicones demonstrate thermal stability even at elevated temperatures with most silicone elastomers remaining stable and elastic up to 200°C while modified products can withstand temperatures as high as 300°C [40]. The high bonding energy of the silicon to oxygen (Si-O_2) backbone provides stability against breakdown by UV irradiation. The bonding energy of Si-O_2 bonds is 444 kJ/mol. Shortwave sunlight at 300 nm has an energy content of about 6.2×10^{-22} kJ (i.e., 398 kJ/mol) and can therefore not cleave Si-O_2 bond that remains stable [40].

A considerable variation in the electrical and physical properties exist within the different RTV SR coating product's blends/formulations. Variations depend on numerous factors which includes the relative amounts of reinforcing fillers in the coatings, curing components affecting the degree of cross-linkage in the polymer, primers for improving adhesion to the insulator surface and coating thickness. The nature, composition and quantity of the fillers are critical in determining the tracking and erosion resistance properties of RTV SR coatings [10].

Figure 12: Example of RTV SR coating peeling on a porcelain insulation

RTV SR coatings can last for over 20 years depending on the service conditions which can produce excessive contamination, biological growth, excessive electrical and/or environmental stresses. Low-quality RTV SR material and/or poor application thereof can cause a loss of hydrophobicity accompanied by signs of chalking, fading, and peeling [10]. This leads to degradation and premature ageing of the RTV SR coating as seen by the example given in Figure 12.

2.6.2 Other typical components in RTV SR coating blends

By differing proprietary formulations of the RTV SR coatings the electrical and physical properties can be optimized for e.g., arc degradation resistance, adhesion promotion and long-term hydrophobicity. Fillers reinforce the elastic silicone network and help adjust rheological properties. For increased tracking and erosion resistance, various alternative filler materials (,e.g., Alumina Trihydrate (ATH), fumed silica or quartz), are often incorporated in the coating

formulation [10]. The included bonding agent ensures proper adhesion of the coating to the ceramic surface. In the case of some formulations, a bonding agent is not included in the main material, and then a primer may be applied on the substrate prior to the application of the RTV SR coating. RTV SR coating products can also be classified as one-part ready to use coatings and two-part coatings where the accompanying catalyst must be added to the main coating prior to use [10].

Naphtha usually acts as a carrier medium to transfer the RTV SR coating to the insulator surface. The silicone and other components are usually dispersed into a solvent such that the solvent evaporates moisture and the air triggers vulcanization forming a solid rubber layer [10]. The type of solvent, cure system chemistry, temperature and humidity determine the speed at which curing takes place. Note that Naphtha and other flammable solvents are forbidden for use on energized insulators. Solvent-free and water-based RTV Coatings have been experimented with to meet increasingly stringent environmental and safety regulations for live-line application, where a non-flammable solvent is required [10].

2.6.3 RTV SR coating thickness

Thick coatings may provide increased thermal resistance to heat generated from DBA, as found for polluted and wetted insulators, and as such do not allow the heat to be conducted away to the glass or porcelain insulator as quickly as thinner coatings [10]. DBA activity for thicker coatings can result in a higher hot spot temperatures thereby causing thermal degradation of the coating quicker than thinner coatings. However, a very thin coating can also degrade quickly due to wearing from environmental stress. Most manufacturers and utilities recommend thickness in the range of 0.3 mm to 0.5 mm (presently 0.3 to 0.35 mm is adopted) [10]. An example of measuring the RTV SR thickness in-field can be seen in Figure 13.

Figure 13: RTV SR wet film comb thickness measurement observation at a coastal substation near Cape Town.

2.6.4 RTV SR coating's application methods

RTV SR coatings can be applied, manually or automatically, by spraying, brushing or factory dipping to an insulator wholly or partially (normally pin side for cap-and-pin insulators) [10]. Some laboratory tests and published works have indicated that half coated cap-and-pin insulators exhibit comparable performance when compared to fully coated insulators [10]. Station line post insulators, as shown in Figure 14 (a) below, uses the RTV SR application procedure the most, but the uniform application thereof on site can be challenging due to complicated working conditions, e.g. working at heights as shown in Figure 14 (b) and high wind conditions.

Alternative methods for coating application onto glass cap-and-pin strings [10]:

- Glass cap-and-pin insulators have been growing interest to adopt a factory pre-coated insulator solution within expertly controlled curing facilities during the manufacturing phase.
- The coating of discs prior to stringing in the vicinity of the installation site.
- Rotational removal of the insulators in service using live-line techniques. Once removed, the insulators can be coated in a well-equipped, environmentally controlled facility established close by and then be re-installed under live-line maintenance conditions.

A coating layer with excellent quality and finish can provide the following advantages [10]:

- No line outages are necessary.
- Cost advantages with respect to the alternative of removing and discarding the existing insulators and installing new pre-coated units.

Pre-coated insulators are now considered by some utilities worldwide and are mandating the adoption of the viable solutions during the design phase itself [10]. In 2020, around 10 million coated glass cap-and-pin insulator units were expected to be in use, with extrapolated data indicating ten times increase by 2030, bringing the total number of such pre-coated insulators in use to 100 million [10].

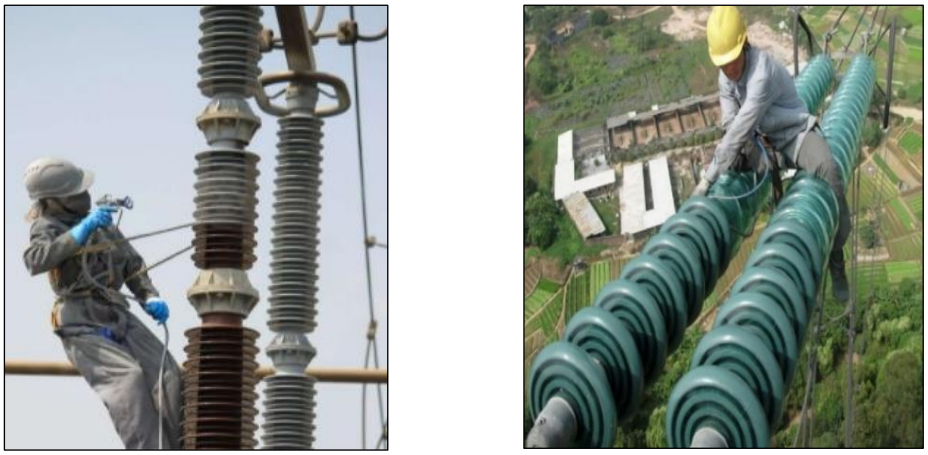

(a) **(b)**

Figure 14: (a) Application of sprayed insulator RTV SR coating on HV station line post insulator [41]. (b) HV glass cap and pin insulator string on the right [10].

2.7 Superhydrophobic Coatings Definition and Preparation

Advanced coatings have been developed the past few decades to ensure better performance of outdoor insulators in highly polluted environments and to reduce the capital cost of transmission infrastructure. Advantages such as low wettability, high thermal- and ultraviolet resistance, self-cleaning, self-healing low ice adhesion strength and delayed freezing time are offered by these advanced coatings [11].

The wettability of a surface depends on the balance of adhesive forces (between liquid and solid surface) and cohesive forces (within liquid) when a water droplet rests on a flat solid surface. Hence, a water contact angle (θ) is formed between the flat solid surface and the water droplet. This contact angle can be described as the tangent angle between the liquid vapour interface at the three-phase boundary as shown in Figure 15 [11].

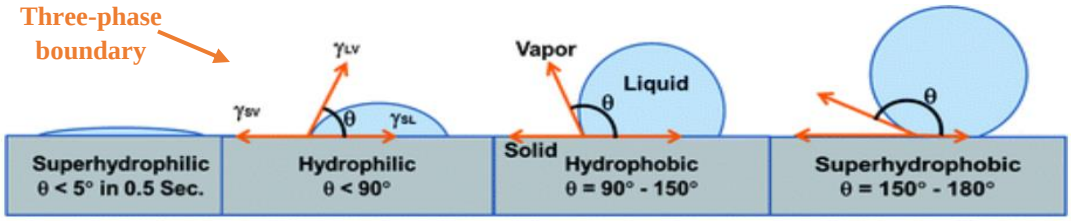

Figure 15: Schematic diagram representing the water contact angle on a superhydrophilic, hydrophilic, hydrophobic and superhydrophobic surface respectively.

Superhydrophobic surfaces offer a contact angle θ > 150˚ and a Contact Angle Hysteresis (CAH) or Sliding Angle (SA) < 10˚ [26]. The superhydrophobic property is being widely developed for industrial applications due to the self-cleaning effect which was inspired by the lotus leaf. A self-cleaning surface repels water and forms water droplets on its surface which will then "sweep off" pollution particles when water droplets roll off the surface when disturbed, referred to as the Lotus effect. Therefore, fabrication of a superhydrophobic surface having self-cleaning properties can effectively address issues associated with contaminated insulator surfaces.

A superhydrophobic surface is fabricated by roughening up the existing low surface energy material by depositing another low surface energy material within the existing material [26]. Silicone rubber is a low surface energy material, and it can be roughened sufficiently to produce a superhydrophobic surface.

Arshad et al [11] presented a detailed review on the properties and applications of superhydrophobic (advanced) coatings in outdoor high voltage insulation. Based on this literature review, the performance of superhydrophobic coatings seem promising in reducing the risk of pollution build up on insulators, especially for use on glass cap-and-pin disc insulators. Furthermore, this review discussed recommendations for electrical tests which can be useful to characterise the electric performance (leakage current, flashover voltage, surface resistance etc.) of superhydrophobic coatings [11]. In conclusion, the paper suggested that more work is needed to standardise tests and procedures (outdoor and laboratory) to evaluate the long-term durability of superhydrophobic coatings.

2.8 Existing Graphene doped RTV SR and Epoxy Resin Studies

Graphene powder is a two-dimensional, atomically thick sheet made up of sp^2 carbon atoms organized in a honeycomb configuration and is ready for practical application in the preparation of polymer nanocomposites which has unique electrical, mechanical, and thermal properties [28]. All the aforementioned properties have been improved significantly when a suitable amount of graphene was dispersed into different polymer hosts such as Polystyrene (PS), Polyurethane (PU), Poly Methyl Methacrylate (PMMA) and Poly Vinyl Alcohol (PVA) [28].

Dong *et al* in [28] studied the incorporation of a low loading of graphene dispersed into a polymeric composite material and obtained a significant enhancement of the mechanical property [28]. Figure 16 shows the acquired Scanning Electron Microscope (SEM) images of the graphene doped polymeric composite with a loading of 1 wt% graphene nanosheets transferred into a polytetrafluoroethylene mould. The images demonstrate that the graphene nanosheets achieved a good random dispersion within the PDMS matrix when the solution-blending method is used [28].

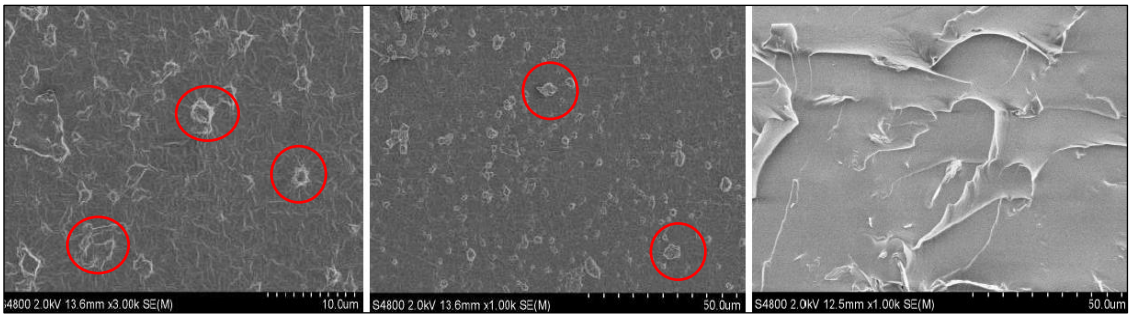

Figure 16: SEM images of graphene/RTV Silicone rubber composite. Red circles indicate graphene aggregates in the PDMS matrix [28].

Furthermore, a corrugated morphology is displayed by the material surface due to (1) the material shrinkage occurring during the crosslinking or (2) the corrugation and scrolling of graphene sheets in the PDMS matrix [28]. The images from Figure 16 also reveals that there are a few graphene aggregates (encircled red) in the PDMS matrix, caused by the weak interaction between graphene nanosheets and the PDMS matrix [28]. This study indicates that more work is required to enhance the interaction between the graphene nanosheets and the PDMS matrix.

In another study J. Zhang et al. [43] The thermal conductivity property of an epoxy resin sample was increased 1.6 times after the addition of 0.1 wt% graphene. J. Zhang et al. [43] describes the reasons that account for the enhancement by incorporating inorganic nanoparticles into a polymer matrix improves the Partial Discharge (PD) resistivity of the polymeric insulation. [43]. When using Ohm's law, the high electric conductivity of inorganic nanoparticles promotes the dissipation of charge and in return reduces the charge induced field (i.e., volume resistivity decreases). Therefore, resulting in a rise of partial discharge inception voltage and then decreases PD intensity for embedded electronics/devices [43].

Contrastingly, conductive pathways are advanced when doping graphene nanoparticles into an epoxy resin matrix, the resin subsequently acts as a scattering site, which excites the electron to

transfer energy and allowing it to transmit energy [43]. Thus, when a graphene filler is used at sites where charge accumulates, the local electric field strength of charged sites decreases due to higher voltages required for PD to take place.

Lastly, J. Zhang et al. [43] results also show that the addition of graphene into an epoxy resin sample increased the contact angle from about 88° to 102°, which indicate an enhancement of the hydrophobicity property.

3. RESEARCH METHODOLOGY

3.1 Introduction

This chapter defines the research methodology developed to test the Pristine Graphene (PG) or Nanoplatelet Graphene (NPG) doped RTV SR coated samples. The experimental investigation methods for each step below given in the research methodology are used to answer the research questions/hypothesis as outlined in Chapter 1. The methods evaluate, filter and characterize the Graphene doped RTV SR coating specimens using a five-step approach as shown in Figure 17. The five-steps together with its applicable standard(s) or technical brochure are as follow:

1. Surface Resistivity Tests (ASTM D257-14 [1] and D4496-21 [1])
2. Hydrophobicity Test (IEC 62073 [3])
   a. Method 1: Contact Angle
   b. Method 3: Spray Bottle
3. Hydrophobicity Transfer Tests (CIGRE TB 442 [4])
4. Inclined Plane Tests (IEC 60587 [5])
5. Outdoor/Mobile Rig Tests (IEC 60815 [34] and CIGRE TB 361 [29])

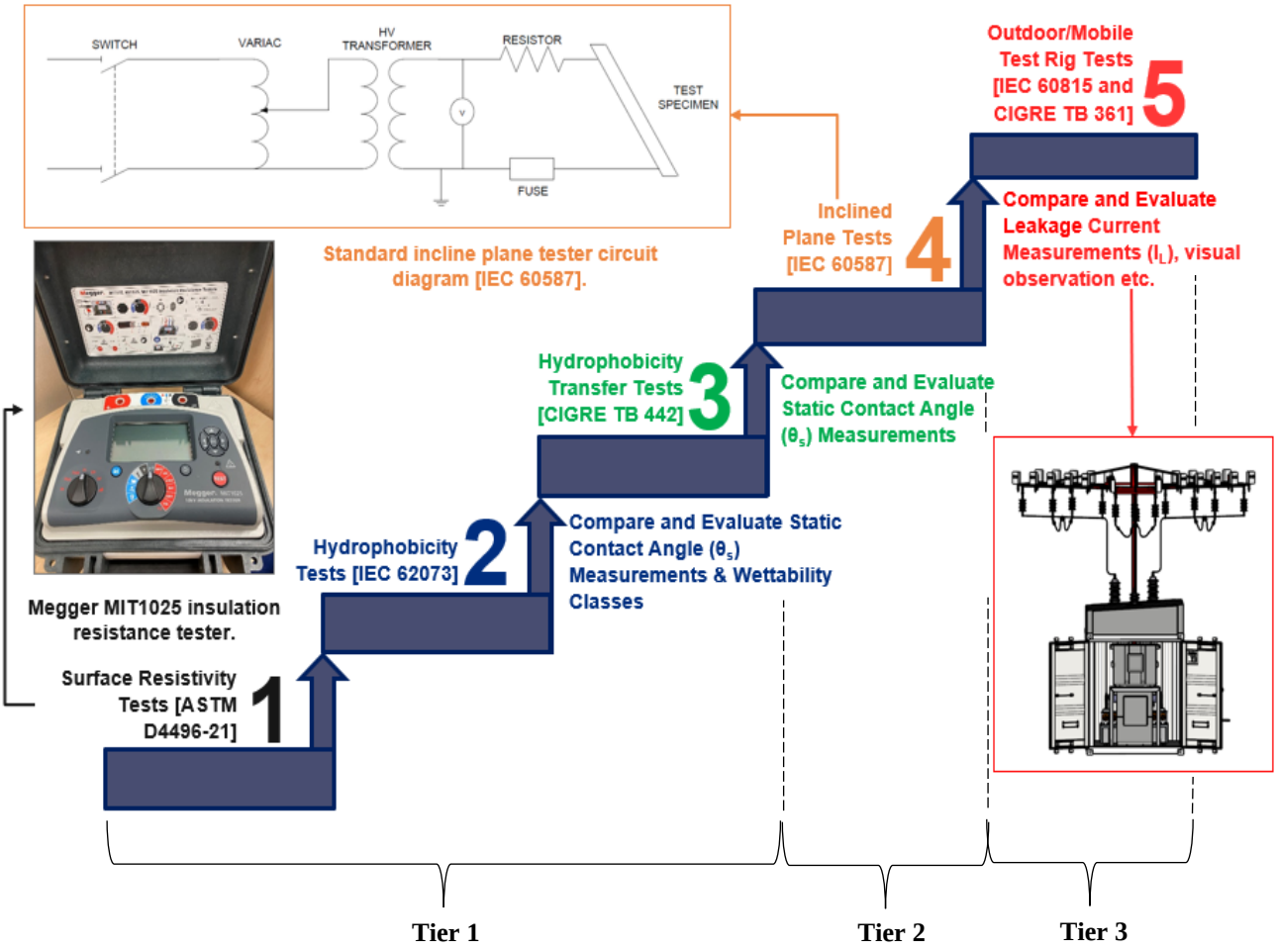

Figure 17: Research methodology experimental test method steps with a three-tier approach as basis.

3.2 Experimental Test Sample's Baseline Data

Two different Batches of coatings were prepared and sprayed onto ceramic tiles' top surfaces with a certain thickness and left to dry. Thereafter, test with methods one to four described in the previous section were used to test the sample coatings quantitively and qualitatively. The dimensions of the test samples were 120 mm x 50 mm x 6.7 mm (as per IEC 60587 [5] requirements for IPTs) and weighed approximately 57 g each. Variability was minimized in this project by using a single formulation of commercially available porcelain tiles which were coated with Graphene doped RTV SR. The coating Batches wt%'s, thicknesses and number of samples are summarised in Table 5.

It was noted that the coating appears darker for PG samples as the graphene wt%'s increases due to PG flakes having a bigger surface layer area of 3000 m^2/g than to NPG flakes which have about 1200 m^2/g according to Prof. L. Jarvis.

Table 5: Prepared coating test sample Batches wt%'s, thicknesses and number of samples summarised.

Batch Number	PG/NPG [wt%]	Number of samples NPG doped SR	Number of samples PG doped SR	Approximate coating thickness [mm]
1	0	1	1	0.07
	0.1			
	1			
	2			
	5			
2	0	2	0	0.45
	0.1	2		
	1	3		
	3	2		
	5	2		
	10	2		

3.3 Method 1: Surface Resistivity Tests

3.3.1 Overview

According to J. Dong et al. [28], graphene has a large specific surface area, unique thermal- and electrical properties. This study focuses on the utilisation of a virgin RTV SR coating as a basis for the modified insulating material. To assess its suitability for insulation purposes, it is essential to evaluate the surface resistivity, which is a measure of its electrical properties. The purpose of this test method is to investigate the impact of varying weight percentages of NPG/PG particles in the RTV SR coating vs surface resistivity. Measuring the surface resistivity determines if there are any significant changes in the electrical behaviour of the RTV SR coating as the concentration of NPG/PG graphene particles increases. This analysis is critical in understanding the potential enhancements or modifications in the electrical

insulation performance of the coating, providing valuable insights for improving its overall effectiveness in practical applications.

ASTM D257-14 [1] and D4496-21 [2] are standard test methods developed by the American Society for Testing and Materials (ASTM) for determining the surface resistivity of solid electrical insulating materials and semi-conductive materials, respectively. The surface resistivity is a measure of a material's ability to conduct or resist the flow of electric current across its surface. This test method provides a quantitative measurement of surface resistivity and is widely used in various industries, including electronics, electrical engineering, and materials science.

The ASTM tests involves applying a DC voltage across two electrodes placed on the surface of the material under test. The current passing through the material is measured, and the surface resistivity is calculated using Ohm's law. The test is typically conducted under controlled environmental conditions, such as temperature and humidity, to ensure accurate and consistent results.

The surface resistivity test is valuable for assessing the suitability of materials for applications where electrical conductivity or insulation properties are critical. It helps determine the performance and quality of insulating materials, such as polymers, ceramics, composites, and coatings. The measured surface resistivity can indicate whether a material meets the requirements for specific electrical applications or if it requires further treatment or modification.

Surface resistivity values obtained through ASTM D257-14 [1] and D4496-21 [2] can be used to evaluate the performance of materials in various scenarios, including static electricity dissipation, prevention of electrostatic discharge, and electrical insulation. For example, in the electronics industry, materials with low surface resistivity are desired to prevent the build-up of static charges that can damage sensitive electronic components.

It is worth noting that this study's test methods focus is on surface resistivity rather than volume resistivity. Surface resistivity refers to the electrical resistance between two parallel electrodes placed on the material's surface, while volume resistivity measures the resistance through the bulk of the material.

3.3.2 Method

The ASTM D4496-21, "DC resistance or conductance of moderately conductive materials" [1] is used as a guideline to perform experiments and calculate the surface resistivity of each sample in this research. The test objects were energised at 5 kVDC for 1 minute, with 4-minute resting intervals in between to allow any build-up of electrical charge to dissipate. Three resistance (R_s) values were measured individually after 1 minute 5 kVDC energy exposure. During preliminary tests, at 5 kVDC, it was noted that the surface resistivity characteristic values for the doped NPG/PG RTV SR samples exhibited a significant change (see Chapter 4) and therefore 5 kVDC was chosen as the test voltage for this experiment compared to testing at lower test voltages, e.g., 500 VDC, 1 kVDC and 2.5 kVDC. The following formula is used to calculate surface resistivity [1]:

$$\rho_s = R_s \left(\frac{W}{L}\right), \quad (6)$$

where W, the width of test surface, = 5 cm and, L, the length between electrodes, = 7.2 cm.

3.3.3 Evaluation

The following report information was chosen from both ASTM- D257-14 [1] and D4496-21[2] standards which must be obtained during experiments for assessment:

a. A description and identification of the material.
b. Name, graphene type, wt%, photo and weight.
c. Shape and dimensions of the test specimen.
d. Type of electrodes
e. Conditioning of the specimen (cleaning, pre-drying, hours at humidity and temperature).
f. Test conditions (specimen temperature, relative humidity, etc., at time of measurement).
g. Method of measurement.
h. Applied voltage.
i. Time of electrification of measurement.
j. Measured values of the appropriate resistances in ohms.
k. Computed surface resistivity in ohms (per square)
l. Statement as to whether the reported values are “apparent” or “steady state.” A “steady state” value is obtained only if the variation in the magnitude of the electric current in a circuit remains within 65 % during the latter 75 % of the specific electrification time used for testing. Tests made under any other circumstances are to be considered as “apparent.” Note: All values in this report are steady state.

The equipment checklists and test procedure for the surface resistivity experimental are presented in ANNEXURE A and B, respectively.

3.4 Method 2: Insulator Surface Wettability/Hydrophobicity Tests

3.4.1 Overview

Various test methods for determination of the degree of wetness on insulator surfaces were studied, namely the static contact angle method, the surface tension method and the spray bottle method [3].

The wetting properties of a surface by water are commonly described by the terms hydrophobic (or hydrophobicity) and hydrophilic (or hydrophilicity). A hydrophobic surface is water-repellent, while a surface that is easily wetted by water is hydrophilic [3].

Many different parameters can influence apparent wettability which include type of insulator material, surface roughness, heterogeneities of the surface, chemical composition (e.g., due to ageing) and presence of pollution [3]. The wetting phenomenon of a surface is complex and properties can change over time, due to the influence of the ambient conditions, corona discharge or dry-band arcing. This dynamic wetting behaviour change can be either reversible or irreversible. Thus, the result of the measurement of the wettability may be influenced by conditions to which the insulator has been previously exposed.

The chemical composition of insulator materials determines the dynamic wetting behaviour. Different processes such as oxidation, hydrolysis, migration of low molecular weight compounds formation of complex compounds between e.g., siloxanes and water, rotation of flexible polymer chains, inter- and intra-molecular rearrangements, microbial growth, deposition of contaminants, adhesion and encapsulation of contaminant particles, may take place at different rates, depending on material and ambient conditions [3]. Measurement of the wettability of a surface is readily performed in the laboratory on well defined, homogeneous, smooth and planar surfaces of prepared specimens [3].

3.4.2 Method A – Contact angle method

3.4.2.1 General

When a water droplet rests on a solid surface, the wettability of this surface depends on the balance of adhesive forces and cohesive forces, resultantly a contact angle (θ) is formed between the solid surface and the water droplet as explained in Section 2.7. Advancing and receding contact angle is measured by adding or subtracting water from the droplet [3]. The contact angle is affected by the surface roughness. Polluted surfaces may differ in θ compared to smooth, clean and planar surfaces [3]. IEC 62073 [3] gives the describes the relevant angles as follows.

3.4.2.2 Static contact angle

Figure 18 presents the acting forces between interfaces which are in balance when a drop of liquid rests on the surface of a solid, and a gas is in contact with both. The forces are due to surface tensions acting in the direction of the respective surfaces [3].

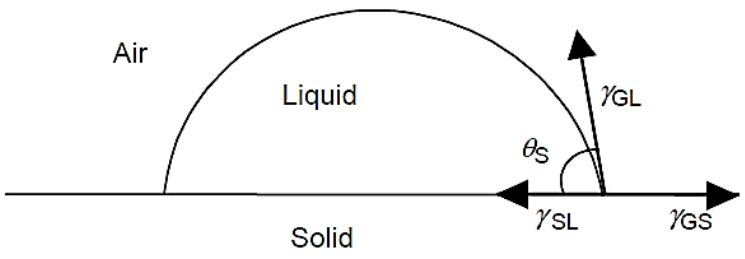

Figure 18: Illustration of static contact angle (θ_s) [3].

$$\gamma_{GL}\cos(\theta_s) = \gamma_{GS} - \gamma_{SL}, \quad (7)$$

where the different symbols are defined as follow:

θ_s (°) is the static contact angle of the edge of the drop with the solid surface

γ_{GL} (°) is the surface tension of the gas − liquid interface,

γ_{GS} (°) is the surface tension of the gas − solid interface, and

γ_{SL} (°) is the surface tension of the solid − liquid interface.

The right side of the equation given above is defined as the surface tension of the solid surface and depends on the interaction between the solid and a particular environment. The surface tension of the solid will be equal to the surface tension of the liquid if the contact angle is 0° and therefore the surface of the solid is then completely wet.

3.4.2.3 Advancing and receding contact angles

The advancing contact angle (θ_a) is the angle inside the water droplet between the solid surface and the droplet surface at the lower part of the droplet when the droplet is on an inclined solid surface as shown in Figure 19. The receding contact angle (θ_r) of a droplet on an inclined surface is the angle inside the droplet (highest part on the inclined surface) between the solid surface and the droplet surface at the droplet's rear end [3]. A completely wetted trace of water is formed as the drop moves along the solid inclined surface if the receding contact angle is zero. The general physical relation between the advancing, receding contact angle and static contact angle (θ_s) is defined as:

$$\theta_r \leq \theta_s \leq \theta_a \quad (8)$$

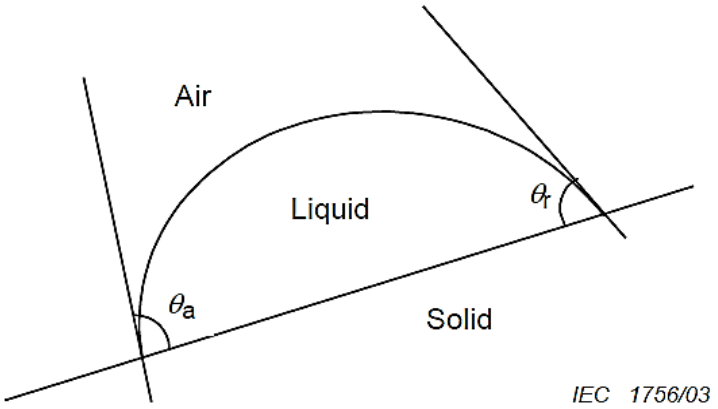

Figure 19: Illustration of the advancing angle (θ_a) and the receding angle (θ_r) [3].

3.4.2.4 Commonly used measurement equipment

Surface tension and contact angle measurements are made using various available commercial equipment, e.g., the Dropometer in Figure 20 (a) or simpler methods such as measurements captured from a magnifying device with a graduated goniometer fixed on a frame. A syringe or micropipette is used for application of a fixed size water droplet on a test specimen [3]. A light projector can be placed behind the droplet and an image of the droplet is then magnified onto a graduated background using a camera, display and/or computer for analysis of the measurements.

(a) **(b)**

Figure 20: (a) Dropometer, measuring surface tension and contact angle made easy using smartphone [43]. (b) Goniometer [44].

3.4.2.5 Measurement procedure

The measurement of the static contact angle (θ_s) is performed by applying a water droplet to the horizontal surface of a test specimen, using a pipette or a syringe with a scale. General recommendations include [3 - 4]:

a) It is recommended to keep the capillary pipette of the syringe immersed in the droplet during the entire measurement in order to avoid vibrations and distortions of the droplet that otherwise may affect the result.

b) According to [3 to 4], the receding contact angle (θ_r) reflects the wetting properties of an insulator more than the advancing contact angle (θ_a) and the static contact angle (θ_s).

c) The test specimen is selected to be as planar as possible and that the size allows for the application of at least three droplets on separate surface areas adjacent to each other. The surface to be measured was not touched and the specimen

was carefully stored until the measurement has been performed. The measurement is performed as soon as possible.

d) The water used should not contain impurities affecting the water surface tension (e.g., solvents, oil residues, etc.). De-ionized water is suitable.

e) Volumes in the range 5 µl to 50 µl may be used. The recommended volume is 50 µl. For rough surfaces, a larger droplet volume is needed. To limit a possible influence of the water droplet volume, the volume is kept as constant as possible when comparing different specimens.

f) The measurement of the contact angles should be performed as soon as possible (within 1 minute) after the application of the water droplet on the surface. This is especially important when the ambient temperature is high and the relative humidity is low, which increases the rate of evaporation of the droplet. If the measurement is performed in a chamber with saturated water vapour, it eliminates the influence of evaporation.

3.4.2.6 Evaluation

The extent of hydrophobicity is to be estimated from static contact angle measurements. Measurement on a single spot of the insulator surface is only valid for that location and not sufficient to draw conclusions on the wettability of the whole insulator material, therefore 3 measurements at different locations are to be taken [3].

3.4.3 Method B – Surface tension method

The surface tension method is the observation of droplets from a series of organic liquid mixtures that will result in different ways the insulator surface will wet with increasing surface tension. This method involves large amounts of liquids to cover a wider surface tension for both hydrophobic and hydrophilic insulators. There are restrictions when using this method for polluted insulator surfaces since the surface tension method is affected by interaction between certain types of surface pollution [3].

3.4.4 Method C – The spray bottle method

3.4.4.1 General

The spray bottle method involves evaluating the insulator surface by visual inspection after the insulator has been exposed to water mist for a short period of time. The wetness of the insulator surface is determined by comparing the appearance of the surface with reference material representing different Wettability Classes (WCs). Figure 21 below shows photos representing the different wettability classes, ranging from WC1, i.e., completely hydrophobic, to WC7, i.e., completely hydrophilic [3].

3.4.4.2 Equipment

A common spray bottle that can produce a fine mist filled with distilled water, can be used for this experiment. The water must not contain any impurities, which could influence the surface tension of the water, such as detergents, solvents, etc. For an easier judgement of droplet shape, it is recommended to use a magnification glass and a lamp during measurements [3].

3.4.4.3 Measurement procedure

A test area of 50 cm^2 to 100 cm^2 must is prepared and the ratio between the length and width of the test area must not be larger than 1:3. The mist is applied from a distance of 25 cm ±10 cm. The surface shall be exposed to the mist for a period of 20 s to 30 s. The amount of water sprayed during the 20 s to 30 s is within 10 ml to 30 ml. The measurement of the wettability is performed within 10 s after the spraying has been completed [3]. A clear picture of the variation of the wettability along and around the insulator must be obtained from the procedure.

3.4.4.4 Evaluation

The appearance on the insulator surface after mist exposure must be identified with one of the seven wettability classes. The criteria for the different WCs are given in Table 6 below. Two visual criteria are used to judge the WC (±1 wettability class) value:

a) the shape of droplets.
b) the percentage part of the surface which is wetted.

Table 6: Criteria for the determination of wettability class (WC) [3].

WC	Definition
1	The discrete water droplets' shape when viewed perpendicular to the surface is practically circular. This corresponds to $\theta_r = 80°$ or larger for the droplets.
2	A major part of the surface is covered by discrete droplets with a shape, as seen perpendicular to the surface, still regular but deviates from circular form. This corresponds to $50° < \theta_r < 80°$ for the majority of droplets.
3	Discrete droplets with an irregular shape cover a major part of the surface. This corresponds to $20° < \theta_r < 50°$ for the majority of droplets.
4	Discrete droplets and wetted traces from the water runnels or water films are observed. This corresponds to $\theta_r = 0°$ for some of the droplets. Water runnels or film covers less than 10% of the observed area.
5	Discrete droplets and wetted traces from the water runnels or water films are observed. This corresponds to $\theta_r = 0°$ for some of the droplets. Water runnels or film covers more than 10% but less than 90% of the observed area.
6	More than 90% but less than 100% of the observed area is covered by water runnels or fil . Small non-wetted areas/spots/traces are still observed.
7	Continuous water film is formed over the whole-observed area.

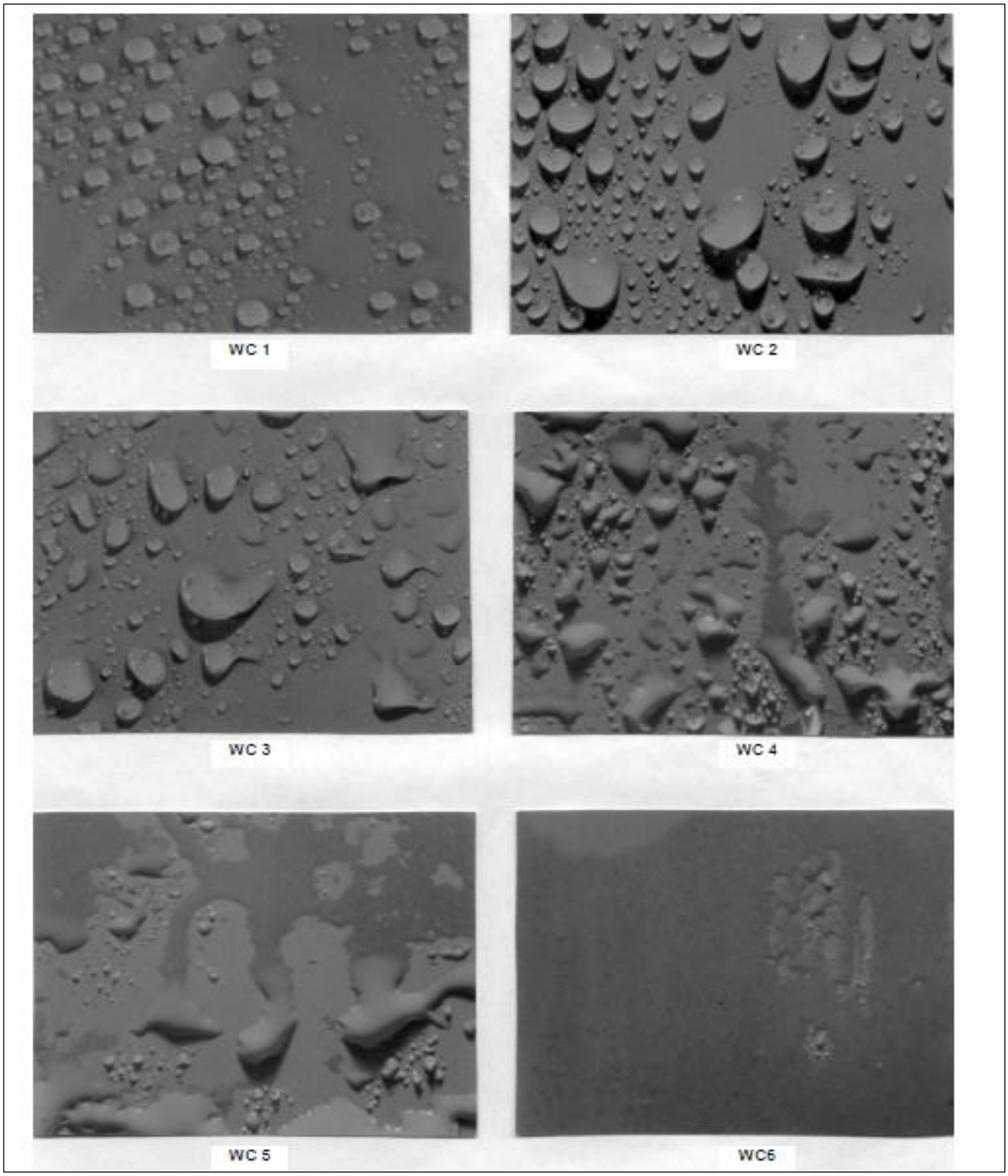

Figure 21: IEC 62073 wettability class comparison reference table [3].

3.5 Method 3: Hydrophobicity Transfer Tests

3.5.1 Overview

Certain silicone elastomers can transfer hydrophobic properties to pollution layers as described in Chapter 2.2. This chapter further elaborates on the HTM mechanism and introduces an intrinsic dynamic hydrophobicity transfer test to prove the diffusion of LMW silicones from the bulk material into the pollution layer when the pollution layer is hydrophilic (see Figure 22) with CIGRE TB 442 [4] as a guideline. The static contact angle method from Chapter 3.4.2 is also used to measure the intrinsic properties of hydrophobicity in this HTM experiment.

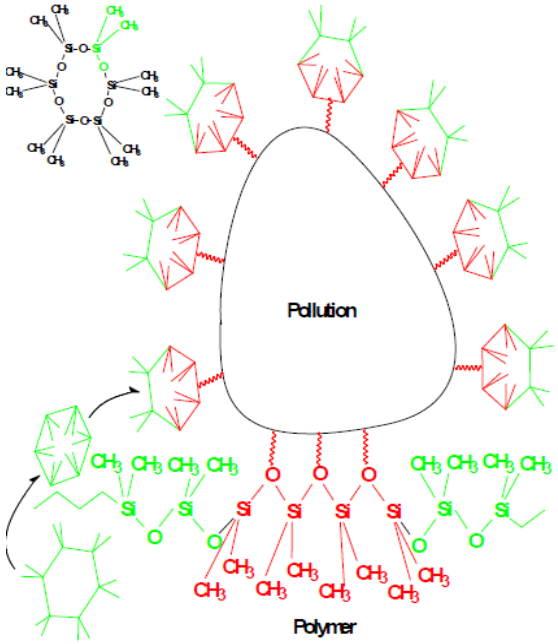

Figure 22: Transfer of hydrophobic properties to pollution layer illustrated [30].

3.5.2 Preparation of polluted test specimens

The test sample's surface must be able to accommodate a test area with dimensions 50 mm x 50 mm and should have a clean surface before the application of the pollution layer. Isopropanol and water are used to clean the sample surfaces before any experiments are performed. After cleaning the surfaces, each sample is stored at room temperature for at least 24 hours [4]. Next, attention must be paid to the thickness of the pollution layer coating and is discussed below.

3.5.2.1 Pollution layer preparation and thickness

The artificial pollution layers in the tests are applied with a defined thickness having a smooth surface without any defects to make the tests reproducible. HTM test results cannot be compared to each other if different layer materials and layer thicknesses are

used. The use of different materials also leads to significantly different results [4]. Common artificial pollution layer practices involve by mixing a slurry based on different silica powders, kaolin or kieselguhr and a liquid. The liquid can be tap water, distilled water or alcohol and can contain a wetting agent or even salts (e.g., NaCl) which is used to produce hygroscopic pollution layers [4]. The solid material used for the pollution layer must be produced in an industrial process (not a natural material from the soil) and must have no surface treatment that is difficult to control and check, e.g., untreated silica powder with a medium grain size of 3 µm (SF600) is recommended in CIGRE TB 442 [4] .

A slurry with a good mixing ratio of silica powder water/isopropanol results in a smooth and plane pollution layer surface. The use of only untreated silica powder and distilled water to produce pollution layers may lead to an uneven pollution layer and to cracks when the slurry dries out, especially with thicker layers [4]. The temperature in the laboratory during the whole test procedure must be kept constant at 23±2°C. To accurately investigate the thickness and the homogeneity of the dried layer (in contrast to the thickness of the adhesive foils explained later) a laser profilometer can be used as seen in Figure 23. Note that after drying of the slurry the thickness of the remaining layer will be less than the wet thickness.

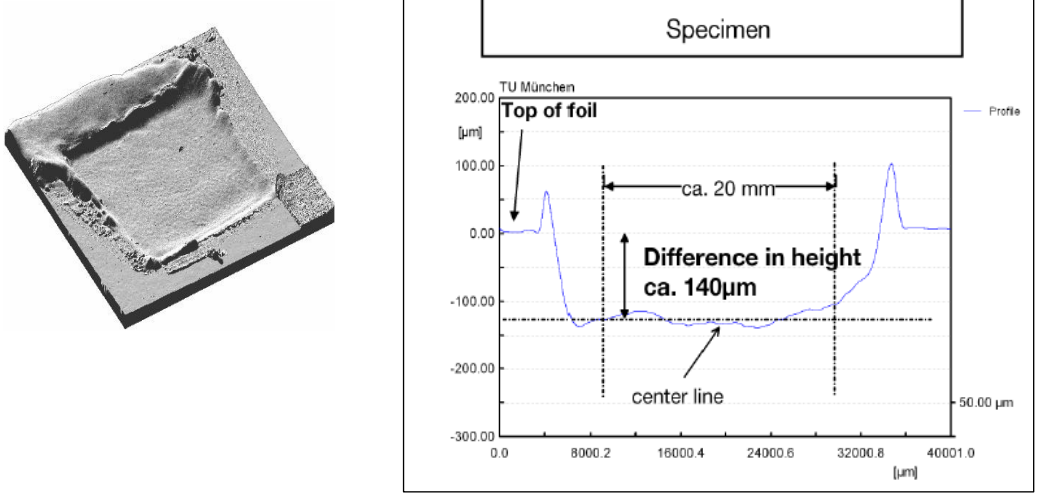

(a) **(b)**

Figure 23: (a) Scanning laser profilometer picture of a specimen with artificial pollution layer [4]. (b) Profile of a specimen with pollution layer, foil thickness 0.36 mm [4].

3.5.2.2 Application of prepared pollution layer slurry

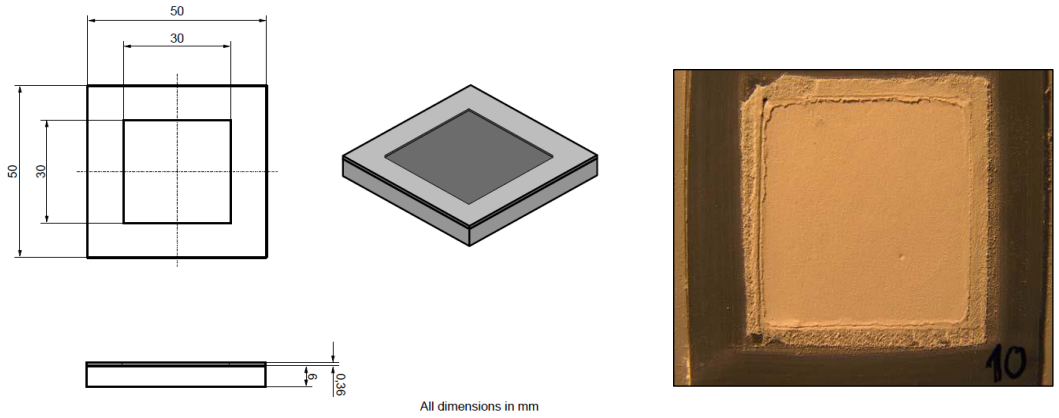

(a) **(b)**

Figure 24: (a) Specimen with adhesive foil and - (b) pollution layer [4].

Before the preparation of the pollution layer slurry, the test sample's surfaces are covered with adhesive foils in such a matter that a window of the dimensions (L x W) 30 mm x 30 mm is obtained as shown in Figure 24. The artificial pollution layer is prepared in the form of a slurry as described in the previous section and is applied, while wet, into prepared frames/window open areas. A plastic stick is used to wipe off the excess slurry. This results in a smooth and even surface. The thickness of the adhesive foils defines the latter thickness of the pollution layer. A thickness of 0.36 mm is recommended [4]. Different layer thicknesses are achieved by adding several foils on top of each other.

3.5.2.3 Influence of humidity during storage on the hydrophobicity transfer

The results of the Round Robin Tests (RRT) from CIGRE TB 442 [4] indicated that HTM tests are influenced by humidity during storage. Therefore, it is decided that test sample's must be stored at a defined relative humidity to avoid possible deficiency of the specimens. After the application of the slurry the samples are be stored as soon as possible at a temperature of (23±2) °C.

3.5.3 Measurement procedure

The measurements are performed with 10 samples and stored as described earlier in this chapter. As soon as the pollution layer is applied, then the start time (0h) of the HTM experiment commences. For the experiment, the contact angle (θ_s) is measured for different time intervals after the pollution layer was applied. Detailed information measurements of the static contact angle of the pollution layer are suggested to be measured at the following time intervals: 8 h, 16 h, 24 h, 32 h, 40 h, and 48 hours as shown in Table *7* [4].

Table 7: Overview of HTM test-series recommended time intervals [4].

Test-Series	Measurement Times [h]				
1	0	8	24	32	48
2	0	16	24	40	48

The measurement of the contact angle must be finished within one minute after the application of the water droplet to the pollution surface. When the water droplet is sucked into the pollution layer within three minutes after its application the θ_s is measured to be 0° regardless the measured θ_s earlier. For each selected time interval, one water droplet, in the range of 5 µl to 10 µl, must be applied in the centre area of the pollution layer of each of the samples as shown in Figure 25. The water droplets should be distributed in the centre area of the pollution layer. Measurements should also take place on different locations for every measurement as with hydrophobicity experiment. This protocol may alleviate the effects of an unequal pollution layer thickness [4].

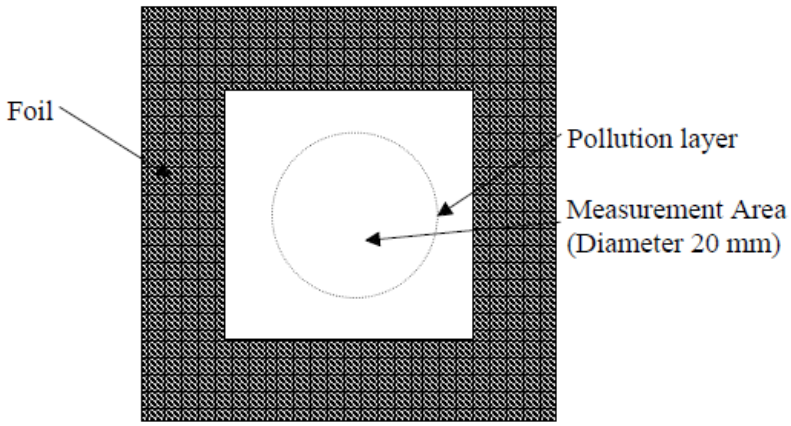

Figure 25: Selected area protocol for water droplet application [4].

3.5.4 Evaluation

No classification of HTM material has been introduced yet, but the CIGRE TB 442 [53] is used in this project as a guideline for evaluation. The ability of hydrophobicity transfer is evaluated according to the time which is needed for the LMW silicones to be transferred into/onto the artificial pollution layers under the conditions given by the recommendations above. Median static contact angles for all sample at the times of measurement, drop volumes (µl), temperature in laboratory (°C) and relative humidity (%RH) in laboratory must be taken note of during experiments for the evaluation and comparison of different materials with regard to the hydrophobicity transfer property, the use of only the static contact angles is sufficient [4]. Figure 26 shows the HTM normalised test results for different polymeric insulating materials tested at various laboratories over a 48h period using the CIGRE TB 442 [4] method.

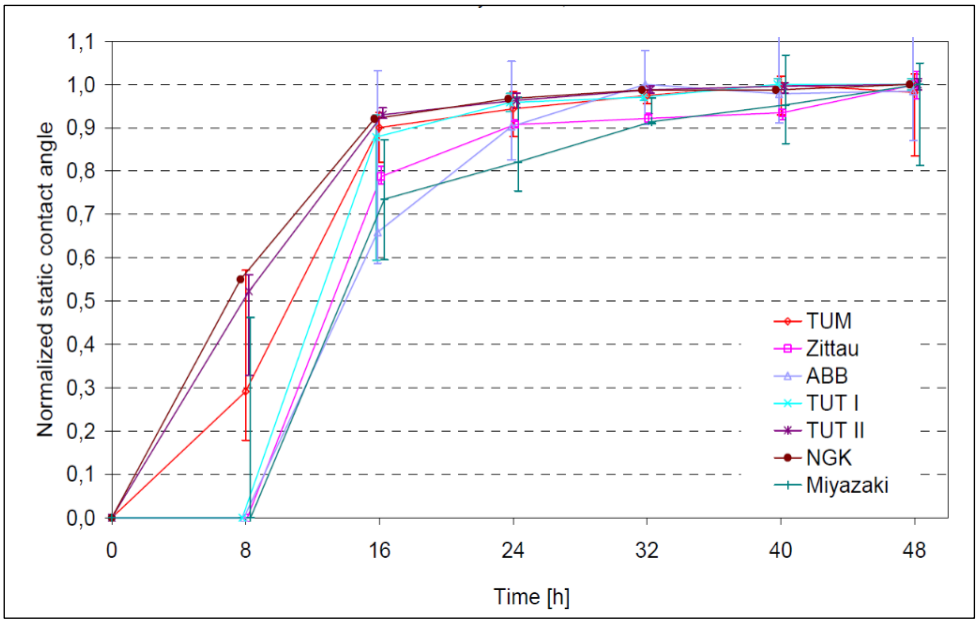

Figure 26: Results from all participating laboratories - normalised to the maximum value including spread [4].

3.6 Method 4: Tracking and Erosion Resistance Tests (Inclined Plane) [IEC 60587]

3.6.1 Overview

Two internationally recognised IPT procedures exist for the testing of composite insulator materials susceptibility to tracking and erosion when energised with HV AC voltages, these being the IEC 60587 [5] standard and the ASTM D2303 standard. Eskom centers most specifications relating to HV Insulators on IEC/CIGRE specifications and guidelines. Hence, for the purposes of this research, the IEC 60587 [5] standard was utilised for AC testing (see Figure 27 and Figure 28). IEC 60587 [5] can be adapted for DC energisation as well.

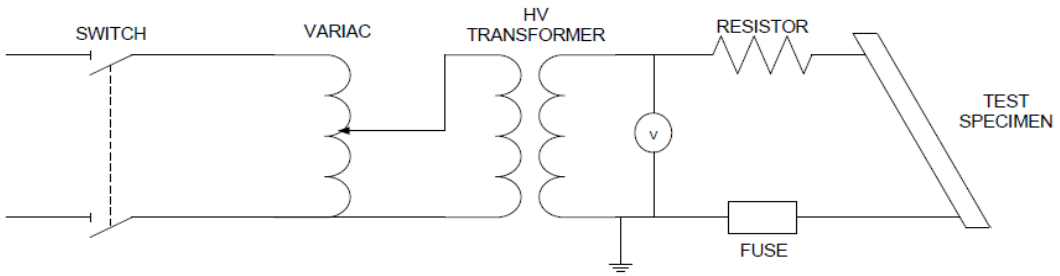

Figure 27: IPT electrical circuit diagram [5].

3.6.2 Tracking and erosion test- methods and parameters

The IEC 60587 [5] standard allows for two methods of testing which can be used for material erosion and tracking experiments:

3.6.2.1 Method One: Constant tracking voltage

The first IPT method stresses the samples at a fixed voltage setting maintained for a 6-hour duration. The IEC 60587 [5] standard recommends test voltages of either 2.5 kV, 3.5 kV or 4.5 kV, at contaminant flow rates of 0.15, 0.3 or 0.6 ml/min. For this project, a test voltage of 3.5 kV_{rms} for AC, at a contaminant flow rate of 0.6 ml/min, was chosen. These test parameters were deemed to be best suited to highlight the resistance to tracking and erosion activity of graphene doped RTV SR coatings.

3.6.2.2 Method Two: Stepwise tracking voltage

IPT method two uses a starting voltage, which is selected and maintained for the first hour, thereafter the voltage is increased in steps of 250 V for each subsequent hour, until failure occurs. The resistance value of a series resistor and the contaminant flow rate must be steadily increased with the increase in voltage for IPT method two [5]. For the purpose of this project, method one was utilised so as to ensure uniformity of test voltage level and contaminant flow rate for all tests conducted [5].

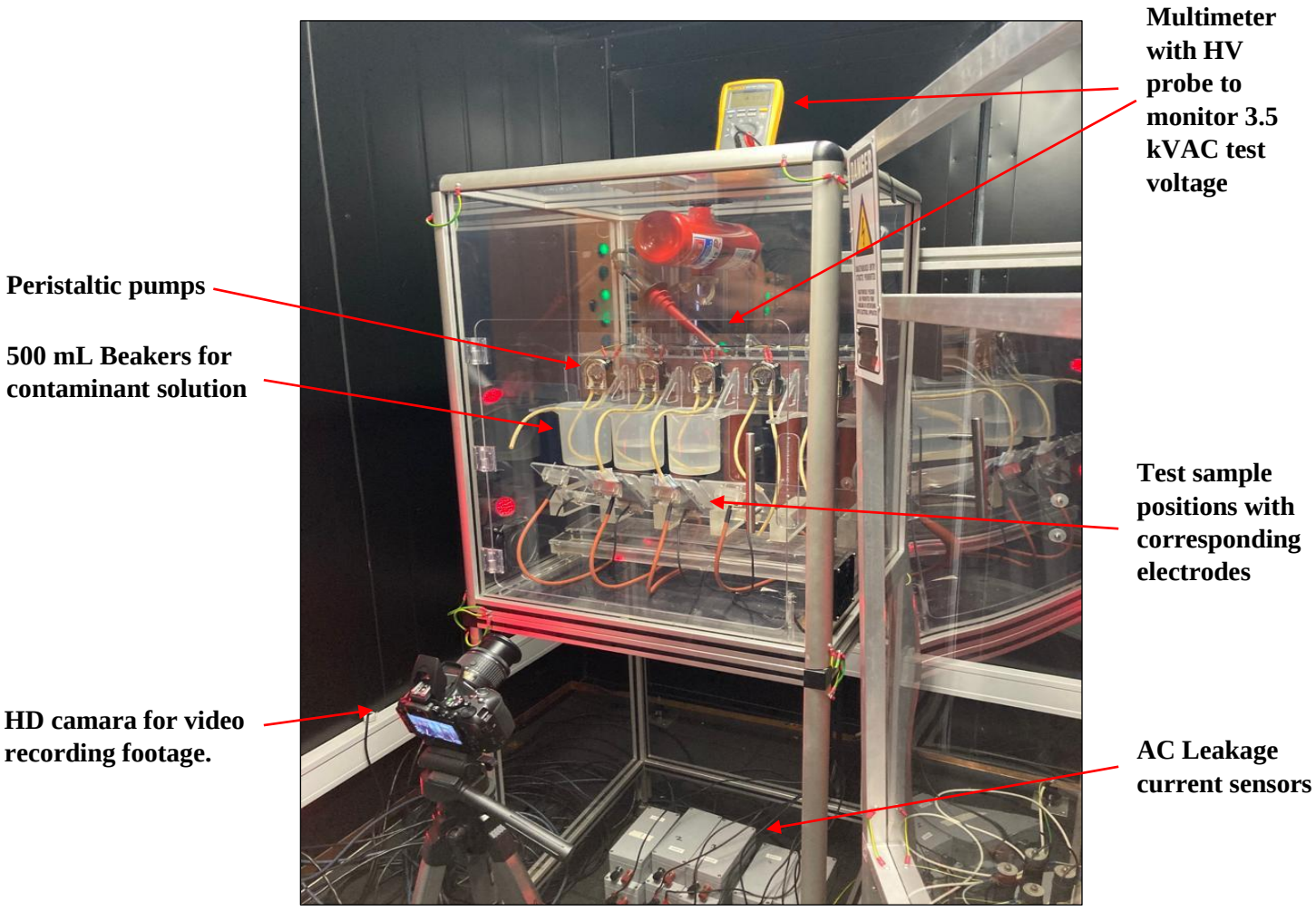

Figure 28: Inclined plane tester setup at Stikland substation.

3.6.3 Choice of electrode material

IPTs were conducted using stainless steel 304 electrodes as specified by IEC 60587 [5] (see Figure 29). The electrodes were 0.5 mm thick and weighed on average 14 g and 4 g for the top and bottom respectively. A master's dissertation by Mr. R. Swinny [45] presents results of research on trying to find an improved/alternative material compared to stainless steel electrodes causing corrosion problems in IPT tests. Carbon glass as a material possesses extreme corrosion resistance and was considered to be a suitable alternative electrode material for the research. Although the carbon glass electrodes eliminated the stainless-steel electrode erosion side effects, it seemed other dynamics resulted in the IPT being radically more severe.

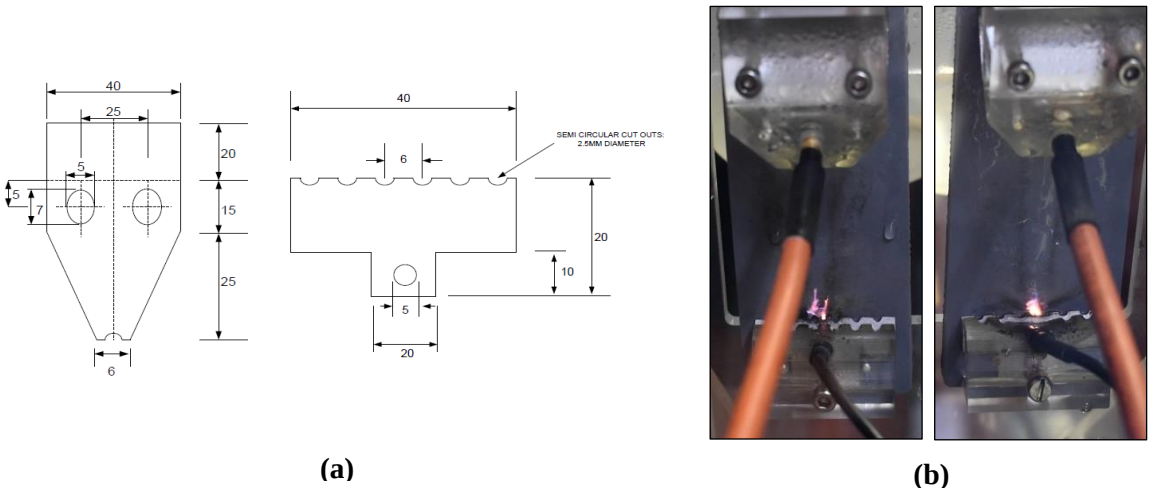

Figure 29: (a) Top (left) and bottom (right) electrodes for inclined plane tester [5]. (b) 2x HTV SR test samples mounted with electrodes in IPT during HVDC test runs.

The research postulated that the carbon glass electrodes utilised in the study had lower thermal conductivity than the steel electrodes, leading to increased surface temperature on the HTV SR material during static DBA and subsequent material breakdown [45]. Stainless steel roughly has a thermal conductivity of 14.4 W/mK, whereas standard glass and carbon have thermal conductivities of 1.05 W/mK and 1.7 W/mK respectively [45].

3.6.4 Choice of contaminant and the flow rate effects during IPT

A combination of ammonium chloride (0.1% ± 0.002 by mass) and Triton X-100, which acts as a wetting agent, is utilised to ensure a contaminant conductivity of 2.53 mS/cm ± 0.03 @ 23°C (resistivity of 3.95 Ω_m) [5]. The flow rate of the contaminant determines the cross-sectional area of the electrolytic pollution layer. Therefore, if the flow rate is increased, the cross sectional are also increases which in turn increase the leakage current flow. A flow rate that is too high will result in high leakage current, leading to flashover, but will not allow for drying of the insulator surface and associated DBA. A flow rate that is too low will not be able to sustain the leakage current required to cause damage. This is confirmed by Bruce et al in [46].

3.6.5 Measurement procedure

ANNEXURE D provides a detailed systematic process which was developed and implemented to ensure reliability, repeatability and safety of all IPT experiments. The procedure provides an outline of the steps followed during pre-testing, actual-testing and post-testing.

3.6.6 Evaluation

IEC 60587 [5] lists two failure criteria:

- Criterion A: Leakage current in excess of 60 mA for longer than 2 seconds (fuse blows), or the specimen exhibits a hole due to intensive erosion or the specimen ignites.
- Criterion B Tracking in excess of 25 mm from the lower electrode, or the specimen shows a hole due to intensive erosion or the specimen ignites.

The SEDIVER coating erosion class guide [7] is also commonly used by utilities to classify tracking and erosion results.

For this project, IPT results were evaluated against both IEC 60587 [5] and SEDIVER [7] criteria.

3.7 Method 5: Outdoor/Mobile Test Rig Tests

The fifth series of tests (Tier 3) is to compare/evaluate the outdoor pollution performance and ageing of the candidate coatings in a natural severe marine environment after a certain period, using the Mobile Test Rig (MTR), in accordance with the IEC 60815 [34] and CIGRE TB 361 [29] for AC power networks. The fifth series of tests were not implemented in this project and can only commence if a modified coating passes all first four series of tests.

However, a portion of the research project did involve the refurbishment of the old KIPTS equipment and final design/build of an MTR which can produce constant 22 kV HVAC and HVDC excitations to evaluate the performance of 30 power line insulators under severe marine environmental conditions. The MTR will also be used to calibrate the old KIPTS with the new KIPTS test facility.

As presented in Figure 30, the previous test rig's equipment was "repackaged" into a standard 3 m shipping container by means of using 3D CAD models developed in Google SketchUp software (see ANNEXURE E.1). Technical design drawings were produced by a chief draughtsman after the final design was finished by me in Google SketchUp (see ANNEXURE E.2).

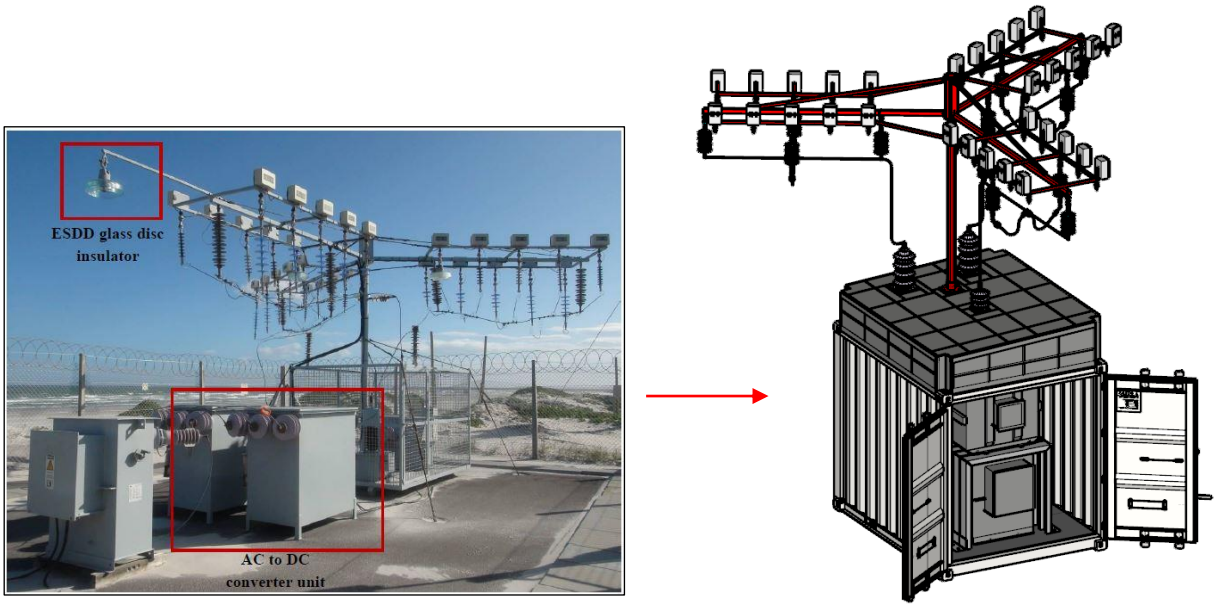

(a) **(b)**

Figure 30: Previous insulator test rig equipment (left). HV equipment "repackaged" into a standard 3 m shipping container by use of Google SketchUp 3D CAD Software (right).

System Nominal Voltage (kV)	System Highest Voltage (kV)	Minimum Electrical Clearance (mm)		Working Clearance (m)	
		Phase-To-Earth (C_e)	Phase-To-Phase (C_p)	Vertical (C_{wv})	Horizontal* (C_{wh})
3,3	3,6	80	110	2,5	1,2
6,6	7,2	150	200	2,6	1,2
11	12	200	270	2,7	1,3
15	17,5	230	310	2,7	1,3
22	24	320	430	2,8	1,4
33	36	430	580	2,9	1,5
44	48	540	730	3,0	1,6
66	72	770	1050	3,2	1,8
88	100	840	1150	3,3	1,9
		(1000)	(1350)	(3,5)	(2,1)
132	145	1200	1650	3,7	2,3
220	245	1850	2300	4,3	2,9
275	300	2350	2950	4,8	3,4
330	362	2900	3600	5,4	4,0
400	420	3200	4000	5,7	4,3

Figure 31: Standard electrical and working clearances for substations from Eskom Operating Regulations for High Voltage Systems documentation.

Technical specifications/designs for each component, e.g., bolts, steel sheets, L-brackets, polycarbonate boxes, 3-phase electrical sockets/plug, thermal insulation, ventilation, entire mansard roof, pole with footing support and flange, square tubing for the three radial arms structures, base support structure for the 50 kVA transformer power supply units, etc were determined (kept confidential). The previous hollow core porcelain AC and DC bushings were also

modelled and accurately placed in the 3D CAD model to prevent possible flashover inside the container during operation (see Figure 31 and Figure 32).

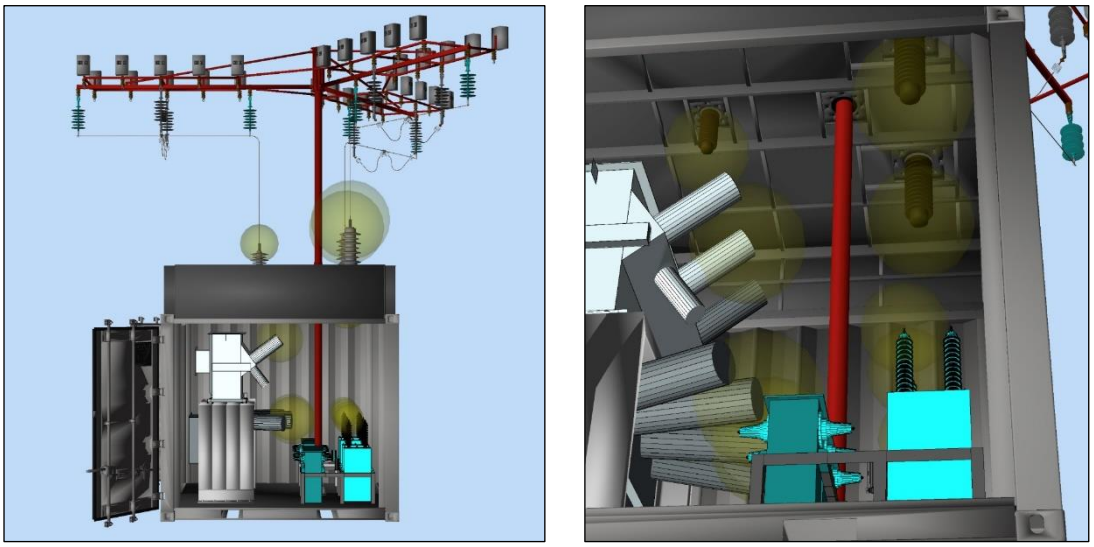

Figure 32: Standard electrical clearances for Eskom substations indicated with yellow spheres in 3D CAD model by use of Google SketchUp 3D CAD Software to determine equipment locations and prevent possible flashover.

4. COATING BATCH 1: EXPERIMENTAL TEST RESULTS FOR PG AND NPG DOPED RTV SR

4.1 Background

A local coating manufacturer was approached whom agreed to provide base RTV SR coating material to be modified by including PG/NPG. The sample coatings were prepared by mixing graphene produced using two methods, i.e., a chemical route (PG) and a mechanical route (NPG), with the base RTV SR coating supplied. Thereafter the coating mixtures, at different doped graphene weight fractions, 0 wt%, 0.1 wt%, 1 wt%, 2 wt% and 5 wt%, also shown in Figure 33, were applied to the upper surface of a clean and flat ceramic tile with a model spray gun at a wet thickness of approximately 0.07 mm. The tile measurements were adopted from the IEC 60587 [5] standard to be used for tracking and erosion tests at a later stage.

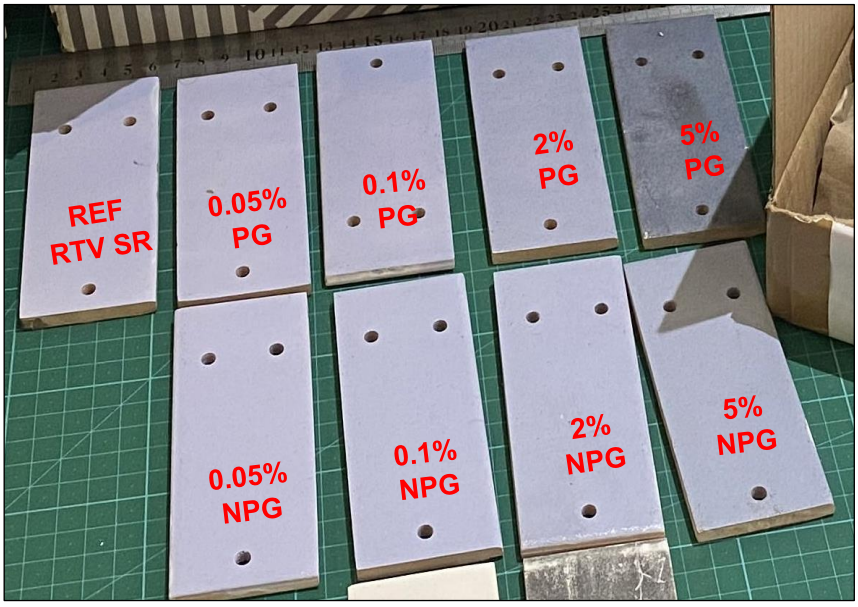

Figure 33: Batch 1 RTV SR coated ceramic tiles with different PG/NPG wt%'s.

The first series of experiments involved the use of an insulation resistance tester to directly determine the insulation resistance performance of each coated ceramic tile sample with the ASTM D257-14 [2] standard used as a guideline. The tiles were electrically charged at 500 V, 1000 V and 2500 V for a period of one minute at each DC test voltage. Current and resistance measurements were logged each second, using the provided instrument software, for one minute of excitation. A ground plate was connected to the positive and negative electrodes after each test for one minute to discharge any build up charge from excitation.

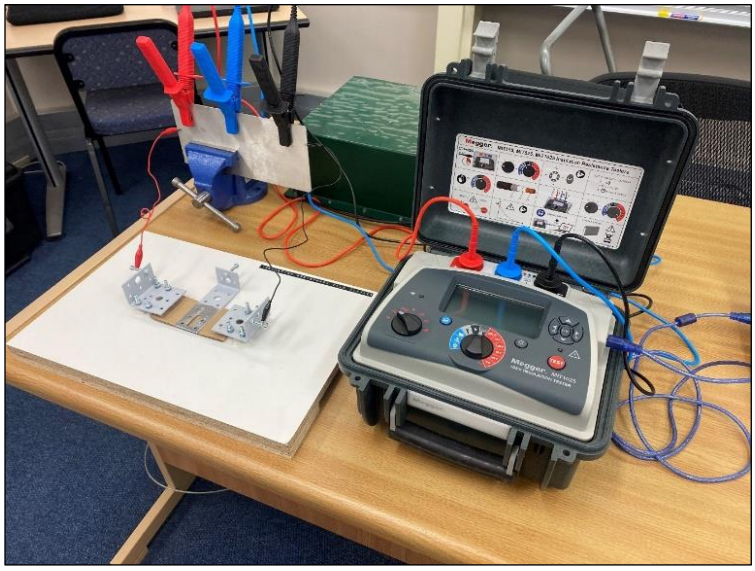

Figure 34: Insulation resistance test setup with ground plate and electrodes.

The second series of tests determined the hydrophobic properties of the coated ceramic tile samples. Two test methods, i.e., contact angle and spray bottle, from IEC 62073 [3] were implemented to evaluate the hydrophobicity/wettability of each PG and NPG doped RTV SR coated ceramic tile sample. The microscope, tile sample test position, micropipette's clamping vice and laptop was placed on separate surfaces to ensure no vibrations/distortions occur during contact angle measurements as shown in Figure 35.

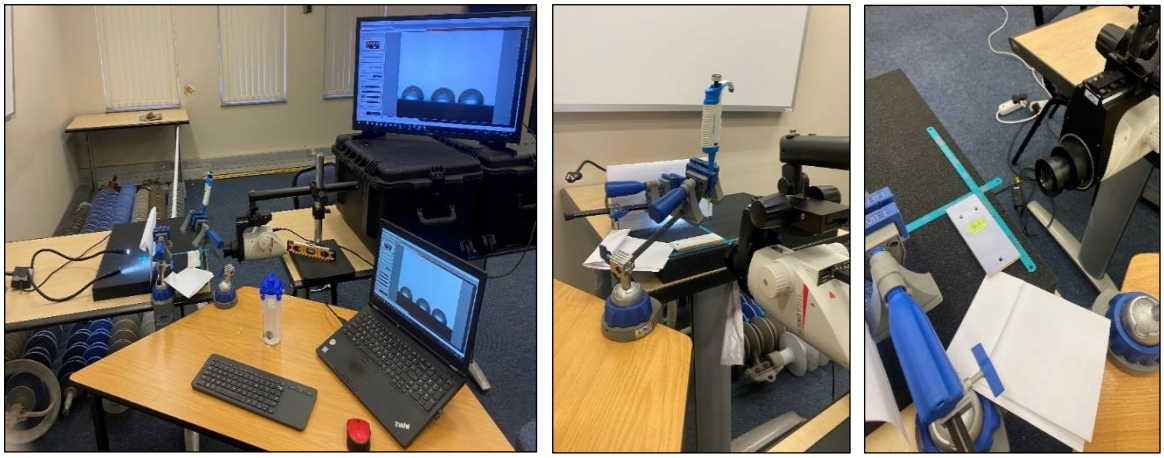

Figure 35: Water droplet contact angle experimental setup with microscope, tile sample test position, variable micropipette, vices and laptop.

The open-source software ImageJ (with Drop Analysis plugin) was used to accurately determine each of the water droplet's contact angles/water droplets shapes from the photos taken using the microscope. Both the resistance and hydrophobicity tests were conducted at laboratory temperature and relative humidity conditions of approximately 22°C and 50%, respectively.

A third series of tests involves an experimental investigation into the hydrophobicity transfer capabilities of each graphene doped RTV SR coating with CIGRE TB 442 [4] as a guideline.

Finally, a fourth series of tests were conducted which was an experimental investigation into the tracking and erosion (accelerated ageing) of the coated ceramic tile samples subjected to 3.5 kVAC excitation in accordance with the IEC 60587 standard [5] using an existing inclined plane tester.

4.2 Insulation Resistance Tests

The goal of the insulation resistance tests was to determine if the PG/NPG doped RTV SR coatings will still exhibit adequate electrical insulation resistance properties. Figure 36 presents an average drop in one minute insulation resistance (using both 1000 V and 2500 V) of 36.7% and 45.7%, for PG and NPG coatings respectively, from 0.1 wt% to 5 wt%. The results also show that PG doped RTV SR coated ceramic tile samples measured higher insulation resistances for each wt% compared to NPG samples at the test voltages >500 V.

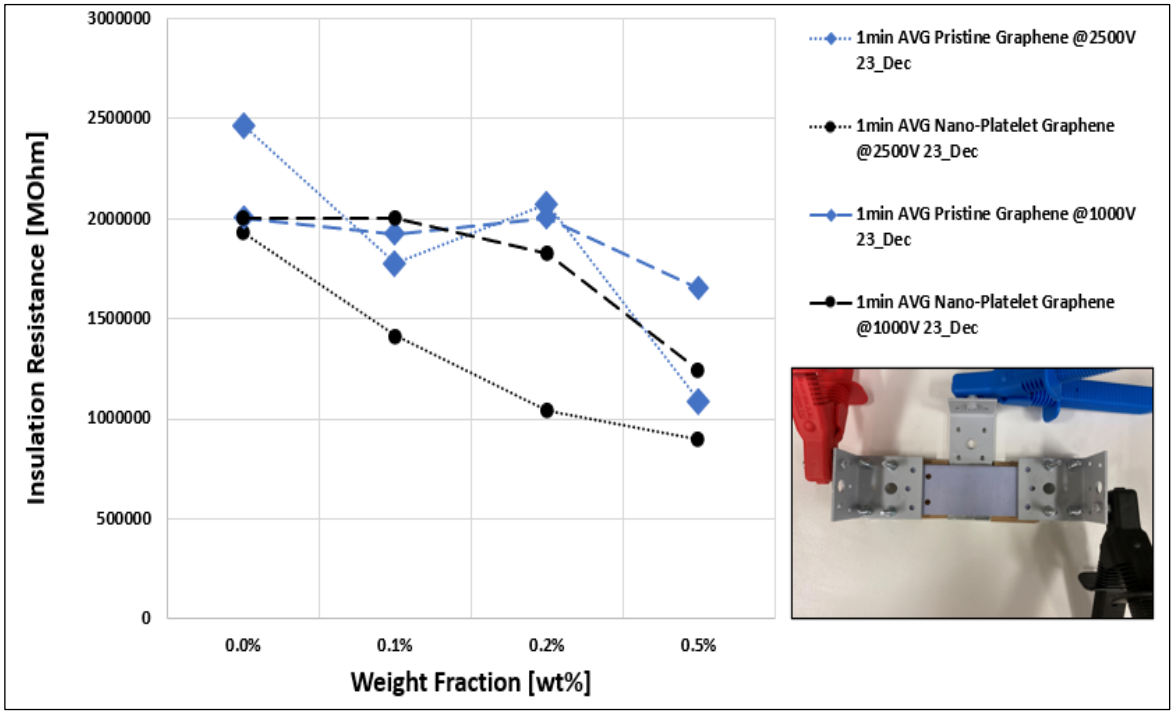

Figure 36: Batch 1 Insulation resistance test results for PG/NPG doped RTV SR coating samples at 500 VDC, 1000 VDC and 2500 VDC respectively.

4.3 Hydrophobicity Tests

4.3.1 Static contact angle measurements

To determine the hydrophobic properties, three 50 µl distilled water droplets were placed adjacent to each other on each coated surface with the use of a variable micropipette in compliance with the test method described in IEC 62073 [3]. An example of this is shown in Figure 37. Six θ_s angle measurements could then be performed in the analysis software described earlier. The coated ceramic tiles and camara were vertically levelled at 90° with a small spirit level to ensure the water droplet angles were accurately projected towards the

camara lens. Three θ_s angle experimental sets were conducted on separate days and an average standard deviation of 5.2° between static contact angles for each weight fraction was calculated.

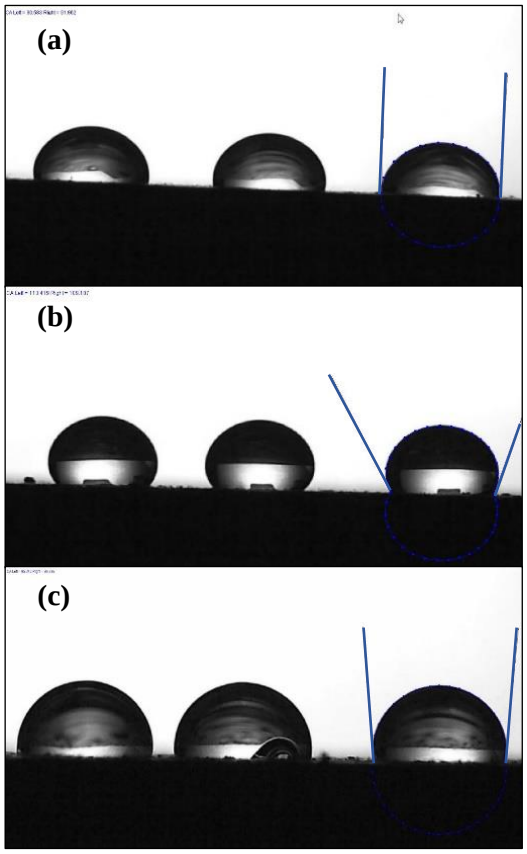

Figure 37: Water droplets on the surface of (a) RTV SR reference coating, (b) 5 wt% PG doped RTV SR coating and (c) 5 wt% NPG doped RTV SR coating. Gas-liquid interfaces indicated for 3rd water droplet in blue.

Figure 38 presents the static CA (°), i.e., hydrophobicity, vs PG/NPG doped RTV SR (wt%) graph. It was noted that there is an approximate 30° increase in hydrophobicity (i.e., higher static contact angle measurements) for 5 wt% PG doped RTV SR coating compared to the RTV SR reference coating and 5 wt% NPG doped RTV SR coating. No significant hydrophobicity enhancement for NPG doped RTV SR at 5 wt% was observed/measured yet. Figure 37 (b) illustrates the beading effect of a water droplet clearly and indicates a lower surface tension force is present within the 5 wt% PG doped RTV SR coating.

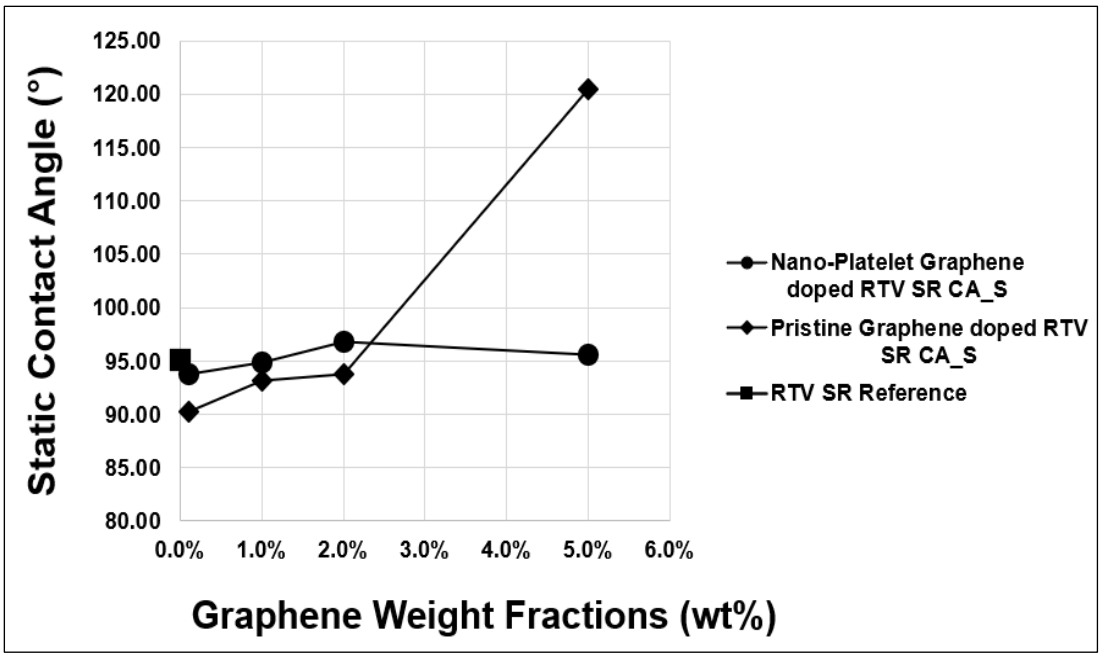

Figure 38: Hydrophobicity static contact angle (θ_s) test measurements for PG, NPG (0.1 wt% to 5 wt%) doped RTV SR coatings and a reference RTV SR coating. Standard deviation of ≈ 5.2° between measurements.

4.3.2 Wettability class measurements

The images Figure 39 to Figure 41 presents the WCs of each coated ceramic tile after spraying each with a fine mist, using a spray bottle, for 30 seconds from a distance of 30±10 cm. Table 8 below contains the final WC results and correlates with the graph given in Figure 38. The 5 wt% PG doped RTV SR coating obtained a WC = 1 and all the other coatings received an average WC = 3. Water droplets easily rolled off the 5 wt% PG doped RTV SR coating when given a tilt angle, demonstrating self-cleaning capability. During the spray bottle test method, it was noted that the 2 wt% PG coating exhibited an unexpected jump in WC, which may indicate a possible error made during the mixing/application of this coating onto the ceramic tile.

Table 8: Wettability class spray bottle method test results.

Coating Type	**Coating Sample Graphene WC vs Weight Fraction [wt%]**			
	0.1	**1**	**2**	**5**
PG doped RTV SR WC	2	2	4	1
NPG doped RTV SR WC	2	3	3	3
RTV SR Reference WC	3			

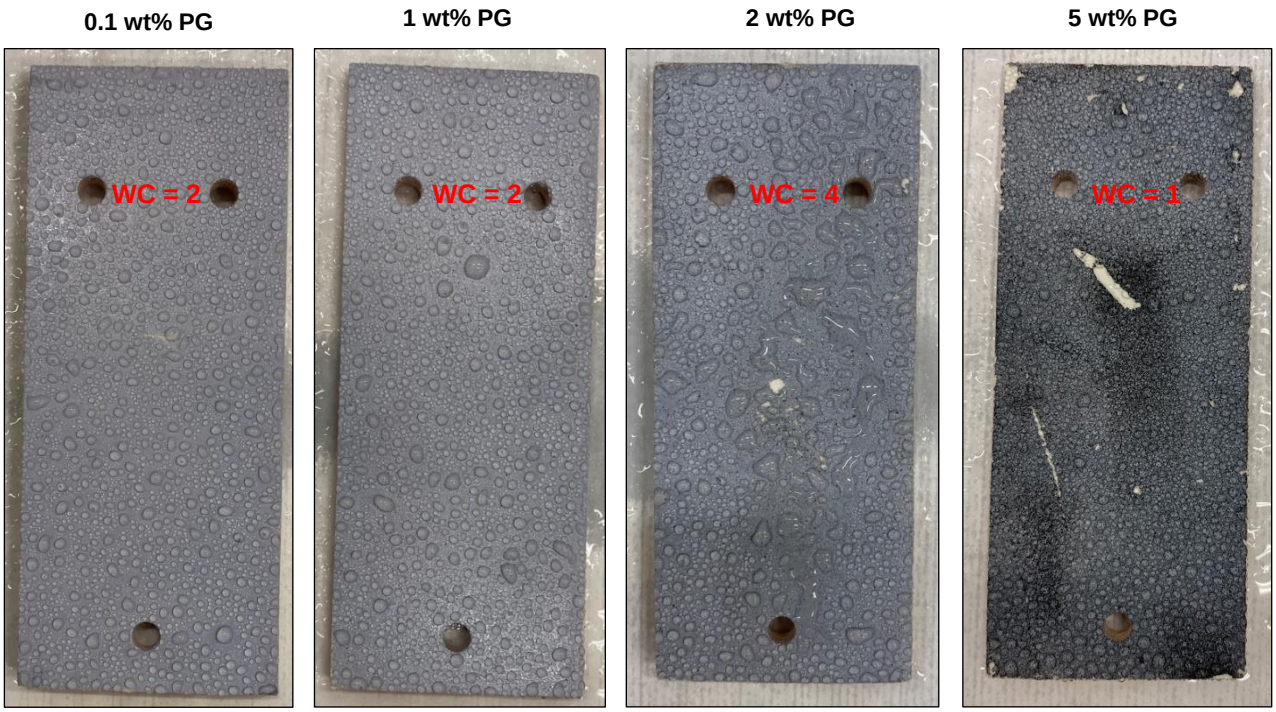

Figure 39: PG doped RTV SR coatings spray bottle test method results photos.

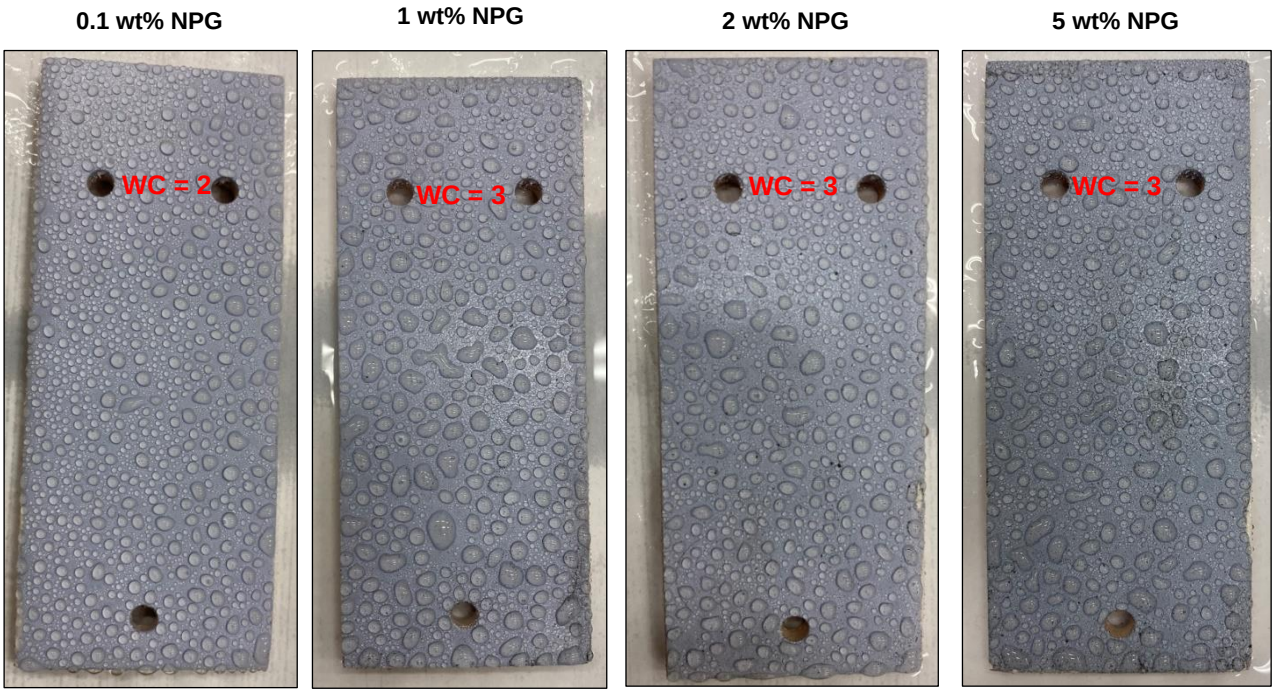

Figure 40: NPG doped RTV SR coatings spray bottle test method results photos.

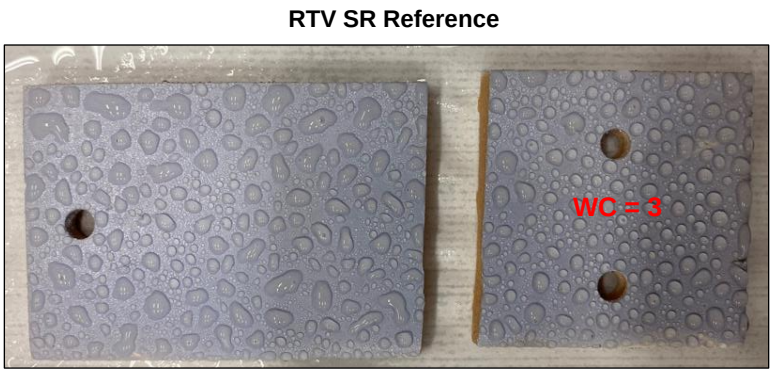

Figure 41: RTV SR coating reference spray bottle test method results photos.

4.4 Hydrophobicity Transfer Tests

A slurry type pollution layer was applied to each coated tile's surface (see Figure 42) after a Kaolin clay powder and Iso-Propyl Alcohol (Iso-propanol: 85%; Ethanol:15%) solution was mixed together for 1 minute according to CIGRE TB 442 [4]. An approximate layer thickness was achieved by the application of five adhesive foil windows (each 70 µm thick) onto the tile's surfaces with a total layer thickness of 0.35 mm (see Figure 42). 10 µL water droplets were applied for θ_s angle measurements at certain time intervals. Unfortunately, no transfer of hydrophobicity was observed for any tile coating's pollution layer after an ≥48 h interval (see Figure 43). The pollution layer thickness is decreased and presented in Chapter 5 to produce feasible θ_s angle results for the coatings.

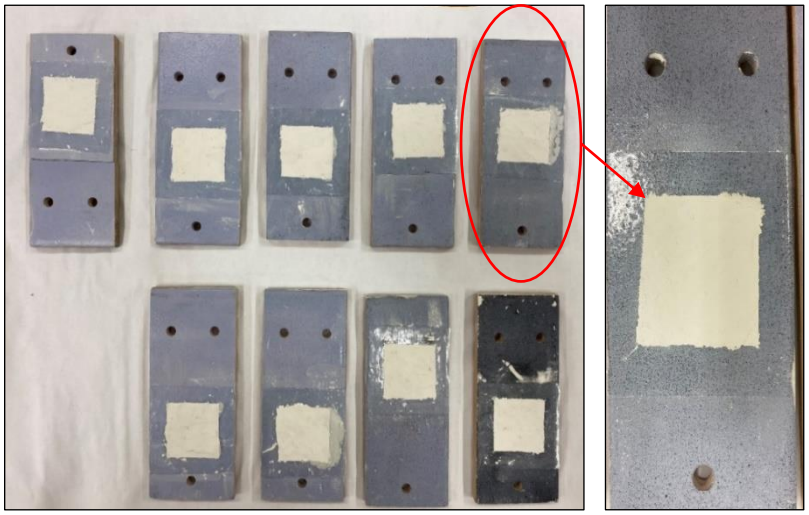

Figure 42: Tile specimens with applied pollution layer slurry.

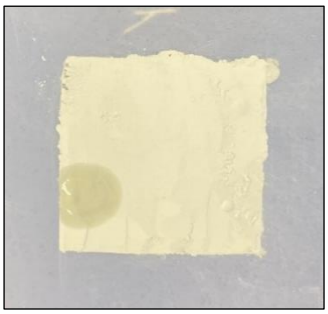

Figure 43: 10 µl Distilled water droplet applied on 4th day on RTV SR reference.

4.5 Tracking and Erosion Resistance Tests

4.5.1 Introduction

Four High Temperature Vulcanised (HTV) SR samples were used to test run the IPT at 4.5 kV DC and AC for 1.5 h, respectively. Figure 44 presents the DC tracking and erosion test is more severe (encircled red) than the AC test.

After the IPT AC- and DC test runs, it was decided to formally test the PG and NPG graphene doped RTV SR coated ceramic tiles from Batch 1 at 3.5 kVAC for 6 h, as per IEC 60587 [5]. The IPT tests was conducted at a lower AC test voltage to serve as a "gentle" test on the thin applied coatings and to clearly show the difference in performances.

Figure 44: Photos of HTV SR material ran with AC or DC tracking and erosion pre-tests. It was observed that DC excitation is more severe than AC.

4.5.2 Results Discussion

The most notable visual observation from the IPTs was that PG at ≥0.1wt% as well as NPG at 5 wt% distributed the electrical activity horizontally alongside the ground electrode surface and upper surfaces of the coating as seen in Figure 45. The good electrical conductivity property of graphene may have assisted with the distribution of DBA activity termination points horizontally alongside the ground electrode.

During IPTs, the ceramic tiles heated up due to heat generated from DBA activity and caused the contaminant to evaporate as soon as an electrical discharge occurred. The test run with HTV SR samples did not heat up due to exhibiting a higher ATH filler content than RTV SR coatings. In the field the RTV SR coating surfaces turns pink from the heat generated by DBA which warms the ceramic material below. From the visual results presented in Figure 46, it can be seen that an increase of PG/NPG wt% content suppresses the amount of RTV SR coating "evaporating" due to heat generated from DBA. The good thermal conductivity property of graphene may have assisted with the distribution and supressing of heat, causing less "hotspots" and lesser pink colourisation of coating surface as PG/NPG wt% content increases.

It is clear from the 0.1 wt% NPG sample, erosion was only concentrated in the middle of the ground electrode, i.e., DBA termination activity was not distributed horizontally compared to the 5 wt% NPG sample. In contrast, smaller erosion (black spots) diameters and horizontal distribution of eroded spots at ground electrodes can be seen in the 5 wt% NPG sample photo far right below (Figure 46).

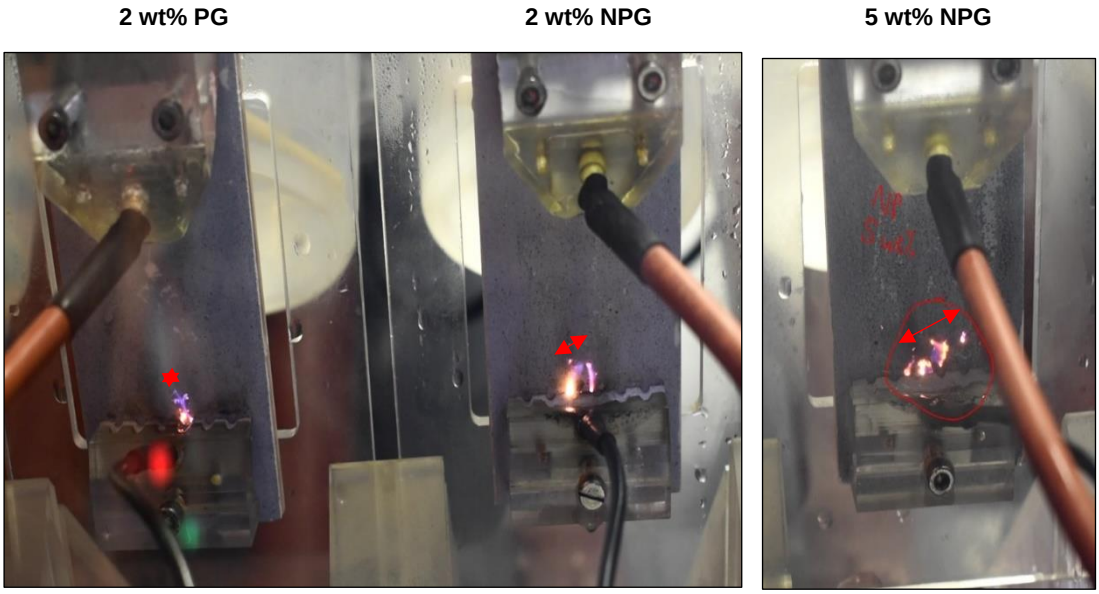

Figure 45: 2 wt% PG (left) and NPG (middle) doped RTV SR. 5 wt% NPG doped RTV SR (right).

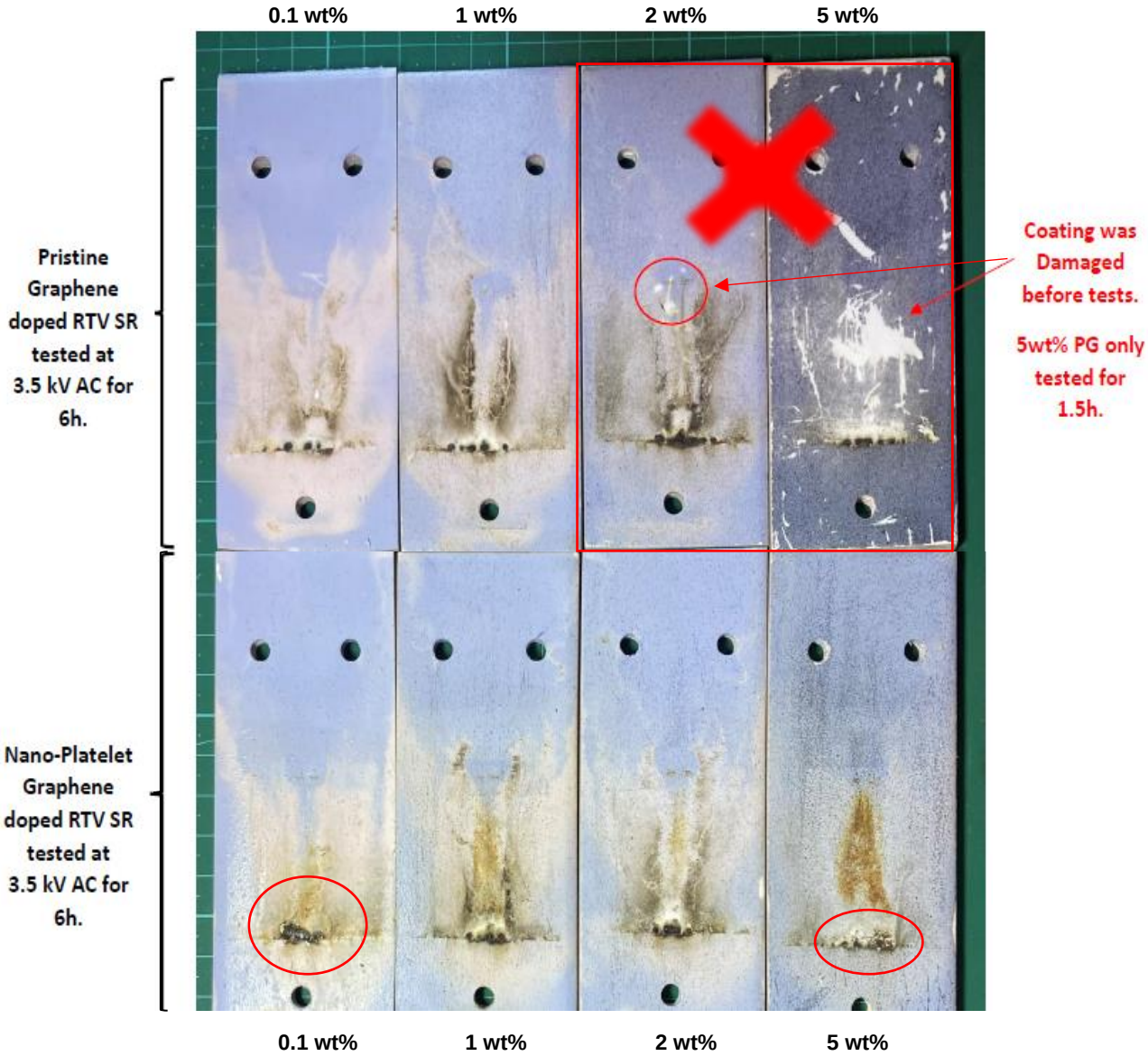

Figure 46: (4 samples above) Photos of Batch 1 PG doped RTV SR coating samples after IPTs. (4 samples below) Photos of Batch 1 NPG doped RTV SR coating samples after IPTs.

No tracking evidence was present on the 5 wt% NPG doped RTV SR coating sample after the end of IPTs. From literature, only erosion of a RTV SR coating causes the ceramic insulator to change back to its uncoated ceramic electrical parameters.

Table 9: Average leakage current measurements from IPT for coating Batch 1.

wt%	Avg. I_{rms} [mA]		Avg. I_{max} [mA] Positive	
	PG	NP	PG	NP
0.1	12.99	14.50	41.83	54.39
1	13.38	15.20	41.13	39.28
2	13.78	15.88	42.00	49.25
5	14.16	18.56	47.36	50.48

Table 9 shows that lower average I_{rms} currents and I_{max} currents were measured for PG doped RTV SR coating samples compared to NPG, this aligns with earlier insulation resistance test results. Overall, the average I_{rms}/I_{max} leakage current increases with an increase in PG/NPG graphene wt% content.

Due to pre-damage of 2 wt% and 5 wt% PG doped RTV SR coating samples, IPT results for Batch 1 PG coatings are inconclusive. No pre-damaged coatings were present in Batch 1 and 2, presented in Chapter 5, for NPG doped RTV SR coating samples.

4.6 Conclusion

- Insulation resistance- and hydrophobicity performance of graphene, i.e., pristine or nano-platelet doped RTV SR coatings has been reviewed. Ceramic tiles coated with a graphene doped RTV SR layer exhibit a lower insulation resistance with an increase in graphene filler weight fraction. Therefore, ASTM D4496-21 [1] test method, which is suitable for measuring electrical resistance of moderately conductive materials is suggested for future experiments. Relatively high (>1000 000 MΩ) specimen insulation resistance steady-state results were obtained using the D257-14 [2] standard as a guideline.

- The hydrophobicity standard deviation results (5.2°) indicate that there may be a need improvement in the contact angle measurement instrumentation used.

- The graphene doped RTV SR coatings used in this experiment did not display any superhydrophobicity characteristics. A lot more research, investigation and field data are necessary to develop such coatings for commercial application.

- Although further measurements must be conducted before a definite conclusion is drawn, using pristine graphene as a filler seem promising in increasing the hydrophobicity of the base RTV SR coating due to an approximate 30° increase in static CA measurements from

90° to 120°. This was to be expected from original, pure, unoxidized pristine graphene compared to the nano-platelet oxidized (hydrophilic in nature) counterpart.

- Based on the literature review, it is concluded that more work is needed to characterize the hydrophobicity transfer, tracking and erosion performance of the graphene doped RTV SR coatings for HV outdoor insulation. IEC and CIGRE test methods to be used are given and will be useful in the performance characterization of these coatings.

- From the results presented in section 4.5.2, there is clear evidence that PG & NPG's good electrical and thermal properties alters the performance of the RTV SR coating, mainly distribution of dry band activity (DBA) and supressing heat generated at one spot.

- The 5 wt% PG sample coating was only tested for 1.5 h due to coating damage beforehand.

- A 0 wt% graphene doped RTV SR coating must be tested to serve as a proper reference to clearly investigate RTV SR coating enhancements/performance changes.

- Severe adhesion problems were noted on PG doped RTV SR sample ≥ 5 wt% and must be investigated. There is uncertainty pertaining the adhesion properties of the PG doped RTV SR coatings. Preparation of another coated tile Batch for laboratory testing may be useful to obtain indication on the long-term performance which include parameters, but not limited to, RTV formulation, filler percentage, optimum surface preparation techniques, role of coating thickness etc.

- Overall thin applied coatings may alter results and therefore no formal conclusion can be made from the modified PG/NPG RTV SR coating Batch 1 test results but was used to guide and improve experimental tests/setup for Batch 2.

5. COATING BATCH 2: EXPERIMENTAL TEST RESULTS FOR NPG DOPED RTV SR

5.1 Background

In the previous chapter, PG and NPG doped RTV SR coatings were investigated with four different experimental test methods (see Figure 17). Some test results concluded that there is a reduction in insulation resistance as the PG/NPG graphene wt% increases. However, all results were not conclusive due to the coating not conforming to a thickness of between 0.3 mm and 0.5 mm as recommended in CIGRE TB 837 [10]. Therefore, a second Batch of NPG graphene doped RTV SR coatings with wt%'s of 0 wt%, 0.1 wt%, 1 wt%, 3 wt%, 5 wt%, and 10 wt% were produced, as shown in Figure 47. Two samples of each wt% was prepared for experimental testing (three samples of 1 wt% was prepared). The coating's wet thickness was increased from approximately 0.07 mm of Batch 1 to approximately 0.45 mm for the new Batch, i.e., Batch 2.

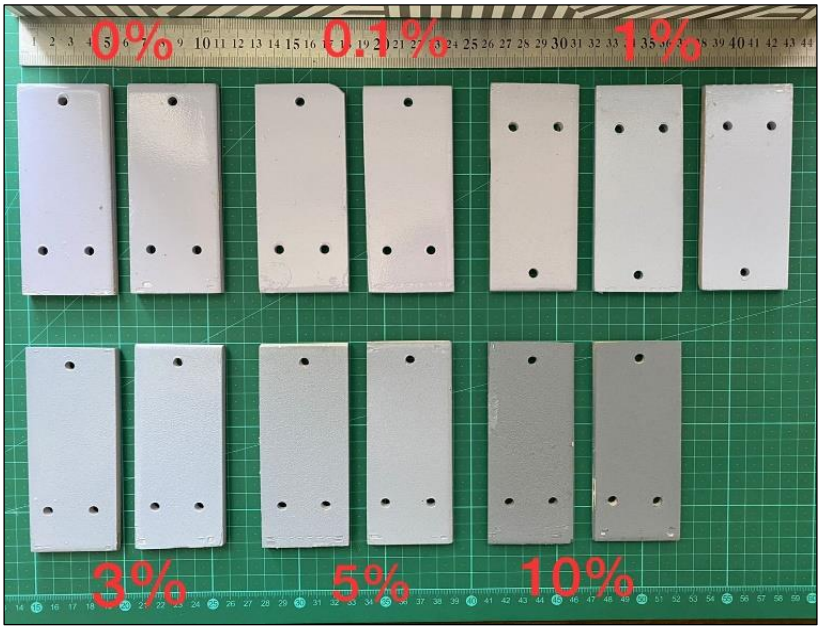

Figure 47: Batch 2 NPG doped RTV SR coated ceramic tiles at approximately 0.45 mm thickness.

From the Batch 1 experiments, it was established that a higher resolution camara must be used for hydrophobicity measurements in order to accurately capture each de-ionised water droplet shape and accurately measure contact angles with ImageJ software. The Leica DMS300 microscope (2.5 MP) was replaced with a Nikon 100D5600 (24 MP) as shown in Figure 48.

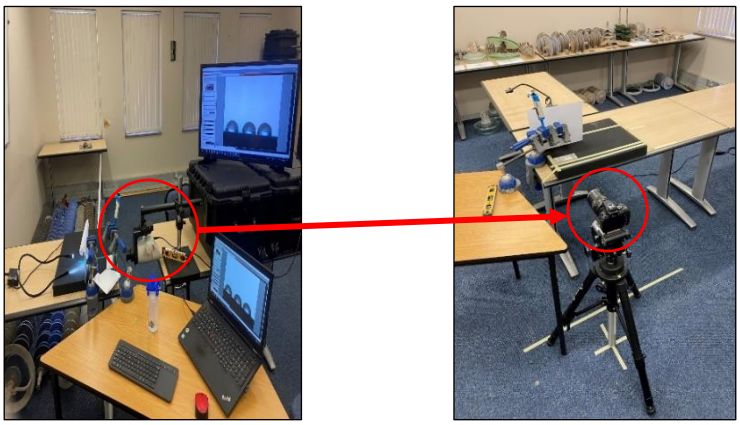

Figure 48: Replacement of Leica DMS300 microscope to Nikon 100D5600 for more accurate hydrophobicity contact angle measurements.

When Batch 2 surface resistivity tests were started, the average resistivity measurements observed were very low compared to test results from Batch 1. Through investigation, it was found that the wooden board surface used for insulation resistance measurements started to conduct between the bolts used to clamp electrodes. Higher humidity levels during the rainy winter months in Cape Town may have caused the damage.

Therefore, the experimental test setup was reconfigured by using plastic spring clamps, as shown in Figure 49 on the right, to secure the steel electrodes onto the tile specimens which rests on an approximately 6 mm thick rubber surface as seen below. The surface resistivity tests then produced valid results.

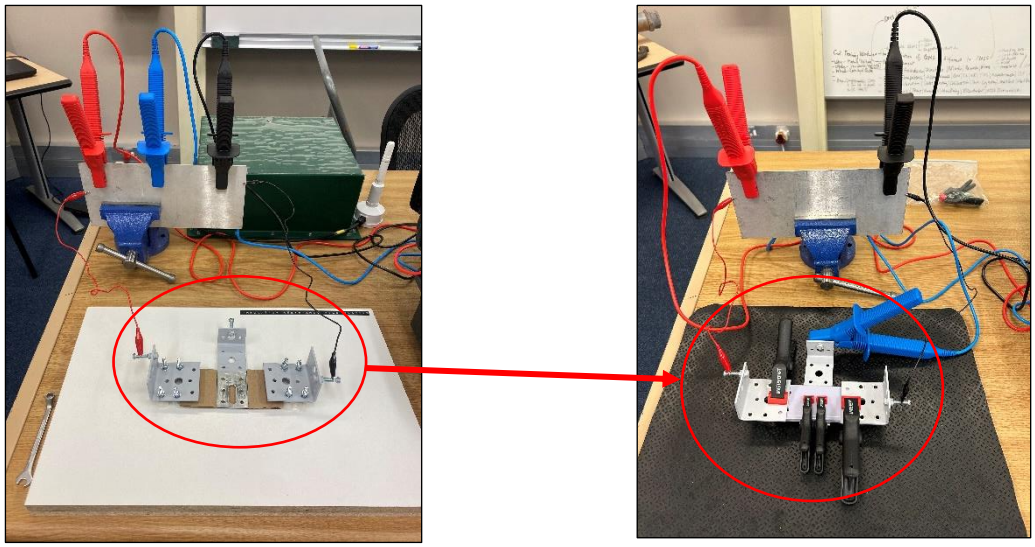

Figure 49: Newly adopted surface resistivity experimental test setup.

5.2 Surface Resistivity Tests

The goal of the surface resistivity tests was to determine if the approximative NPG doped RTV SR coatings still exhibit adequate electrical insulation resistance properties. From the graph presented in Figure 50, the surface resistivity drops exponentially from approximately 6.88 TΩ/cm^2 to approximately 0.15 TΩ/cm^2 (97,82% decrease) when increasing to 10 wt% NPG.

The standard deviation is also indicated on graph with error bars which was calculated from 12 datapoints (both samples for each NPG wt% combined) over a 2-day period. The standard surface resistivity deviation was very small for the RTV SR virgin sample and > 5 wt% NPG samples, indicating that the test method is stable and repeatable. However, the standard surface resistivity deviations for 0.1 wt% ≤ NPG ≤ 3 wt% were more "unstable". Possibly due to mixing imperfections in the mixing and application process (imperfect dispersion of graphene nanoplatelets was seen from microscope photos between samples at a similar wt%).

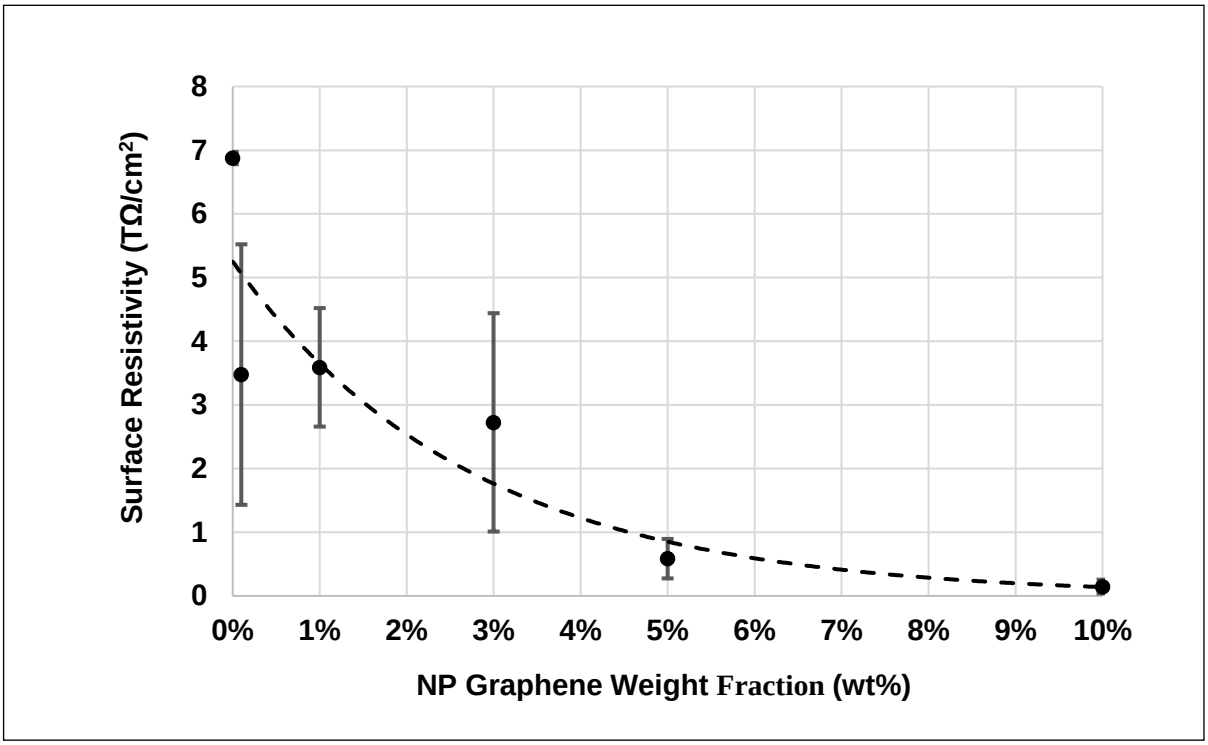

Figure 50: Surface resistivity (TΩ/cm^2) vs weight fraction (wt%) at a 5 kVDC test voltage for an NPG doped RTV SR coating (≈0.45 mm thick.) applied on a ceramic tile.

Finally, it was again clear that NPG enhances the flow of electrical charge within the modified coating as seen from the surface resistivity test results. From the electrical current results, an average of 350 µW of power dissipated during the 10 wt% NPG surface resistivity tests. The surface resistivity test method's accuracy can be improved by refining the dispersion of graphene at 0.1 wt% > NPG < 5 wt% and improving the test apparatus shown in this report, e.g., electrode design, build etc.

5.3 Hydrophobicity Tests

The extent of hydrophobicity can be estimated by evaluating the water droplet static CA variations between each NPG doped RTV SR sample as recommended in IEC 62073 [3]. Test methods (1 and 3) were performed on a stable horizontal surface and the results thereof are discussed in the following sections. If the static CA of the material increases above 90°, it indicates that the material is hydrophobic or >150° it is superhydrophobic.

5.3.1 Static Contact Angle Measurements

Twelve static CAs (method 1) were measured for each NPG wt% sample from 50 µl de-ionised water droplets, after placing each droplet with a micropipette on a clean sample's top surface in a controlled environment (known as the Sessile drop technique). The water droplet shape depends on the material of the sample and the physical and chemical states of its surface [4]. ImageJ software was then used to determine the static CA measurements/drop shape analysis with 3 decimal precision from high resolution (24 MP) black\white contrast photos within approximately 3 s. The results are shown in the graph in Figure 51. It was found that there is about approximately 10° difference between the RTV SR and 10 wt% NPG doped SR surface static CA measurements. Therefore, indicating a slight increase in hydrophobicity of the unfilled RTV SR coating. The standard deviation is also calculated from twelve measurements at each wt% over a 2-day period.

The standard deviation also shows an increase in static CA measurements for an increase in NPG wt%.

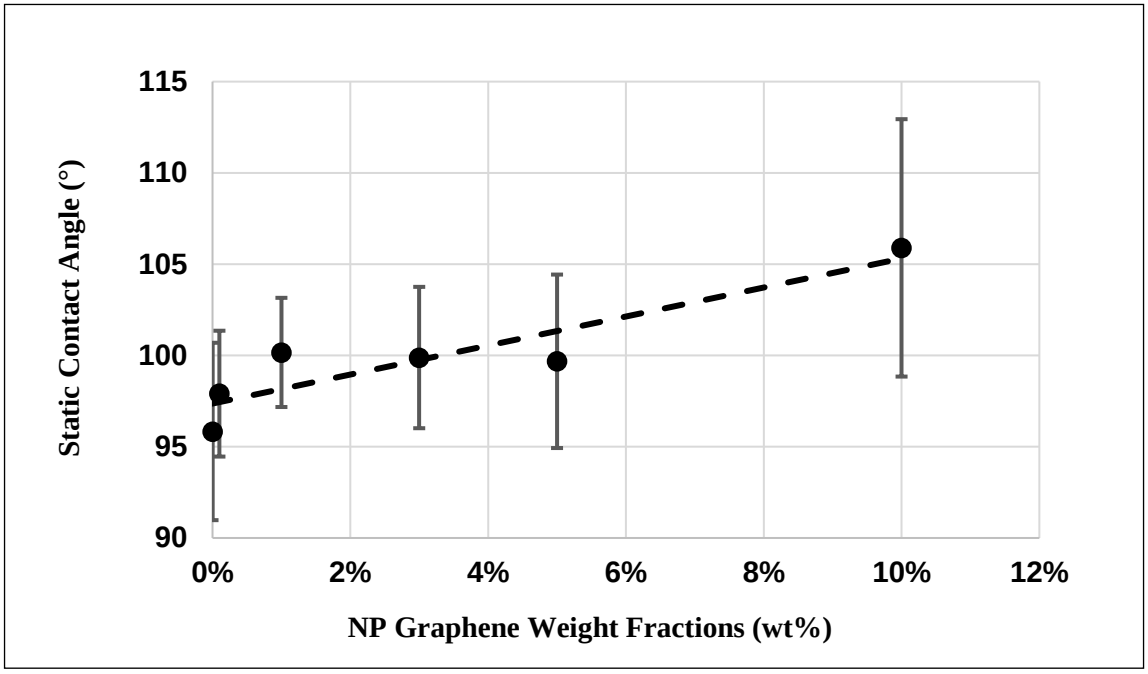

Figure 51: Static CAs (°) vs weight fractions (wt%) for an NPG doped RTV SR coating (≈0.45 mm thick.) applied on a ceramic tile.

Figure 52 and Figure 53 proves from a visual perspective that the water droplet shape changes on the coating's surface during static conditions for an increase of NPG wt% into the RTV SR matrix.

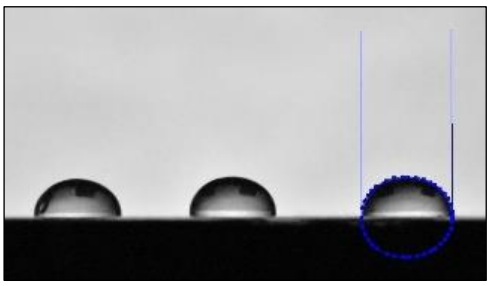

Figure 52: RTV SR reference coating black/white contrast photo with 50 µl water droplet shape at position 3.

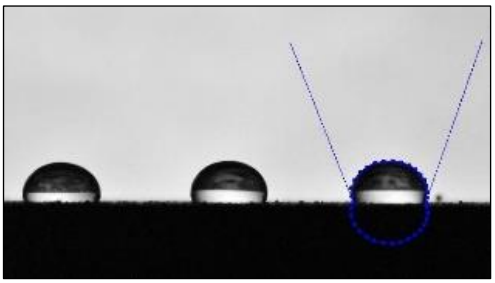

Figure 53: RTV SR reference coating black/white contrast photo with 50 µl water droplet shape at position 3.

The accuracy of the hydrophobicity performance test method used in this project can be improved by using software and hardware which are integrated together to measure receding angles (better indication of hydrophobicity level) and increase repeatability of results, e.g., water droplet placement without any disturbances and precise 2D-CAD water droplet shape modelling.

5.3.2 Wettability Class Measurements

The spray bottle test (method 3) given in IEC 62073 [3] was used to determine the WC of each sample at different NPG wt%. De-ionised water droplets were sprayed from a distance of 20±10 cm for 30 seconds onto each sample's top surface, 10 seconds thereafter, a high-resolution photo was taken, as shown in Figure 54 and Figure 55. After comparing the photos to the reference table given in IEC 62073 [3], a WC of 1 was measured for all samples. Unfortunately, this test method could not reveal the slight increase in hydrophobicity as the NPG wt% increases.

Figure 54: RTV SR reference (left), 0.1 wt% NPG doped RTV SR (middle) and 1 wt% NPG doped RTV SR coating's spray bottle test method results by using IEC 62073 [3].

Figure 55: 3 wt% NPG doped RTV SR (left), 5 wt% NPG doped RTV SR (middle) and 10 wt% NPG doped RTV SR coating's spray bottle test method results by using IEC 62073 [3].

5.4 Hydrophobicity- Recovery and Transfer Tests

Two sets of experiments were implemented to measure Hydrophobicity- Recovery (HR) and Transfer (HT) properties respectively. At first, it was very difficult to retrieve any HT results with a approximately 0.07 mm coating thickness (Batch 1) and approximately 0.35 mm pollution layer thickness with CIGRE TB 442 [4] as a guideline. The hypothesis was that a 0.45 mm coating thickness (Batch 2) will increase the amount of LMW silicone fluid present within the bulk material of the coating. However, no HT results were obtained for Batch 2 after 2 days with a 0.35 mm pollution layer thickness. Therefore, the HR test method below was implemented and used as a test run to see if any HR even occurs with a very thin pollution layer.

5.4.1 Hydrophobicity Recovery Measurements

A thin pollution layer of Sikron SF600 silica powder (3 µm grain size) was gently applied onto each sample's top surface by means of a paint brush. Immediately thereafter, a 10 µl de-ionised water droplet was applied to the coating's polluted surface and two static CA measurements were taken by use of the test method given in Section 3.4.

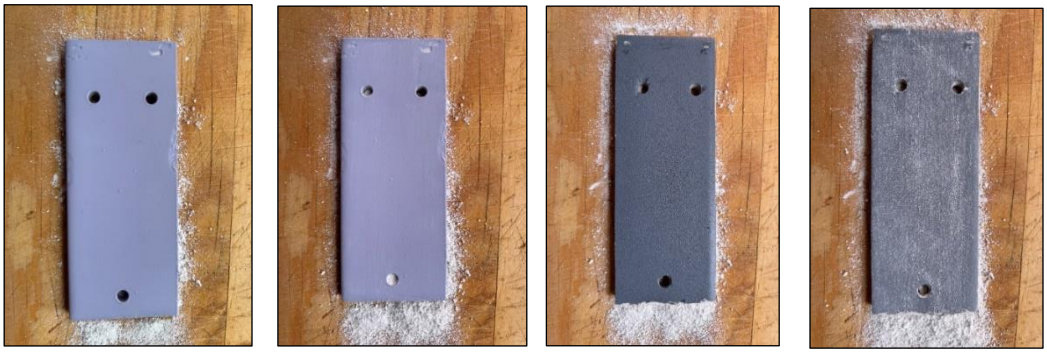

Figure 56: Before and after application of Sikron SF600 silica powder pollution layer by paint brush on RTV SR (left) and 10 wt% NPG doped RTV SR (right).

High resolution photos of water droplet shapes at 0 h and 1 h are shown in Figure 57 for RTV SR reference and 10 wt% NPG doped RTV SR coating samples respectively. Figure 58 presents the average static CA measurements for each sample at different NPG wt% after 0 h/ 1 h of hydrophobicity recovery. The dashed red line represents the average static CA measurements, produced in Section 5.3.1, and is used as a threshold for this HR experiment. From Figure 58, after 1 h the RTV SR reference coating static CAs recovered from approximately 70° to approximately 95° and the NPG 10 wt% from approximately 70° to approximately 118°.

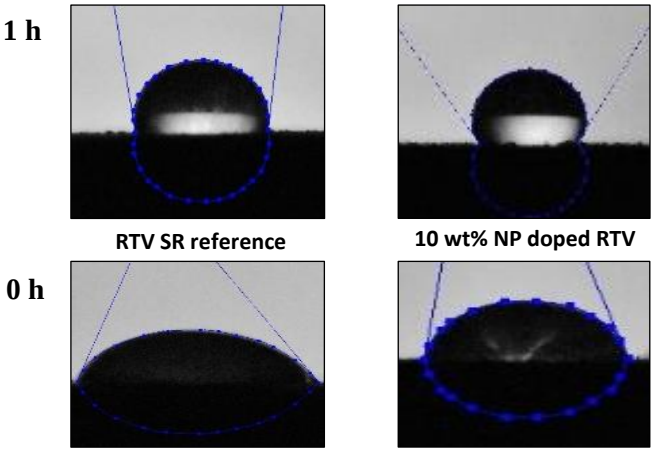

Figure 57: Water droplet shapes at 0 h and 1 h after application of Sikron SF600 silica powder pollution layer by paint brush on RTV SR (left) and 10 wt% NPG doped RTV SR (right) coatings.

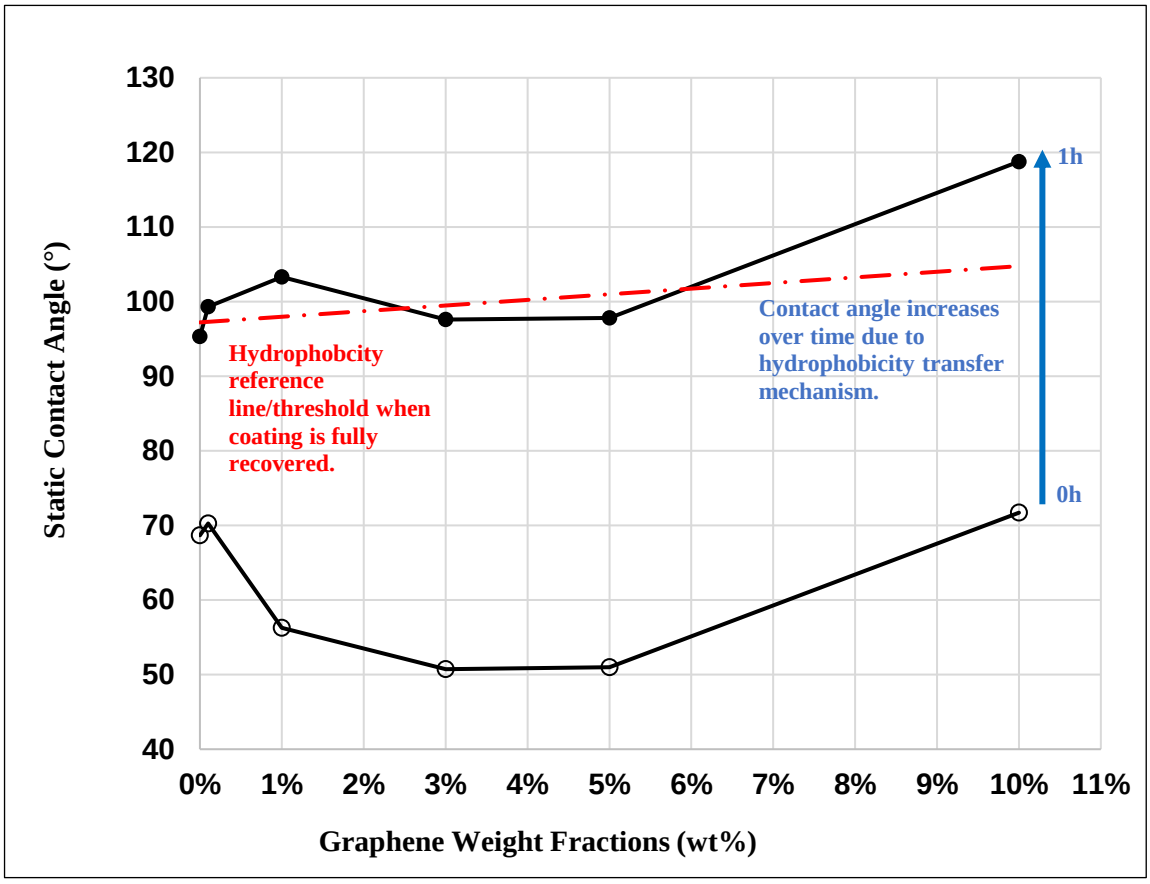

Figure 58: Hydrophobicity recovery test run results for all samples.

This HR test run may have shown that the HT mechanism is still present, however the test method used itself is not repeatable due to difficulty of applying a similar pollution layer thicknesses by paint brush. Therefore, the following section used a specific HT test method, CIGRE TB 442 [4], which is more repeatable and reliable for LMW silicone transfer experiments.

5.4.2 Hydrophobicity Transfer Measurements

A slurry type pollution layer was applied onto each coated tile's surface consisting of a Sikron SF600 silica powder and Iso-Propyl Alcohol (Isopropanol: 85%; Ethanol:15%) solution mixed together. A pollution layer thickness of approximately 0.07 mm thick was measured by the application of one adhesive foil window onto each coating's top surface representing the total pollution layer thickness. A thinner pollution layer thickness (reduced from 0.35 mm to 0.07 mm) was chosen to allow the amount LMW silicones available within the bulk layer of the material in coatings to diffuse quicker.

An HTV SR composite material, RTV SR coating (approximately 0.45 mm thick.) and 10 wt% NPG RTV SR coating (approximately 0.45 mm thick.) test samples were used in this HT experiment. The graph in Figure 59 shows the CA measurements made at 0 h, 25 h, 44 h, 65 h and 91 h for each sample. All the samples recovered to approximately 99% within the first 25 hours and static CA measurements settled after approximately 65 h. A static CA measurement difference

of approximately 10° was again noted at 65 h and 91 h between the RTV SR reference and 10 wt% NPG doped SR samples, which was also evident in measurements from Section 5.3.1. The standard deviation between two static CA angle datapoints are also shown for each time interval. It was noted that there was a decrease in static CA measurement for RTV SR coating at 44 h, which may be due to the pollution layer being slightly thicker than other measurement locations, slowing down HT.

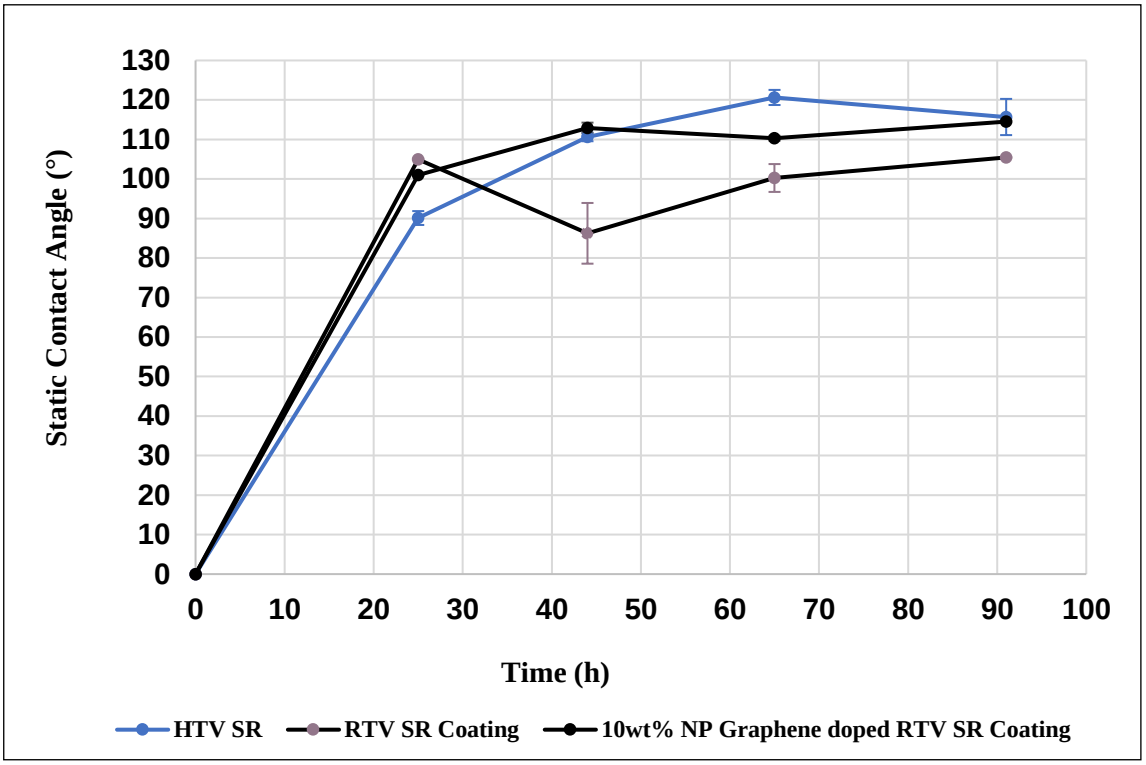

Figure 59: Hydrophobicity transfer static CA test results for HTV SR composite material, RTV SR coating (≈ 0.45 mm thick.) and 10 wt% NPG RTV SR coating (≈ 0.45 mm thick.) at 0 h, 25 h, 44 h, 65 h and 91 h.

The photos shown in Figure 60 prove that the 10 µl water droplet shapes did remain stable on each pollution layer after 65 h, signifying LMW silicones have diffused into the pollution layer and encapsulated the pollution particles. Finally, it can be concluded that the NPG particles does not inhibit the hydrophobicity transfer mechanism of the RTV SR coating with NPG weight fractions >0.1 wt%.

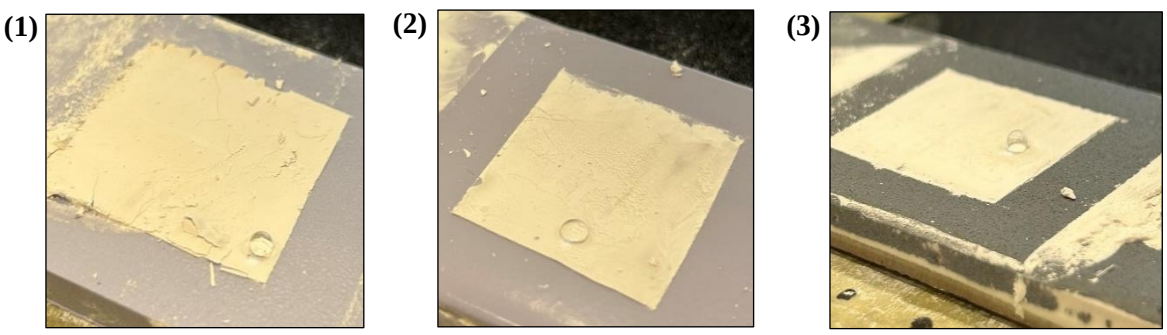

Figure 60: 10 µl Water droplet placement on pollution layers (≈0.07 mm thick.) for (1) HTV SR composite material, (2) RTV SR coating (≈ 0.45 mm thick.) (2) and (3) 10 wt% NPG RTV SR coating (≈ 0.45 mm thick.) after 65 h, signifying HT.

5.4.3 Hydrophobicity Transfer Test Results Discussion and Hypothesis

From the previous sections it was proven that the diffusion of LMW silicones is not inhibited by NPG particles doped within the RTV SR matrix and the hydrophobicity transfer mechanism remains present. As seen earlier, higher static CA measurements for the 10 wt% NPG doped RTV SR coating were measured compared to the RTV SR virgin coating. Now, a concept/hypothesis has come to light due to this phenomenon.

Graphene is a two-dimensional, atomically thick sp_2 carbon atom sheet organized in a honeycomb configuration as shown in grey in Figure 61 [28][47]. Graphene/natural rubber nanocomposites were also prepared and studied by J. Dong et el. [28]. The study suggests that strong interfacial interactions were present between the nano filler particles, graphene oxide, and the rubber matrix after performing mechanical tests, determining molecular dynamics, investigating strain induced crystallization.

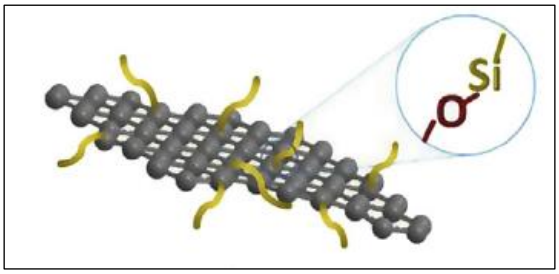

Figure 61: Graphene oxide and Silicone-Oxide interfacial interaction [48].

If there is a chemical and physical crosslink between the NPG sheets (stacked on top of each other) and this RTV SR rubber matrix, then the following hypothesis is proposed:

When hydrophobicity transfer [49] occurs on an NPG doped RTV SR coating surface, many LMW silicones are physically entangled within free floating NPG sheets and crosslinked by means of van der Waals forces, throughout the bulk material and being transferred together as a “package” to encapsulate a pollution particle, as illustrated in Figure 62. Better HT results are expected for a pollution layer applied on 10 wt% NPG RTV SR coating compared to a pollution layer applied on a virgin RTV SR coating.

The LMW silicones i.e., wears a “scratchy” jacket of graphene nanosheet particles (forming a package) and increases its the surface roughness, lowers the surface tension and improves the hydrophobic state of the encapsulated pollution particle over time until steady state is reached.

Lastly, if NPG has a good bonding affinity with the rubber matrix, the overall void volume of NPG coatings may have decreased, and the amount of LMW fluid available may not have decreased with an increase in NPG wt%.

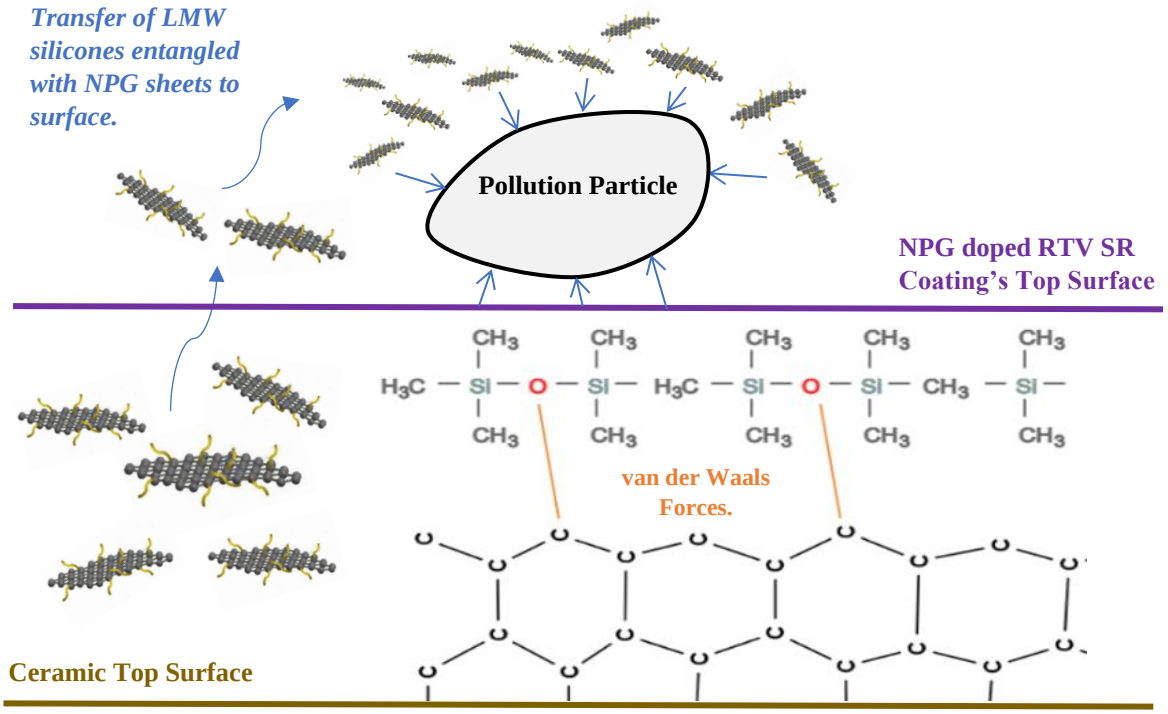

Figure 62: Illustration of how NPG doped RTV SR bulk material LMW silicones and NP graphene has nanosheet particles entangled and bonded together by van der Waals forces, forming small packages, which then migrates via HT to the pollution particle, finally encapsulating it .

5.5 Tracking and Erosion Resistance Tests

5.5.1 Visual Observations and Measurements

Tracking and erosion (accelerated ageing) resistance tests were performed with NPG doped RTV SR coatings using an Inclined Plane Tester (IPT) (see ANNEXURE D) according to IEC 60587 [5]. Four coatings (thickness of approximately 0.45 mm) with different NPG doped RTV SR weight fractions (0 wt%, 3 wt%, 5 wt% and 10 wt%) applied on approximately 6.7 mm ceramic thick tiles and were tested at an AC excitation voltage of 3.5 kV. DC excitation voltage tests were not performed, due to being more destructive than AC, which may produce inconclusive results for this investigation. The coating experiences thermal degradation over time from high temperatures caused by DBA activity.

A solution of 0.1 % ± 0.002 % Ammonium Chloride and 0.02% ± 0.002 % isooctylphenoxypolyethoxyethanol (Triton X-100) with a conductivity of 2.53 mS / cm was used during tests at a flowrate of 0.6 ml/min. The following visual observations were made for the RTV SR reference and the 10 wt% NPG doped RTV SR coatings during IPT tests (also see Figure 63):

1. Severe electrical discharge activity near earth (cathode) electrode of 10 wt% NPG doped RTV SR coating. Small explosive sounds were also heard from the 10 wt% NPG doped

RTV SR coating's surface during DBA activity and discharging events near earth electrode.

2. Severe combustion, ignition and electrical discharge activity near earth electrode of 10wt% NPG doped RTV SR coating.
3. Most severe tracking and erosion burning activity stretching from cathode to anode (after 13 minutes) on 10 wt% NPG doped RTV SR coating (left). Only DBA present on RTV SR coating reference surface (right).

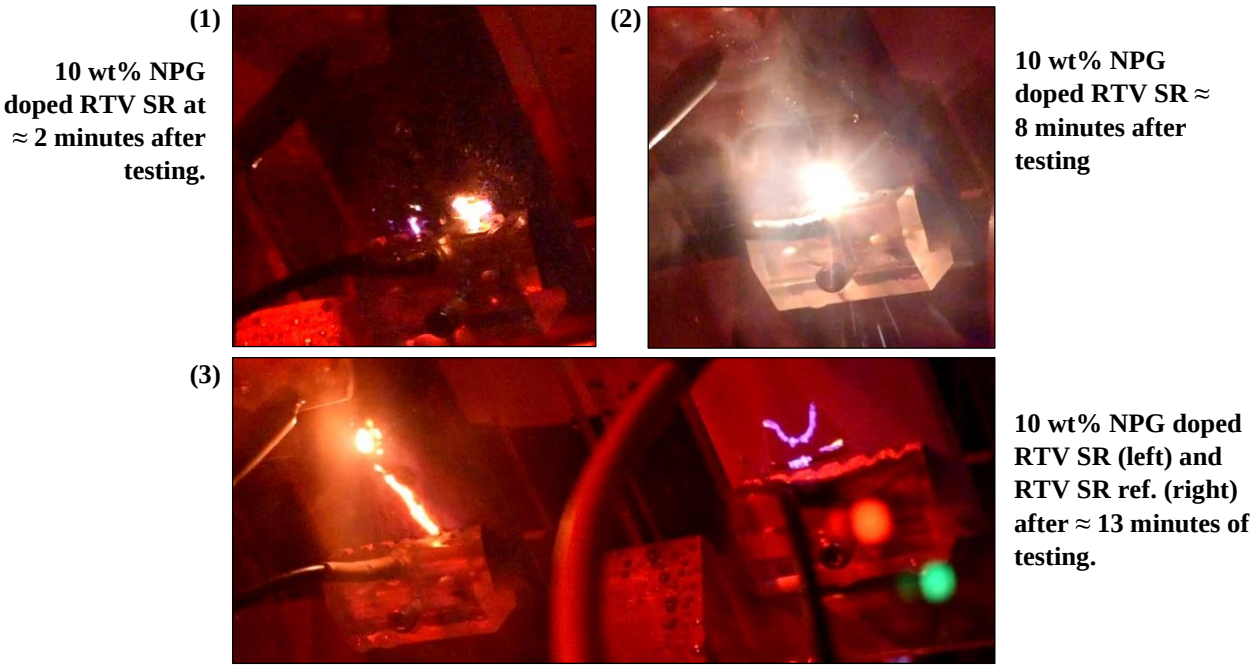

Figure 63: Combustion, ignition and electrical discharge activity on 10 wt% NPG doped RTV SR coating (top: both and bottom: left) and DBA activity on RTV SR reference coating (below: right) during IPTs at 3.5 kVAC.

The NPG doped RTV SR coatings did not survive the IPT within the first approximately 14 minutes of testing. and Table 10 and Figure 64 contains the tracking and erosion results from the IPTs. Tracking lengths were measured, erosion results were compared and determined from the commonly used SEDIVER Coating Erosion Class guide [26].

Table 10: IPT test time and tracking length results for NPG doped RTV SR coatings for 0 wt%, 3 wt%, 5 wt% and 10 wt%.

NPG Weight Fraction [wt%]	Test Time [min]	Tracking Length [mm]	SEDIVER Coating Erosion Class	Comment
0	13	0	CE0	No tracking or erosion present. Slight blackening of material near earth electrode. Entire IPT test was stopped at 13 minutes due to the excessive failing of 10 wt% NPG doped RTV SR sample.
3	15	30	CE5	Severe tracking and erosion up to support material of coating caused by combustion, DBA and burning events. Specimen failed the test.
5		20	CE5	Severe tracking and erosion up to support material of coating caused by combustion, DBA and burning events. Specimen failed the test.
10	13	42	CE5	Severe tracking and erosion of coating up to support material caused by combustion, DBA and burning events. Specimen failed the test.

5.5.2 IPT Results Discussion

The NPG doped RTV SR coating test specimens shown in Figure 64 had a noticeable tendency to ignite/combust compared to the RTV SR reference coating during IPTs. The white powder shown in Figure 64 is the by-product of the thermal decomposition process of the ATH also contained within the rubber matrix and releases water of hydration during severe electrical discharging events.

The highest wt% NPG doped RTV SR coating (10 wt%) as seen in the IPT results, Table 10, produced the longest tracking length of 42 mm from the cathode, exceeding the anode, and had the shortest test time of 13 minutes compared to the 3 wt% NPG and 5 wt% NPG doped RTV SR coatings which produced shorter tracking lengths of approximately 35 mm at a slightly longer test time of 15 minutes. Lastly, the virgin RTV SR reference coating had no signs of severe material degradation after 13 minutes of tracking and erosion testing.

The IPTs thus showed that an increase in NPG wt% into this specific RTV SR mixture increases the severity and speed of the thermal combustion process of the ATH filler. A similar discovery was made by C. Wang et.al. [50] in Section 3.3 were a compounding mixture of and ATH and NPG (ATH/NPG) thermogravimetric analysis curves were determined. C. Wang et.al results

concluded that the thermal decomposition of ATH/NPG imitates at a lower temperature in comparison to ATH [50].

0 wt% NPG doped RTV SR after 13 minutes

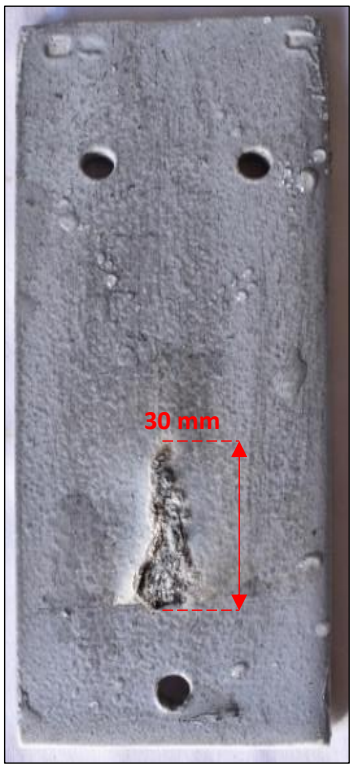

3 wt% NPG doped RTV SR after 15 minutes

5 wt% NPG doped RTV SR after 15 minutes

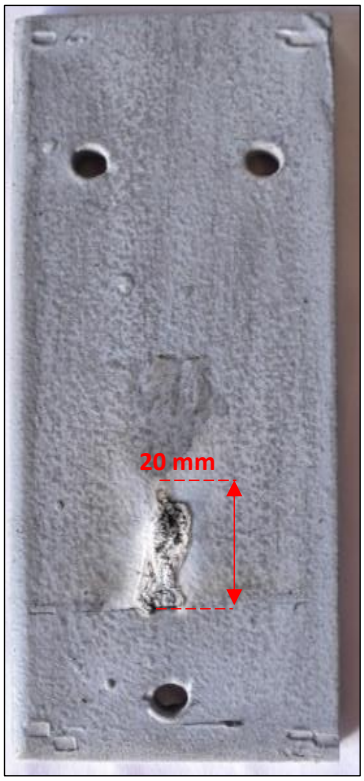

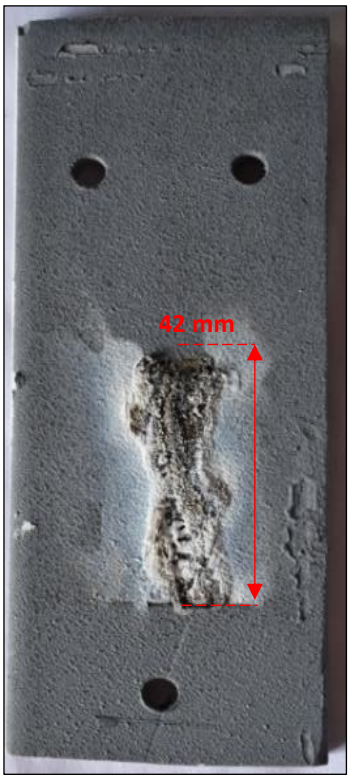

10 wt% NPG doped RTV SR after 13 minutes

Figure 64: RTV SR reference, 3 wt% NPG doped RTV SR, 5 wt% NPG doped RTV SR and 10 wt% NPG doped RTV SR after IPTs.

6. FINAL CHAPTER

6.1 Answers for Hypothesis and Research Questions

6.1.1 Hypothesis

The hypothesis states that PG/NPG graphene has the potential to enhance the electrical performance of RTV SR coatings and improve pollution performance properties when compared to traditional coatings used on ceramic insulators.

Supporting evidence:

1. The evaluation of hydrophobicity, recovery, and transfer properties showed promising results, including an increase in static contact angle measurements for both PG and NPG. The presence of hydrophobicity recovery and transfer mechanisms was evident with the addition of NPG.
2. A new hypothesis, from experimental data, suggests that if there is a physical entanglement and/or interfacial interaction between the LMW silicones and the NP graphene sheets, the pollution layer will develop a similar hydrophobicity level to that of a clean graphene-doped coating surface after a certain amount of time.

Disadvantage found from insulation resistance and accelerated ageing tests:

1. It was presented that PG/NPG doped RTV SR coatings showed a significant reduction in insulation surface resistivity compared to the reference RTV SR coating. This indicates a decrease in electrical insulation resistance, which is crucial for preventing flashovers caused by pollution deposits.
2. The conclusion also mentions that the addition of NPG particles to the RTV SR mixture lowers the combustion temperature of the ATH filler, resulting in faster ignition of material during electrical discharging events, found in IPTs.

6.1.2 Research Question

What is the optimal dispersion concentration of PG and NPG filler in a RTV SR host to achieve significant improvements:

1. …in **pollution performance** to those of superhydrophobic coatings on AC high-voltage ceramic insulator materials?

   Approximately 5 wt% PG and 10 wt% NPG increases the static CAs with of the modified coatings with approximately 30° and 10° respectively which both is not above > 150°, thus not superhydrophobic.

   Hydrophobicity- recovery and transfer mechanism was happily not inhibited by the addition of NPG into RTV SR coating samples, a crucial mechanism required from polymeric insulation materials to improve pollution performance.

2. …in **electrical properties** comparable to those of superhydrophobic coatings on AC high-voltage ceramic insulator materials?

   NPG doped RTV SR material combusts/ignites during IPTs at concentrations above > 3 wt% as explained in Chapter 5.

   Doping PG into RTV SR still requires further investigation into its electrical properties, i.e., IPTs.

   From experiments, insulation surface resistivity decreases for both PG and NPG doped RTV coatings as graphene wt% increases.

6.2 Conclusion

Important properties from the modern day polymeric composite insulators such as surface resistivity, hydrophobicity, hydrophobocity transfer/recovery, tracking and erosion resistance were used to investigate and evaluate the performance of the PG and NPG doped RTV SR coatings at different wt%'s. The research methodology given and setup in Figure 4 was a good guideline to develop and the modify the virgin RTV SR insulator coating.

From an electrical insulation resistance perspective, the NPG doped RTV SR coatings >3 wt% had more than twice the reduction in insulation surface resistivety compared to the reference RTV SR coating. From the inclined plane tests, it was also confirmed that an addition of NPG particles to this RTV SR mixture lowers the combustion temperature of the ATH filler and therefore ignites the NPG filled coating at a faster rate during electrical discharging/DBA events. It also seems that a thicker RTV SR coating with NP graphene as a filler increases the combution probability.

Good performance was obtained from evaluating the hydrophobcity-, recovery and transfer properties, in this project. A approximately10% increase in static CA measurements were found for a 10 wt% NPG compared to the unfilled RTV SR coating. Both the hydrophobicity- recovery and transfer mechanisms were still present with an addition of NPG into the RTV SR matrix.

After hydrophobicity transfer, comparable "large" static contact angles were measured as with a clean 10 wt% NPG doped RTV SR coating surface. Hence, a hypothesis has been derived that if there is a physical entanglement and/or interfacial interaction between LMW silicones and the free floating NPG sheets within the bulk layer of the modified coating material (by means of van der Waals forces), then the NPG sheets are transferred along with the LMW silicone fluid as a package to the surface during HT and encapsulates the pollution particles. Resulting the pollution layer to develop a similar hydrophobicity level to that of a clean NPG doped RTV SR coating surface after a certain amount of time.

Finally, the finalised MTR design will allow Eskom to build, commission, operate, maintain and perform further insulation research work in a natural severe marine environment, enabling Eskom to regain its position as a leading institute in high voltage insulator research. More insight can then be obtained in the operation of high voltage insulators, leading to improved design and selection of insulators for the distribution and transmission networks.

6.3 Recommendations

- Modify and setup the inclined plane tester to evaluate hydrophobicity- resistance and transfer principles according to CIGRE TB 837 [10].

- Research alternative fillers and chemical methods which will not decrease the combustion temperature of the ATH filler when adding NPG.

- Perform thermogravimetric analysis of modifed coating and study the chemical and physical phenomena as a function of weight vs. temperature in a heated oxygen/nitrogen atmosphere [10]. Thereafter compare the thermogravimetric analysis results to the IPT results.

- Heat up the modified coating for different temperatures and wt%'s. Compare hydrophoobicity level/changes.

- When, a modified coating has passed methods 1. to 4. in Figure 4 (preliminary tests), outdoor pollution performance- and ageing tests of the candidate coatings must then be performed in a natural severe marine environment in accordance with the IEC 60815 [34] and CIGRE TB 361 [29].

- Further investigate the LMW silicones and NPG hydrophobicty transfer "package" hypothesis presented in this research by other means, e.g., the Soxhlet test, which can produce quantitative measurements for the extraction of LMW left in silicone. Also investigate pollution particle surface.

- Measure the thickness and homogeneity of the dried pollution layer more accurately with a laser profilometer and to the thicknesses produced from the adhesive foil method.

- Perform Scanning Electron Microscopy (SEM) studies to determine the morphological features, chemical interactions within the SR matrix and characteristics of the modified coating samples [5].

- Improve NPG mixing and dispersion quality into RTV SR coatings. NPG is cheaper and easier to prepare than PG and brings down costs of the modified coating tremendeously. It is recommended to explore the optimum use of NPG as a filler compared to expensive PG filler.

- Addressing the need for standardised tests to evaluate RTV SR coatings on ceramic insulator materials is still crucial. While the IPT method was used in this study to assess tracking and erosion resistance, further research is necessary to establish specific testing protocols for RTV SR coatings. Future work should focus on investigating and validating appropriate testing methodologies that simulate real-world operating conditions, including environmental factors like temperature, humidity, and pollution levels. Additionally, exploring the correlation between laboratory-based tests and field performance through long-term field studies can provide valuable insights into coating durability, pollution resistance, and overall electrical performance. Collaboration among researchers, industry experts, and regulatory bodies is vital to develop consensus-based testing procedures that are widely accepted and adopted by the industry. By conducting further research on standardised tests, this study will contribute to advancing the field, supporting the development

of reliable testing protocols, and promoting the widespread adoption of RTV SR coatings for effective pollution mitigation in high-voltage electrical systems.

- It is evident that graphene appears to enhance the electrical conductivity properties of base RTV SR coating. Therefore, a notion surfaced that a semi-conductive coating material which can govern a small leakage current along the doped conductive graphene flakes, may possibly heat up the insulator's surface and prevent fog, mist, light rain, or snow from forming, therefore preventing flashover. From literature resistive glazed porcelain insulators exhibits semi-conductive characteristics.

6.4 Future Work

Further investigate, evaluate, and compare the experimental test results of the PG doped RTV SR samples with the results of the NPG doped RTV SR samples. This comparative analysis will provide valuable insights into the influence of different types of graphene powders (PG and NPG) on the pollution performance and electrical properties of the coating. By systematically examining and comparing the performance of the two types of graphene-doped coatings, a comprehensive understanding of their respective advantages and limitations can be obtained.

The investigation should include various key performance parameters such as insulation resistance, hydrophobicity, hydrophobicity transfer, and tracking and erosion resistance. These parameters should be measured and analysed for both the PG and NPG doped RTV SR samples under similar test conditions and pollutant exposure. This knowledge can be used to guide the selection and optimisation of graphene materials for future applications in high-voltage insulation systems.

Moreover, the findings can be utilised to develop guidelines and recommendations for the design and formulation of graphene-doped coatings tailored to specific environmental conditions and performance requirements. This will contribute to the development of advanced and reliable insulation solutions for HVAC ceramic insulators, enhancing their resistance to pollution and improving their overall electrical performance.

Overall, investigating, evaluating, and comparing the experimental test results of PG and NPG doped RTV SR samples will provide valuable insights and pave the way for further advancements in the field of graphene-based coatings for electrical insulation applications.

In addition to the future work recommendations, it is highly recommended to investigate and study the corona activity between different weight wt%'s of graphene-doped room temperature vulcanised RTV SR. Corona activity refers to the phenomenon of partial discharge or electrical discharge occurring in the presence of high voltage gradients.

The study of corona activity can provide valuable insights into the electrical performance and breakdown characteristics of the graphene doped RTV SR coatings. By varying the wt%'s of graphene powder dispersed into the SR host, it is possible to examine the impact of different concentrations on corona inception voltage, corona discharge intensity, and corona extinction voltage.

REFERENCES

[1] ASTM: D4496-21, “Standard Test Method for D-C Resistance or Conductance of Moderately Conductive Materials”, 2021.

[2] ASTM: D257-14, “Standard Test Methods for DC Resistance or Conductance of Insulating Materials”, 2014.

[3] SANS/IEC: 62073, “Guidance on measurement of wettability of insulator surfaces”, Edition 1.0, 2003.

[4] CIGRE TB442, “Evaluation of Dynamic Hydrophobicity Properties of Polymeric Materials for Non-Ceramic Outdoor Insulation”, Working Group D1.14, December 2010.

[5] SANS/IEC: 60587, “Electrical insulating materials used under severe ambient conditions – Test methods for evaluating resistance to tracking and erosion”, Edition 3.0, 2007-05.

[6] B.S. Limbo, “Insulator Ageing with HVAC and HVDC Excitation using the Tracking Wheel Tester”, MSc Thesis, 2009.

[7] Guide 1, 92/1, “Hydrophobicity Classification Guide” STRI, 1992.

[8] W. Vosloo, “A Comparison of the Performance of High Voltage Insulator Materials in a Severely Polluted Coastal Environment”, PhD Thesis, March 2002.

[9] W. Vosloo, R. Davey, “Power Utility Perspective on Natural Ageing and Pollution Performance of Outdoor Insulators”, IEEE Electrical Insulation Magazine Vol. 36, No. 4, 2020.

[10] CIGRE TB837, “Coating for improvement of electrical performance of outdoor insulators under pollution conditions”, Working Group B2.69, June 2021.

[11] Arshad, G. Momen, M. Farzaneh and A. Nekahi, “Properties and Applications of Super hydrophobic Coatings in High Voltage Outdoor Insulation: A Review”, TDEI, 2017.

[12] Y.Y. Quan, and L.Z. Zhang, “Facile fabrication of superhydrophobic films with fractal structures using epoxy resin microspheres”, Appl.Surf:Sci., vol. 292, 2014.

[13] I. Karapanagiotis, D. Grosu, D. Asianidou and K.E. Altantis, “Facile method to prepare superhydrophobic and water repellent cellulosic paper”, J.Nanometer, vol. 2015, 2015.

[14] Z. Guo, W. Liu and B. Su, “Superhydrophobic surfaces: From natural to biomimetic to functional”, J.Colloid Interface Sc., vol. 353, 2011.

[15] S. Seyedmehdi, H. Zang and J. Zhu, “Superhydrophobic RTV silicone rubber insulator coatings”, Appl.Surf:Sci, vol. 258, 2012.

[16] A. Seyedmehdi, H. Zhang and J. Zhu, “The role of ATH in superhydrophobic silicone rubber coatings for High Voltage insulators”, in 28th International Power Sytem Conference, 2013.

[17] S.M. Braini, A. Haddad, and N. Harid, “The performance of nano coating for High Voltage Insulators”, in 46th International Universities Power Engineering Conference, 2011.

[18] T. Omote, M. Abe, K. Nose, M. Kasatani, M. Meda and K. Hondo, “Investigation on prevention of corona audible noise for contaminated insulators”, in The 20th International Conference on Electrical Engineering, 2014.

[19] I. Ramalla, B.K. Gupta and K. Bansal, “Effect on superhydrophobic surfaces on electrical porcelain insulator, improved technique at polluted areas for longer life and reliability”, Int.J.Eng.Technol., vol. 4, no. 4, 2015.

[20] F. Wang, G. Wen, F. Fan, T. Zhang and J. Li, “Turn hydrophobic to superhydrophobic of composite insulators by surface fluorination”, in ICHVE, 2016.

[21] J. Wu and A. Schnettler, “Degradation assessment of nanostructured superhydrophobic insulating surfaces using multi-stress methods”, IEEE Trans.Dielectr.Electr.Insul., vol. 15, no. 1, 2008.

[22] J. Wu, C. Cornelissen and A. Schnettler, “Investigation on the flashover performance of nanostructured insulating surface with ‘Lotus-Effect[R]’ under wet conditions”, in ISH, Pilsen-Czech, 2015.

[23] F. Madidi, G. Momen and M. Farzaneh, “Development of a stable TiO2 nanocomposite self-cleaning coating for outdoor applications. Article ID 7958152”, in Advances in Material Science and Engineering, 2016.

[24] G. Maghsoudi, R. Momen, R. Jafar and M. Farzaneh, “Direct replication of micro-nanostructures in the fabrication of superhydrophobic silicone rubber surfaces by compression molding, Applied Surface Science”, vol. 458, 2018.

[25] G. Maghsoudi, R. Jafari, G. Momen and M. Farzaneh, “Micro-nanostructured polymer surfaces using injection molding: A review”, Materials Today Communication, vol. 13, 2017.

[26] R. Jafari and M. Farzaneh, “Development a simple method to create the superhydrophobic composite coatings”, Journal of Composite Materials, vol. 47, no. 25, 2013.

[27] J.M. George, A. Le Du and S. Prat, “Evaluation of innovative hydrophobic surfaces for overhead line insulators”, in ISH, Budapest-Hungary, 2019.

[28] J. Dong, P. Wang, D. Sun, Y. Xu and K. Li, “Preparation and Characterization of Graphene/RTV Silicon Rubber Composites”, TTP, 2013.

[29] CIGRE TB361, “Outdoor Insulation in Polluted Conditions: Guidelines for selection and Dimensioning: Part 1: General Principles and the AC Case”, Working Group C4.303, June 2008.

[30] W. Vosloo, C. de Tourreil, R. Macey, “Practical guide to outdoor high voltage insulators”, CP, 2004.

[31] CIGRE TB691, “Pollution Test of Naturally and Artificially Contaminated Insulators”, Working Group D1.44, July 2017.

[32] CIGRE TB518, “Outdoor Insulation in Polluted Conditions: Guidelines for selection and dimensioning: Part 2: The DC Case”, Working Group C4.303, December 2012.

[33] Pietersen D, “The development of a methodology to compile insulator pollution severity application map for South Africa”, University of Stellenbosch, April 2005.

[34] SANS/IEC: 60815-1, ”Selection and dimensioning of high-voltage insulators intended for use in polluted conditions Part 1: Definitions, information and general principles”, Edition 1.0, 2008-09.

[35] CIGRE TB555, “Artificial Pollution Test for Polymer Insulators Results of Round Robin Test”, Working Group C4.303, October 2013.

[36] 4 Ways to Avoid Insulator Flashovers, “https://www.midsunikm.com/post/ways-to-avoid-insulator-flashovers”, [Accessed: 4 July 2023].

[37] ANSI C29-13, “American National Standard for Composite Insulators Distribution Deadend Type”, Edition 1, 2010.

[38] E. Ramesh,U. Joshi, “Investigation into the Effect of Corona on Insulators”, IJERT (ISSN:2278-0181), 2018.

[39] W. Thipprasert, A. Yawootti and A. Rupdee, “Effect of test conditions on ageing deterioration of Composite Insulator Using the Tracking Wheel Test”, GMSARN International Conference, 2018.

[40] J. Lambrecht and K. Hindelang, “Chemistry and properties of Silicones,” in Power Engineers Handbook”, INMR, 2018.

[41] Insulator Spray-Coating, “https://www.slideshare.net/NeeleshArora1/powergrid-vizag-400-kv-and-hvdc-yard-epsilon-rtv-insulator-coating”, [Accessed: 27 April 2021].

[42] J. Zhang et al, “Improvement in Anti-static Property and Thermal Conductivity of Epoxy Resin by Doping Graphene”, IEEE Electrical Insulation Magazine Vol. 27, No. 2, 2020.

[43] Dropletlab, “https://dropletlab.com/wp-content/uploads/2020/04/Brochure.pdf”, [Accessed: 6 July 2021].

[44] PhysioSupplies.eu, “https://www.physiosupplies.eu/plastic-goniometer-20-cm”, [Accessed: 6 July 2021].

[45] R. Swinny, W. Vosloo, J.C. Bekker “Investigation into the influence of electrode material on the IEC Inclined Plane test procedure (IEC 60587) when applied for Direct Current (DC) voltages”, Masters Dissertation, March 2021.

[46] G.P. Bruce, S.M. Rowland and A. Krivda, “DC Inclined-plane testing of silicone rubber formulations”, Annual Report Conference on Electrical Insulation Dielectric Phenomena, 2010.

[47] H. Zhang, W. Xing, H. LI, Z Xie, G. Huang, J. Wu, “Fundamental researches on graphene/rubber nanocomposites”, Advanced Industrial and Engineering Polymer Research 2 32-41, 2019.

[48] F. Farhang, M. Ehsani and S.H. Jazayeri, ”Effects of the Filler Type and Quantity on the Flashover Voltage and Hydrophobicity of RTV Silicone Rubber Coatings”, Iranian Polymer Journal 18 (2) 149-157, 2009.

[49] H. Janssen, A. Herden and H. Karner, “LMW Components in Silicone Rubbers and Epoxy Resins”, 11th ISH, 1999.

[50] C. Wang, J. Wang, Z. Men, Y. Wang and Z. Han, “Thermal Degradation and Combustion Behaviours of Polyethylene/Alumina Trihydrate/Graphene Nanoplatelets”, MDPI Journal, 2019.

ANNEXURE A – Equipment/Software Checklists for Chosen Experiments

SURFACE RESISTIVITY TESTS

1) Megger MIT 1025 Device
2) PowerDB 11.2 Advanced Software
3) USB-B to USB-A Cable
4) Insulation Resistance Test Tile Clamper
5) Surgical Gloves
6) Nikon 100D5600
7) 1x Temperature and Humidity Sensor
8) Timer

HYDROPHOBICITY TESTS

1) Variable Micropipette 10 µl to 100 µl. *Work at 50 µl.*
2) Micropipette Syringes
3) De-ionized/Distilled water
4) Capped Bottle for Distilled Water
5) Surgical Gloves
6) Nikon 100D5600
7) 2x Dremel Vices
8) Small Spirit Level
9) ImageJ Drop Analysis Software
10) x1 Temperature and Humidity Sensor/Hygrometer
11) Spray Bottle
12) Timer

HYDROPHOBICITY TRANSFER TESTS

1) Variable Micropipette 10 µl to 100 µl. *Work at 10 µl.*
2) Micropipette Syringes
3) De-ionized/Distilled water
4) Capped Bottle for Distilled Water
5) Surgical Gloves
6) Nikon 100D5600
7) 2x Dremel Vices
8) Small Spirit Level
9) ImageJ Drop Analysis Software
10) 1x Temperature and Humidity Sensor/Hygrometer
11) Timer
12) Adhesive Foil (3 Foils Thick at 0.36 mm, 0.12 mm each recommended) (*A foil thickness of 70 micron was used for this project*)
13) Scissors
14) Untreated Silica Powder with medium grain size 3µm (SIKRON SF600)/Kaolin

powder/Diatomaceous earth
15) Isopropanol
16) Digital Gram Scale
17) Teaspoon
18) Plastic Stick/Spatula for Mixing and Scraping
19) Polyethylene Storage Container with small holes in lid
20) Desiccant (Calcium Chloride Crystals)

INCLINED PLANE TESTS

1) 30x Electrodes pairs (0.5 mm thick) manufactured from stainless steel (Grade 304) as per IEC 60587
2) 4 mm Bolts and Nuts for Electrodes
3) Stikland Inclined Plane Tester with AC Transformer and DC Rectifier
4) Ground Stick
5) Control Panel
6) 3 kΩ Limiting Resistors
7) 63 mA Fuses
8) Paper Clips
9) Filter Paper
10) Scissors
11) Syringes and Needles to Measure Contaminant Flow Rate and to mix contaminant.
12) Online Leakage Current Analyzer (OLCA)
13) Laptop with installed OLCA analysis software.
14) 2x AC Current Measurement Boxes (Calibrated) with Cabling
15) 2x DC Current Measurement Boxes (Calibrated) with Cabling.
16) OLCA Temperature and Relative Humidity Sensor
17) "1 % ± 0.002 % mass NH_4Cl (ammonium chloride) and 0.02 % ± 0.002 % mass isooctylphenoxypolyethoxyethanol in distilled or de-ionized water. The contaminant should have a resistivity of 3.95 Ωm ± 0.05 Ωm at 23°C.
18) 3x 1L Beakers
19) De-ionized/Distilled water
20) Teaspoon
21) Surgical Gloves
22) Isopropanol
23) Citizen CX301 Precision Balance Scale
24) Timer
25) Nikon 100D5600
26) Tektronix High Voltage Multimeter
27) High Voltage Probe
28) Conductivity Meter with Thermometer
29) Inclined Plane Tester Checklist and Procedure Hardcopies
30) Coated Tile Test Specimens
31) 1200 Grit Sandpaper

ANNEXURE B – Surface Resistivity Experimental Test Procedure (using ASTM D257-14 and D4496-21)

Figure 65: Insulation resistance experimental test setup with Megger 1025 device, plastic spring clamps, insulation resistance test device electrodes, capacitive discharging ground plate etc.

1. Ensure the Megger 1025 IRT device is switched OFF and all 3x test leads/electrodes are disconnected.

2. Connect PC to the Megger 1025 IRT device via an USB cable and setup the PowerDB software for timed (set to 1 minute) insulation resistance tests - 60010.

3. Measure the laboratory temperature and humidity using a hygrometer.

4. Confirm all Insulation Resistance Tile Clamping Device (IRTCD) electrode's conduction path resistances are the same resistance as the probe resistance measured when shorted. It must be roughly 1.4 Ohms for a Fluke CNX3000 multimeter.

5. Wear surgical gloves at all times to prevent contamination of coated tile samples when touching.

6. Carefully remove the coated tile sample from its plastic container bag and check for any visible surface contamination such as dust, hair, damage etc.

7. Remove visible contamination by gently wiping the sample's surface with cotton swab and Iso-Propyl alcohol.

8. Gently position the tile sample perfectly between the IRTCD positive and negative electrodes as well as on top of the guard electrode and secure with plastic spring clamps. Ensure the electrode's test setup rests on a approximately 6 mm thick rubber surface.

9. Press the IRTCD positive and negative electrodes downwards until it makes contact with the tile’s upper coated surface. (Don’t press the IRTCD electrode too hard against the tile sample’s surface, otherwise the tile will break).

10. Clamp the Megger’s positive, negative and guard test leads to the connection bolts of the IRTCD clamps/electrodes.

11. Take picture of coated tile sample.

12. Switch the Megger device ON by turning the settings knob to the Insulation Resistance Timed function position and by setting the voltage knob to 5 kVDC.

13. Open the S1/MIT Dialog on PC to view measurements and select "Start New Live Stream". Enter a suitable test name, e.g., "Tile Specimen %, Graphene Type, Test Voltage, Test Time, Test No."

14. Press the Megger’s red TEST function knob for 3 seconds to start insulation resistance tests. Save all the voltage, current and resistance measurement results as a .csv file on PC after 1 min has passed.

15. Do 3x sets of 1-minute insulation resistance measurements with 4-minute rest intervals in between at 5 kVDC test voltages. During rest intervals ground all electrodes to a ground

plate before the next IR measurement is done to ensure any capacitive build up within the tile is drained properly.

16. Turn OFF the Megger device after all 9x sets of insulation resistance measurements are completed at the required test voltage.

17. Carefully remove the tile sample without scratching its surfaces and place it back into its respective plastic container bag.

18. Repeat steps 6. to 17 for all coated tile samples.

ANNEXURE C – Hydrophobicity Tests
ANNEXURE C.1 – Hydrophobicity Contact Angle Measurement Experimental Test Procedure (using IEC 62073)

Figure 66: Hydrophobicity contact angle measurement test setup with high resolution camara and makro lense. A combination of other equipment such as a variable micropipette (10 µl to 100 µl), white LED light for high contrast photos and highly manoeuvrable vice grips helps with placing droplets with minimal disturbances.

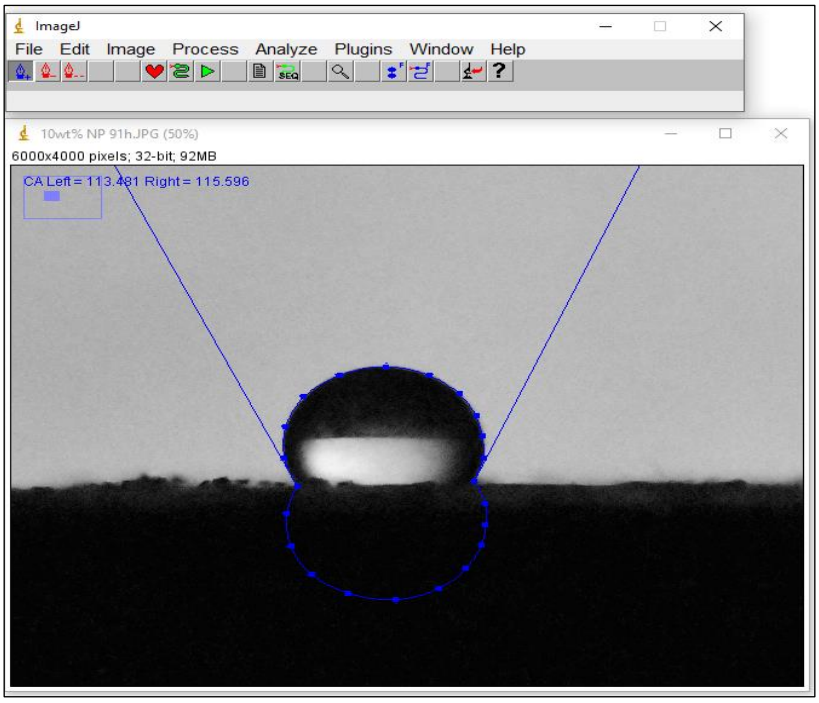

Figure 67: Hydrophobicity high-precision contact angle measurement with ImageJ software.

1. Setup a high-resolution Nikon camara with makro lense attached on adjustable stand.

2. Position the camara in such a way that the tile's horizontal surface can be captured.

3. Place a piece of clean A4 paper vertically behind the tile specimen's test position and let a bright white LED light shine through the

paper from behind to ensure a monochrome picture contrast is captured.

4. Ensure no camara and tile specimen vibrations/distortions occur during water droplet application which may affect results.

5. Measure the laboratory temperature and humidity with a hygrometer.

6. Set the variable micropipette to a droplet volume of 50 µl.

7. Wear surgical gloves at all times to prevent contamination of coated tile samples when touching.

8. Carefully remove the coated tile sample from the container and check for any visible surface contamination such as dust, hair, damage etc.

9. Remove visible contamination by gently wiping the sample's surface with cotton swab and Iso-Propyl alcohol. Allow time to dry.

10. Gently position the tile sample in front of the camara.

11. Focus the camara lens onto the tile specimen surfaces by adjusting its horizontal position and zooming knob accordingly.

12. Use a small spirit level to vertically level the tile specimen 90 degrees in front of the camara.

13. Use a small spirit level to vertically level the camara 90 degrees in front of the tile specimen.

14. Take pictures of vertically levelled camera lens and tile specimens.

15. Connect a clean/new syringe to the micropipette.

16. Transfer 50µl of distilled/de-ionised water into the micropipette.

17. Turn off laboratory ceiling lights to ensure monochrome contrast pictures are captured.

19. Transfer a 50µl of distilled/de-ionised water droplet from the micropipette onto the surface of the tile specimen. 3x Droplets must be applied on separate surfaces adjacent to each other for measurements.

Note: Use a Dremel vice (connected to a separate table/surface) to hold the micropipette steady during droplet placement and immersed within the droplet during measurement.

20. Repeat steps 1 to 19 for all tile specimens.

21. Import photos to Image J (with Drop Analysis Plugin) software to accurately measure/analyse the static contact angles of each applied water droplet.

ANNEXURE C.2 – Hydrophobicity Spray Bottle Experimental Test Procedure (using IEC 62073)

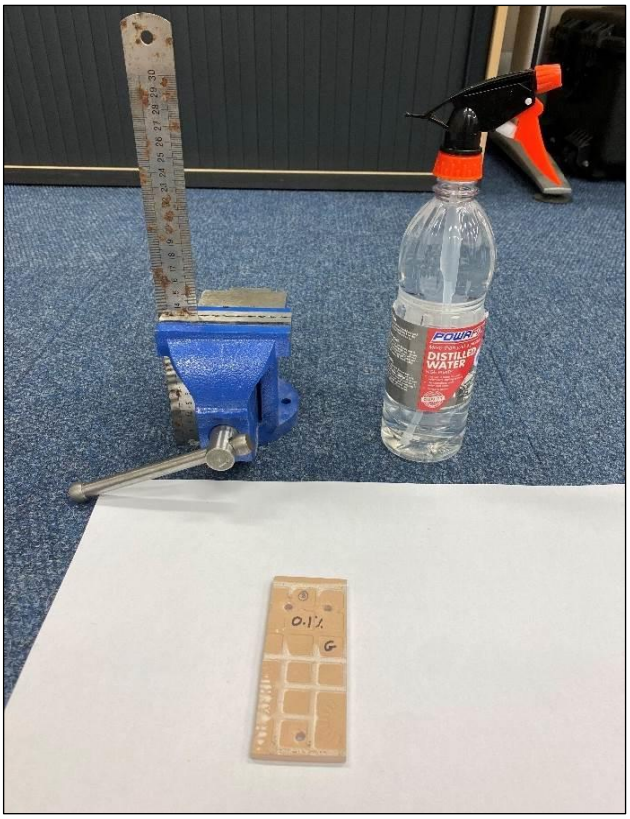

Figure 68: Hydrophobicity wettability class measurement setup.

1. Measure the laboratory temperature and humidity with a hygrometer.

2. Fill a spray bottle, which can produce a fine mist, with distilled/de-ionised water.

3. Fasten a 30cm ruler vertically to a vice and place it near the test position to be used as a spray distance reference point.

4. Wear surgical gloves at all times to prevent contamination of coated tile samples when touching.

5. Carefully remove the coated tile sample from the container and check for any visible surface contamination such as dust, hair, damage etc.

6. Remove visible contamination by gently wiping with fingers (with surgical gloves on) over the sample until visibly clean.

7. Gently position the tile sample in front of the vice and ruler setup.

8. Apply the mist onto the coated tile area for a period of 30s from a distance of 25 cm ±10 cm.

9. Perform wettability measurements within 10s after spraying has been completed. Note: The measurement shall be performed in such a way that a clear picture of the variation of the wettability along and around the coated area is obtained.

ANNEXURE D – Inclined Plane Experimental Test Procedure (using IEC 60587)

See next page.

INCLINED PLANE TESTER PROCEDURE & CHECKLIST

TEST TITLE: _____

DATE: _____

INDEX

STEP 1: IPT PREPARATION	√
1. Fill in workers register.	
2. Ensure safety screens in front of HV transformer and capacitor bank.	
3. Ensure entire work area is safe, the MCB is SWITCHED OFF and VARIACS are SET TO 0 V.	
4. Ensure the capacitor bank drain switch is in the CLOSED POSITION.	
5. Place the earth stick next to the control panel.	
6. Setup all electrical equipment correctly for HV test: AC, DC+ or DC-.	
7. Setup multimeter and high voltage probe.	
8. Setup LC equipment correctly for HV test: AC, DC+ or DC -.	
9. Calibrate the LC equipment with OLCA software on laptop.	
10. Note the temperature and humidity via the OLCA software in the table below. Remember to take a photo of measurements.	
11. Open IPT front cabinet door.	
12. Prepare two test sample bays by cleaning all necessary electrodes with 1200 Grit sandpaper and electronic cleaner. Clean all electrodes with distilled water afterwards and wipe dry.	

TEST ENVIRONMENT CONDITIONS		
Temperature (°C)		Photo Nr:
Relative Humidity (%)		

STEP 2: TEST SAMPLE PREPARATION	√
1. Ensure a clean and safe working area for test sample preparation and photos.	
2. Mark 2x test samples with Unique Test Name (UTN) on a surface not subject to test and note the UTNs in the table below.	
3. Take detailed close-up photos of each sample's written UTN (rear) and front view. Note the photo numbers in the table below.	
4. Take detailed close-up photos of each sample's Anode and Cathode electrodes. Note the photo numbers in the table below.	
5. Weigh the test samples and electrodes with an electronic scale. Note the measurements in the table below.	
6. Roughen the top surface of each sample with 1200 Grit sandpaper.	
7. Spray each sample with distilled water and note the Hydrophobicity Class (HC) values in the table below. Gently wipe down the water droplets from both sample's surface afterwards.	

TEST SAMPLE 1 INFORMATION			
Sample 1 Unique Test Name			
PHOTO NUMBERS			
Unique Test Number	Before:	N/A	
Front View	Before:	After:	
Anode Electrode	Before:	After:	
Cathode Electrode	Before:	After:	
HC	Before:	After:	
WEIGHTS			
Test Sample (g)	Before:	After:	Δ:
Anode Electrode (g)	Before:	After:	Δ:
Cathode Electrode (g)	Before:	After:	Δ:
HYDROPHOBICITY CLASS			
HC	Before:	After:	
TEST SAMPLE 2 INFORMATION			
Sample 2 Unique Test Name			
PHOTO NUMBERS			
Unique Test Number	Before:	N/A	
Front View	Before:	After:	
Anode Electrode	Before:	After:	
Cathode Electrode	Before:	After:	
HC	Before:	After:	
WEIGHTS			
Test Sample (g)	Before:	After:	Δ:
Anode Electrode (g)	Before:	After:	Δ:
Cathode Electrode (g)	Before:	After:	Δ:
HYDROPHOBICITY CLASS			
HC	Before:	After:	

STEP 3: IPT TEST RUN	√
1. Fasten each test sample with 3x Stainless Steel (SS) and 3x SS bolts to test bays 2 and 3 respectively. Ensure both the electrodes and filter paper are fitted correctly to ensure proper flow of contaminant over each tile's surface.	
2. Fill a beaker with 500 mL distilled water and measure the conductance. Add measurements in the table below.	
3. Add 0.1 % ± 0.002 % Ammonium Chloride and 0.02% ± 0.002 % isooctylphenoxypolyethoxyethanol (Triton X-100) to the solution until a conductivity of 2.53 mS / cm is measured.	
4. Divide the 500 mL solution into x2 beakers (each 250 mL) and place the beakers into their respective test positions.	
5. Fit the contaminant supply tubes into the folds of the filter paper and beakers respectively.	
6. Ensure the entire testing area is clean and safe from debris.	
7. Close the IPT door and ensure the safety lock switch is in the CLOSED POSITION.	
8. Make sure that all electrical connections are sound and check earth connections.	
9. OLCA SWITCHED ON and running.	
10. If doing DC tests, ensure the capacitor bank drain switch is in the OPEN POSITION.	
11. SWITCH ON supply at MCB.	
12. SWITCH ON the HV equipment at the main control panel by turning RED knob.	
13. HOLD the YELLOW alarm switch for 3s to stop sounding alarm.	
14. SWITCH ON the main supply of the motors with the GREEN light ON.	
15. SWITCH ON motor 2 and 3 with both GREEN lights ON.	
16. Establish flow rate and flow over the surfaces for both samples.	
17. When a constant flow rate is established setup video camara to record test positions (1^{st}, 3^{rd} and 5^{th} Hour – 20 min intervals) and take photos.	
18. Check if VARIACS are SET TO 0 V.	
19. Press the GREEN START button on the main control panel to start IPT.	
20. Slowly TURN UP the VARIAC OUTPUT until the required test voltage is measured by the multimeter.	
21. Note the START TIME in the table below at 0 min Interval Time.	
22. Keep checking the test samples during energisation to see that there are not any problems e.g., contaminant flow errors, contaminant volume level, sample burning, flashovers, voltage drops/spikes etc. ➢ If a sample fails: • Note the time and SWITCH OFF supply as described in STEP 4. • Remove failed sample from test position. • Remove contaminant supply to that test position by removing supply tube. • Disable HV supply to that test position. • Resume tests on other samples, noting time of re energization. ➢ If anything is goes entirely wrong: • Press the RED EMERGENCY STOP button on the main control panel • SWITCH OFF supply as described in STEP 4.	

CONTAMINANT INFORMATION		
BEAKER 1		
Conductivity (mS / cm)	Before:	After:
Temperature (°C)	Before:	After:
Volume (mL)	Before:	After:
BEAKER 2		
Conductivity (mS / cm)	Before:	After:
Temperature (°C)	Before:	After:
Volume (mL)	Before:	After:

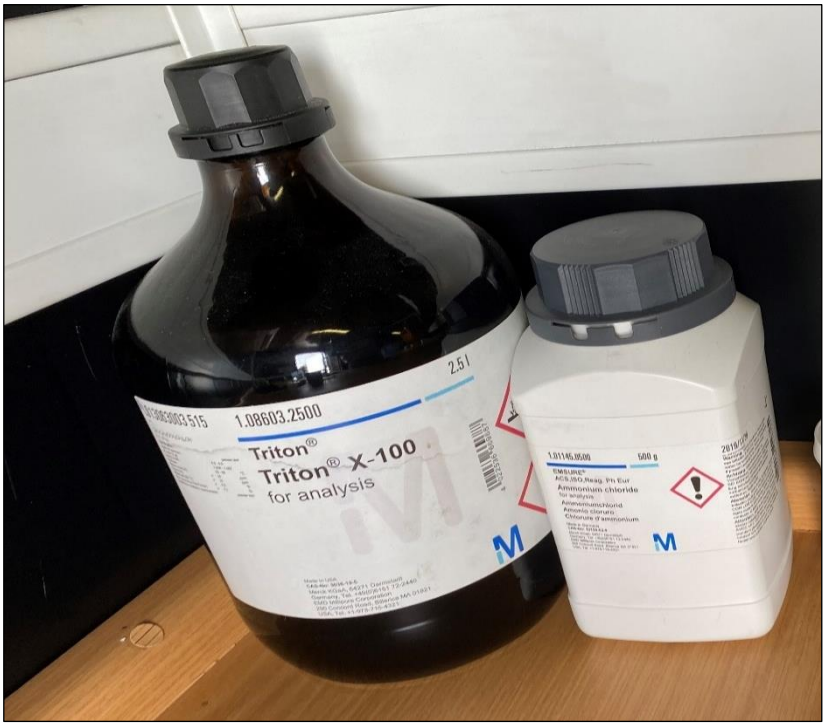

Figure 69: Ammonium chloride (left) and isooctylphenoxypolyethoxyethanol, Triton X-100, (right) used as conductive solution for incline plane tests at a flow rate of 0.6 ml/min.

VISUAL OBSERVATIONS DURING IPT (Tracking, erosion, punctures etc.)	
1. Interval Time: 00:00 – 00:15	
2. Interval Time: 00:15 – 00:30	
3. Interval Time: 00:30 – 00:45	
4. Interval Time: 00:45 – 01:00	
5. Interval Time: 01:00 – 01:30	
6. Interval Time: 01:30 – 03:00	
7. Interval Time: 03:00 – 05:00	
8. Interval Time: 05:00 – 06:00	

GENERAL Notes / Comments:

STEP 4: END OF IPT TEST RUN	√
1. Slowly TURN DOWN the VARIAC OUTPUT until the 0 V POSITION.	
2. Press the RED STOP switch.	
3. SWITCH OFF motor 2 and 3 with both GREEN lights OFF.	
4. SWITCH OFF the main supply of the motors with the GREEN light OFF.	
5. SWITCH OFF the HV equipment at the main control panel by turning RED knob.	
6. SWITCH OFF supply at MCB.	
7. If doing DC tests, drain the capacitor bank by setting the switch in the CLOSED POSITION with an earth stick.	
8. Make sure that all electrical connections are sound and check earth connections.	
9. Place the earth stick next the control panel.	
10. Note the FINISH TIME in the table above.	
11. Open IPT front cabinet door and carefully remove samples tested and beakers.	
12. Measure each beaker's contaminant conductivity and volume level. Add measurements in the table above.	
13. Take detailed close-up photos of each sample's front view. Note the photo numbers in the table above.	
14. Take detailed close-up photos of each sample's Anode and Cathode electrodes. Note the photo numbers in the table above.	
15. Weigh the test samples and electrodes with an electronic scale. Note the measurements in the table above.	
16. Do a final visual observation of both test samples.	
17. Spray each sample with distilled water and note the HC values in the table above. Gently wipe down the water droplets from both sample's surface afterwards.	
18. Download and analyse OLCA leakage current data for both test samples.	

FINAL Notes / Comments:

ANNEXURE E – Mobile Test Rig Design
ANNEXURE E.1 – MTR LV & HV Electrical Wiring Layout Diagram and 3D CAD Models

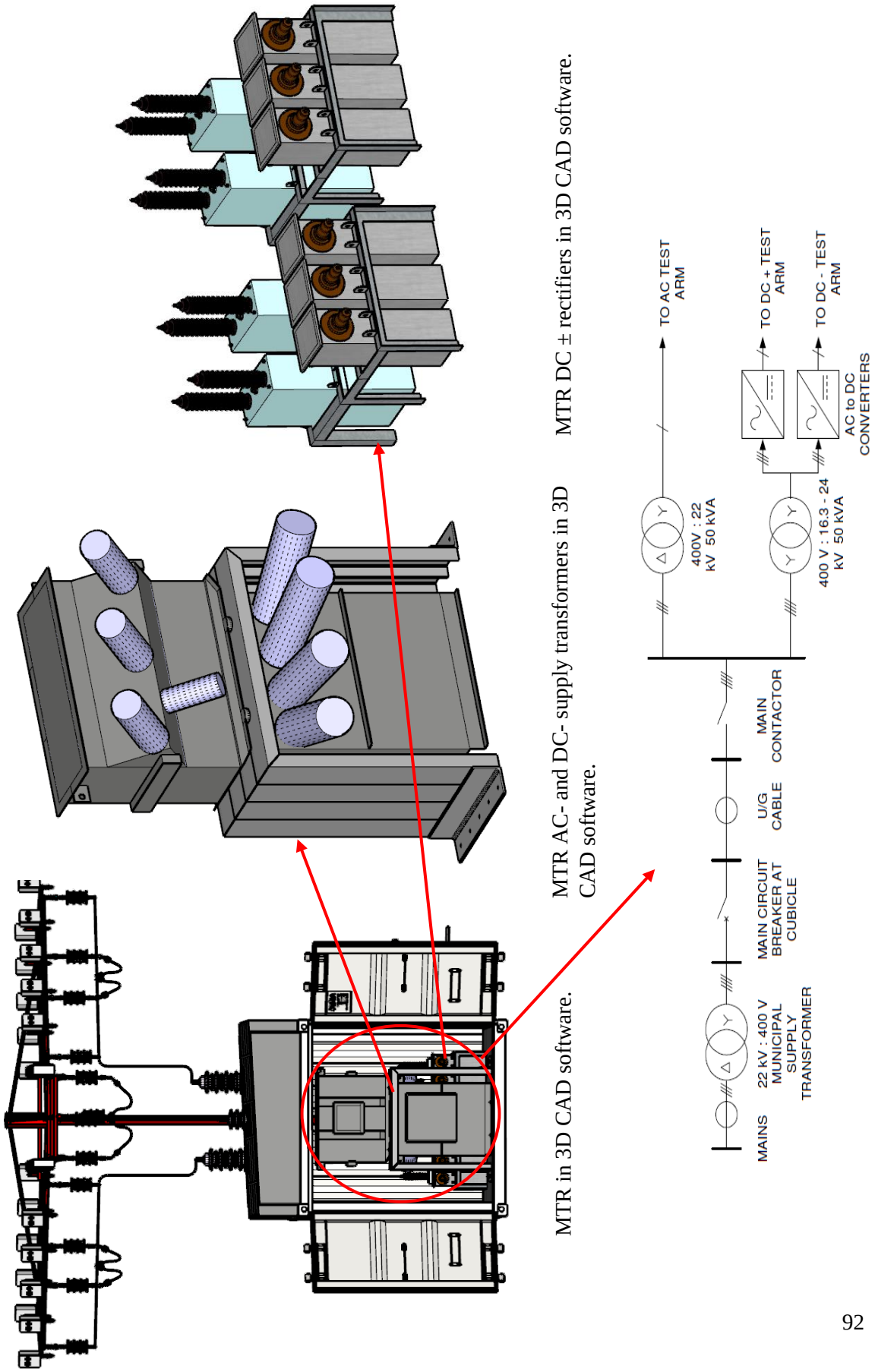

ANNEXURE E.2 – High Level Overview of MTR Technical Design Drawings